Structure of Multi-Temperature Sensitive Core-Shell Microgels

PhD Thesis

submitted in partial fulfilment of the requirements
for the degree of "Doktor rerum naturae"
to the Faculty of Mathematics and Science of the
Christian-Albrechts-University of Kiel

Ingo Berndt

Kiel 2005

This PhD work was carried out at the Institute of Physical Chemistry at the Christian-Albrechts-University of Kiel from July 2001 until April 2004 and continued at the Institute of Physical Chemistry at the RWTH Aachen from May 2004 until November 2005 supervised by Prof. Dr. Walter Richtering.

I certify that this thesis does not incorporate, without acknowledgement, any material submitted for a degree or diploma at any university, and that, to the best of my knowledge, it does not contain any material previously published or written by another person except where due reference is made in the text. The work in this thesis is my own, except for the contributions made by others as described in the acknowledgements.

Ingo Berndt

Referent:	Prof. Dr. Walter Richtering
Korreferent:	Prof. Dr. Regine von Klitzing
Tag der Disputation:	20. Dezember 2005

Zum Druck genehmigt.

Kiel, den

Der Dekan

Short Summary

The internal and overall structure of multi-temperature sensitive core-shell microgels was studied in this work.
The particles consist of chemically cross-linked networks of two temperature-sensitive polymers, poly-*N*-isopropylacrylamide (PNIPAM) and poly-*N*-isopropropyl*meth*acrylamide (PNIPMAM), which exhibit lower critical solution temperatures (LCST) at 34 and 44 °C in aqueous solution. The particles were prepared in a two-step seed-and-feed polymerization to obtain a core-shell morphology, which allows a spatial separation of the two polymers with sensitivity to different quantities of the environmental stimulus temperature.
The influence of shell thickness, i.e. the shell/core mass composition, and the cross-linker content of the shell on the overall structure of PNIPAM core-PNIMAM shell microgels were investigated by means of dynamic light scattering (DLS). It was found that the particle size decreased in two distinct transitions upon heating at temperatures according to the core and shell component, respectively. The core transition at 34 °C became less pronounced for higher cross-linked and thicker shells.
Small-angle neutron scattering (SANS) was used in order to explore the internal structure. A new core-shell form factor model was developed and employed to fit the obtained data. Real space information on the particle structure was obtained from an analytical expression of the form factor calculating radial density profiles. The structure of the core-shell microgels was evaluated at temperatures above, between and below the LCSTs of the two polymers. At high temperatures the radial density distribution is well described by a two-box profile with narrow interface at the particle surface and at the core-shell interface where both networks interpenetrate. Decreasing the temperature below the shell LCST revealed a highly swollen shell, a broadened core-shell interface and increased dimensions of the core. The core expansion was explained by lateral stretching forces exerted to the core from the swollen shell. Thicker shells developed stronger forces and thus led to more expanded cores. At a temperature below the core LCST both core and shell were highly swollen, however, the swelling of the core was restricted. The cross-linked shell polymer close to the core-shell interface was stretched to a maximum extent and prevented further swelling of the core.
An inverse PNIPMAM core-PNIPAM shell microgel was investigated for comparison. Already DLS indicated a mutual influence of core and swelling as the particle sizes observed for the core-shell particle were smaller than for the parent core at temperatures between the LCSTs. The form factor model demanded for modifications to allow an asymmetric shape of the interface between core and shell. The analysis of data taken at 39°C validated the core compression by the collapsed shell and further revealed an inhomogeneous swelling of the core due to loosely cross-linked chains in the periphery which did not interpenetrate with the shell network.
The calorimetric properties of the core-shell microgel series with varied shell/core mass ratios were examined by means of differential scanning calorimetry (DSC) and compared to the structural information obtained from SANS. Two thermal transitions were found at temperatures correlated to the LCSTs of the components. A shift of the core transition towards higher temperatures was observed with increased shell masses and could be explained by a "chemo-mechanical" model. The forces which are exerted from the swollen shell to the core partially compensate the thermodynamic shrinking force of the core and thus the transition temperature is increased. In case of a very high shell mass a third thermal transition was observed between the LCST. The very thick shell led to a significant expansion of the core and the third transition corresponds to reorganized hydrogen bonds which are formed by the stretching of polymer chains close to the core-shell interface.
The transition heats of the PNIPMAM shells were much smaller compared to a pure PNIPMAM microgel. The comparison with SANS results revealed a restricted swelling in the confined geometry of a shell and could explain the lower heats.

Kurzzusammenfassung

In der vorliegenden Arbeit wurde die Struktur mehrfach temperatursensitiver Kern-Schale-Mikrogele untersucht.
Die Teilchen bestehen aus kovalent vernetzten Polymernetzwerken der beiden temperatursensitiven Polymere Poly-*N*-Isopropylacrylamid (PNIPAM) und Poly-*N*-isoproplymethacrylamid (PNIPMAM), die untere kritische Entmischungstemperaturen (LCST) bei 34 bzw. 44 °C aufweisen. Die Teilchen wurden in zwei aufeinander folgenden Schritten hergestellt, so dass eine Kern-Schale-Morphologie erhalten wurde, die eine räumliche Trennung der unterschiedlich temperatursensitiven Polymere erlaubte.
Der Einfluß der Schalendicke, gegeben durch das Massenverhältnis von Schale zu Kern, und der Vernetzungsdichte der Schale auf das temperatursensitive Verhalten von PNIPAM Kern-PNIPMAM Schale-Mikrogelen wurde mit dynamischer Lichtstreuung (DLS) untersucht. Es wurden zwei getrennte Übergänge in den Teilchengrößen bei Temperaturen beobachtet, die den LCSTs der beiden Polymere entsprechen. Der Übergang bei 34 °C war nicht so stark ausgeprägt bei Teilchen, die eine dicke oder sehr stark vernetzte Schale hatten.
Die interne Struktur der Teilchen wurde mit Kleinwinkel-Neutronenstreuung (SANS) untersucht. Ein neues Kern-Schale-Formfaktor-Modell wurde entwickelt, um die experimentellen Daten anzupassen. Die räumliche Struktur wurde dabei durch radiale Dichteprofile beschrieben. Es wurden Messungen bei Temperaturen oberhalb der LCST der Schale, zwischen den beiden LCSTs und unterhalb der LCST des Kerns durchgeführt. Bei hohen Temperaturen wird die Dichteverteilung sehr gut durch zwei kastenartige Profile mit schmalen Grenzflächen an der Teilchenoberfläche und an der Kern-Schale-Grenze beschrieben, wo sich die beiden Netzwerke gegenseitig durchdringen. Bei niedrigeren Temperaturen unterhalb der LCST der Schale wurden eine aufgequollene Struktur der Schale, eine verbreiterte Kern-Schale-Grenze und eine radiale Streckung des Kerns beobachtet. Die Streckung des Kerns wurde durch lateral wirkende Kräfte erklärt, die von der Schale auf den Kern ausgeübt werden. Dabei wurde festgestellt, dass dickere Schalen stärkere Kräfte entwickeln müssen und zu einer stärkeren Streckung des Kerns führen. Bei Temperaturen unterhalb der LCST des Kerns war die Quellfähigkeit des Kerns eingeschränkt. Das vernetzte Schalenpolymer an der Kern-Schale-Grenze konnte aufgrund der Vernetzung nicht weiter anquellen und verhinderte so das weitere Quellen des Kerns.
Zum Vergleich wurde ein inverses PNIPMAM Kern-PNIPAM Schale-Mikrogel untersucht. Bereits die Teilchengrößemessungen deuteten auf einen gegenseitigen Einfluß auf das Quellvermögen von Kern und Schale hin: Im mittleren Temperaturbereich zwischen den beiden LCSTs war das Kern-Schale-Teilchen kleiner als der zugrunde liegende Kern. Das Formfaktor-Modell musste so verändert werden, dass es einen asymmetrischen Verlauf an der Kern-Schale-Grenze zuläßt. Die Auswertung der 39 °C-Daten bestätigte, dass der Kern in diesem Fall durch die kollabierte Schale zusammengedrückt wurde. Außerdem zeigte das Dichteprofil ein inhomogenes Quellen des Kerns an, das durch gering vernetzte Polymersegmente in den äußeren Bereichen des Kerns hervorgerufen wurde, die sich nicht mit dem Schalennetzwerk durchdringen.
Die kalorimetrischen Eigenschaften von Kern-Schale-Mikrogelen mit unterschiedlichen Massenverhältnissen von Kern zu Schale wurden durch Differentialthermoanalyse (DSC) untersucht und mit den Ergebnissen der Neutronenstreuung verglichen. Es wurden zwei thermische Übergänge entsprechend den LCSTs der beiden Komponenten beobachtet. Es zeigte sich, dass sich das Signal des Kerns mit zunehmender Masse der Schale zu höheren Temperaturen verschob. Um dies zu erklären wurde ein "chemo-mechanisches" Modell vorgeschlagen. Dabei wird die Kontraktion des Kerns durch die entgegengesetzten, von der Schale auf den Kern ausgeübten Kräfte teilweise kompensiert, was effektiv zu einer Erhöhung der Übergangstemperatur führt.
Bei dem Kern-Schale-Mikrogel mit der dicksten Schale wurde ein dritter thermischer Übergang zwischen den beiden LCSTs gefunden. Die sehr dicke Schale führte zu einer starken Streckung des Kerns. Der zusätzliche thermische Übergang wurde mit der Umordnung von Wasserstoffbrückenbindungen erklärt, die stattfinden, wenn die Polymersegmente in der Nähe der Kern-Schale-Grenze gestreckt werden. Es wurde auch beobachtet, dass die Wärmetönungen beim Übergang der PNIPMAM-Schalen deutlich kleiner waren als im Vergleich zu einem reinen PNIPMAM-Mikrogel. Der Vergleich mit den SANS-Daten konnte zeigen, dass das begrenzte Quellvermögen in der eingeschränkten Schalengeometrie für die kleineren Wärmetönungen verantwortlich war.

List of Publications and Presentations

Journal contributions

I. Berndt, J. S. Pedersen, W. Richtering
Temperature-Sensitive Core-Shell Microgel Particles with Dense Shell
submitted.

I. Berndt, J. S. Pedersen, P. Lindner, W. Richtering
Influence of Shell Thickness and Cross-Link Density on the Structure of Temperature-Sensitive Poly-N-Isopropylacrylamide – Poly-N-isopropylmethacrylamide Core-Shell Microgels investigated by Small-Angle Neutron Scattering
Langmuir, in press.

I. Berndt, C. Popescu, F.-J. Wortmann, W. Richtering
Mechanics versus Thermodynamics: Swelling in Multi-Temperature Sensitive Core-Shell Microgels
Angew. Chem. Int. Ed., accepted for publication.

I. Berndt, J. S. Pedersen, W. Richtering
Internal Structure of Multiresponsive 'Intelligent' Core-Shell Microgels
J. Am. Chem. Soc. **2005**, *127*, 9372.

I. Berndt, W. Richtering
Doubly Temperature Sensitive Core-Shell Microgels
Macromolecules **2003**, *36*, 8780.

Patent

W. Richtering, I. Berndt
Heterogene Kern-Schale-Mikrogele mit mehrstufigem Schaltverhalten
Patentschrift DE 102 40 956 B4, **17.03.2005**.

Conference proceedings

I. Berndt, J. S. Pedersen, P. Lindner, W. Richtering
Structure of Doubly Temperature Sensitive Core-Shell Microgels based on Poly-N-Isopropylacrylamide and Poly-N-Isopropylmethacrylamide
42nd Meeting of the German Colloid Society "Smart materials: foams, gels and microcapsules", September **2005**, Aachen.
Progr. Colloid Polym. Sci., accepted for publication.

W. Richtering, I. Berndt, M. Stieger, P. Lindner
Temperature Sensitive Microgel Suspensions: Smart Materials and Macromolecular Push Me-Pull You
Makromolekulares Kolloquium, February **2003**, Freiburg.
Macromol. Chem. Phys. **2003**, *204*, F69.

Oral presentations

I. Berndt, J. S. Pedersen, W. Richtering
A Small-Angle Neutron Scattering Study of Temperature-Responsive Core-Shell Microgels
42nd Meeting of the German Colloid Society, September **2005**, Aachen.

I. Berndt, J. S. Pedersen, W. Richtering
Strukturuntersuchungen an thermosensitiven Kern-Schale-Mikrogelen
1. Zsigmondy Colloquium of the German Colloid Society, April **2004**, Mainz.

I. Berndt, W. Richtering
Thermosensitive Kern-Schale-Mikrogele
Forschungsseminar "Neue Materialien", November **2003**, University of Rostock.

I. Berndt, W. Richtering
Thermosensitive Microgels
6th European School on "Scattering Methods Applied to Soft Condensed Matter", May **2002**, Bombannes, France.

Poster presentations

T. Sobisch, D. Lerche, I. Berndt, W. Richtering
Characterization of thermosensitive PNIPAM microgels by analytical centrifugation
42nd Meeting of the German Colloid Society, September **2005**, Aachen.

I. Berndt, J. S. Pedersen, W. Richtering
Strukturuntersuchungen an thermosensitiven Kern-Schale-Mikrogelen
12th Ostwald Colloquium, March **2004**, Kiel.

I. Berndt, J. S. Pedersen, W. Richtering
Structural Investigation of Thermoresponsive Core-Shell Microgel Particles
Hasylab User Meeting, January **2004**, Hamburg.

M. Stieger, I. Berndt, N. Greinert, W. Richtering, J. S. Pedersen, P. Lindner
Temperature-Sensitive Microgel Suspensions: Smart Materials and Push Me-Pull You Systems
77th American Chemical Society: Colloid and Surface Science Symposium, June **2003**, Atlanta, Georgia, USA.

M. Stieger, I. Berndt, N. Greinert, W. Richtering, J. S. Pedersen, P. Lindner
Temperature-Sensitive Microgel Suspensions: Smart Materials and Push Me-Pull You Systems
Bunsentagung, May **2003**, Kiel.

I. Berndt, W. Richtering
Thermosensitive Kern-Schale-Mikrogele
7. Nachwuchstage der Kolloid- und Grenzflächenforschung der Kolloidgesellschaft e.V., April **2003**, Heidelberg.

I. Berndt, W. Richtering
Thermosensitive Kern-Schale Mikrogele
6. Nachwuchstage der Kolloid- und Grenzflächenforschung der Kolloidgesellschaft e.V., March **2002**, Berlin.

Acknowledgements

First of all I would like to express my gratitude to my supervisor Prof. Dr. Walter Richtering for the opportunity to carry out this work in his research group, his support, advice, and patience throughout this work. He was always open for discussions and new ideas and allowed me great freedom in my research. It was an exciting pleasure to work for him who is so passionate and enthusiastic about his projects.

I would like to thank Prof. Dr. Jan Skov Pedersen from the University of Århus, Denmark. He was an important member of my supervisory panel and spent a lot of time and work with the development of the core-shell form factor model. It was always a pleasure to visit Århus for fruitful and enjoyable discussions.

I thank Prof. Dr. Regine von Klitzing for becoming the co-referee of my work and her hospitable permission to be a guest in her group and to occupy the rooms in the last months of my work.

Further I would like to express special thanks to all my colleagues at the University of Kiel and at the RWTH Aachen. In detail I want to say "Thank you!" to:

• Markus and Stacy. Markus introduced me to the world of microgels and I respect his reliability, competence, and patience in many situations. I thank Stacy for encouraging me to look at things from a different point of view.

• Florian for historical, cultural, and intellectual contributions. The evening with the "Mäusesheriff" was an unforgettable experience.

• Bernd and Edda. I don't thank Edda for coffee and cookies ;-) but for her friendly and social nature. I thank Bernd for his tireless support during long nights at the D11 and computational discussions.

• Franziska for her readiness to help and sympathy not only in the last days of my work.

• Christof as a gifted chemist for discussion, sushi and exciting experiments with dangerous hazards.

• Matthias Soddemann for contact and job offers.

• The members of the Lagaly group, especially Lars, Matthias, Tanja, Gaby and Klaus.

• Frank and Bernhard as temporary office mates.

• The technical staff from the mechanical and electronic workshop.

I also want to thank the local contact team at the D11 Peter Linder, Ralf Schweins and David Boyer for their assistance during the neutron scattering experiments even at nights and weekends.

I am grateful to Prof. Dr. Crisan Popescu and Prof. Dr. Franz-Josef Wortmann from the Deutschen Wollforschungsinstitut in Aachen for their enthusiastic involvement in the DSC data evaluation.

I express my thanks to Prof. Christoph Schick and Dr. Heiko Huth from the Institute of Physics, University of Rostock. They allowed me to carry out the DSC experiments on their machines and supported me during the experiments.

Further I am deeply indebted to many people and friends who are not directly related to this work: Mahatma, Olli, Iris, Jacqueline, Michael, Everall, Che, the sailing team, the Mensa team, Garip´s, Lemmy and August Ernst from Bad Oldesloe.

I am thankful to Uschi and Dieter Rietfort for oriental hospitality in Aachen and the Scary Fives for recovery at excursions and the beautiful presents.

I thank Swantje for everything she has done for me in this period of my life. The times have been difficult and exhausting in the last months, but your love and understanding made me going on. I thank you for every single day!

Last, but certainly not least I, am very grateful to my parents and family, especially my brother Heiko and my uncle Karl and aunt Heinke, for everything they have done for me during all my life.
I dedicate this work to my parents Antje and Hartmut. Their love and vitality are my life long guidance.

Table of Contents

1 Introduction and Motivation

1.1 Hydrogels, Microgels, and "Smart Materials"

Hydrogels are defined as cross-linked polymeric networks that are able to swell in water. The solvent uptake can be up to thousands of times of the weight in the dry state.[1,2]

Hydrogels can be classified according to their chemical and physical properties.[3] The two main categories based on the nature of the cross-linking are physical and chemical cross-linked gels. The first category defines polymeric networks that are bound together by entanglements of polymer chains or other non-covalent attractive interactions between the polymer chains, such as hydrogen bondings, chelating ions, or electrostatic interactions.[4,5,6] Physically cross-linked gels can be dissolved under conditions that weaken the attractive forces between the polymer chains.

The second class of hydrogels are chemically cross-linked gels which exhibit improved structural stability compared to the physically cross-linked analogues. Covalent bonds between the polymer chains are formed throughout the entire network and lead to permanent endurance with respect to the network structure. Commonly, the materials are prepared by co-polymerization of a mono-functional monomer with a cross-linking monomer which has at least two functional groups that are able to polymerize.

Apart from the structural classification, hydrogels can be further distinguished by their responsive behaviour to changes in their environment. Non-responsive gels simply swell upon the uptake of water. In contrast responsive gels display structural changes as a response to certain stimuli, such as temperature,[7] pH,[8] radiation,[9] solvent composition,[10] or salt concentration[11,12] due to functional moieties incorporated in the polymer network. The response arises from competing mechanisms of solvation within the polymer network. In a swollen polymer network, an external stimulus can lead to increased attractive polymer-polymer interactions, which then dominate the polymer-solvent interactions. This causes aggregation of the polymer chains in the network and shrinkage of the network by expelling

the solvent. Hence the dimensions of the entire polymer network are reduced. Due to their ability to react to environmental changes stimuli-responsive hydrogels are often referred to as "smart" or "intelligent" materials.

The size of a hydrogel needs to be mentioned together with its stimuli-sensitivity. So-called macrogels can be prepared on length scales which range typically from millimeters to centimeters. The sizes of microgels on the other hand are on colloidal length scales. Typical dimensions range from a few tens to several hundreds of nanometers. The dimensions affect the time scales in which a responsive hydrogel can react to environmental changes. The reaction time roughly scales with the square of the one-dimensional length scale,[13] which is for spherical particles the surface to volume ratio. Thus the use of macrogels for applications requiring short response times is limited due to their slow reaction often in the order of 1 to 100 seconds.

Although micro- and macrogels may consist of identical monomers and cross-linkers, they differ in their internal structure according to the preparation procedure. Macrogels are prepared under bulk conditions leading to rather homogeneous cross-linked structures. Microgels are usually prepared by emulsion co-polymerization and different steps can be distinguished during the polymerization including nucleation, chain growth and aggregation resulting in a non-homogeneous distribution of polymer chains and cross-links throughout the network.[14]

One of the most widely investigated stimuli-responsive polymers is poly-*N*-isopropylacrylamide (PNIPAM) due to its interesting thermal behaviour in aqueous solution. The entropy driven demixing of linear PNIPAM chains upon heating takes place by a structural "coil-to-globule" transition at a temperature that is higher than the lower critical solution temperature (LCST) of 31-32 °C.[15] Chemically cross-linked PNIPAM microgels exhibit a volume phase transition (VPT) at a temperature slightly higher than the LCST at 34 °C due to the presence of more hydrophilic cross-links in the network (Fig. 1-1).

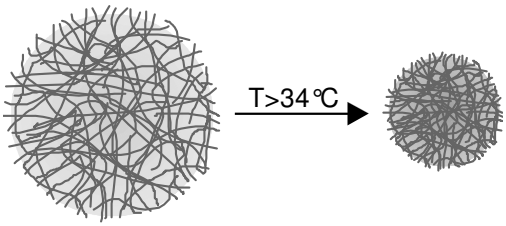

Fig. 1-1: Volume phase transition of a PNIPAM microgel in aqueous solution at a temperature higher than the LCST.

PNIPAM microgels are usually prepared by precipitation polymerization in aqueous solution using the cross-linker *N*,*N´*-methylenbisacrylamide (BIS) as depicted in Fig. 1-2. A surfactant, often sodium dodecylsulfate (SDS) is added to stabilize the dispersion and to control the particle size. The NIPAM monomer is soluble in water at elevated temperatures. When the reaction is started with a radical initiator, usually potassium peroxodisulfate (KPS) that decomposes at elevated temperatures, the monomers grow to oligomers, which become insoluble in water at a certain chain length. The growing oligomers are colloidally instable and aggregate forming precursors to which further oligoradicals attach until the monomer is exhausted. The synthesis of PNIPAM microgels proceeds typically at 70 °C, which is well above the LCST. Therefore the microgels are formed in the collapsed state.

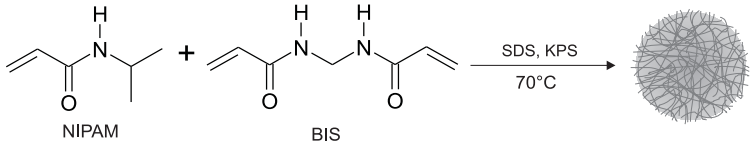

Fig. 1-2: Synthesis scheme for PNIPAM microgels. The NIPAM monomer polymerizes in the presence of the cross-linker BIS resulting in the formation of microgel particles.

Various applications of sensitive microgels are reported such as in drug delivery, biosensors, catalysis and chemical separation.[16] Many applications make use of the fact that microgels expel water from the inside when the LCST is approached. The collapsed or dried particles can be pre-loaded with a solvent containing an active agent which is later squeezed out when

the environmental conditions change and the microgel collapses. A similar mechanism can be applied to separation issues.

The versatility of these materials can be enhanced even further by the incorporation of sensitivity to a second stimulus into the microgel network. Co-polymerization of a temperature sensitive monomer with a pH-sensitive monomer, as for example acrylic acid (AAc), leads to microgel particles which are sensitive to both temperature and pH changes.[17] The incorporation of other suitable monomers can lead to sensitivity towards radiation, solvent composition, or ionic strength. The random incorporation of functionalized co-monomers exhibits the disadvantage that the sensitivities to basically orthogonal stimuli (e.g. pH and temperature) compete and partially compensate when the segments with different sensitivity interfere due to close neighboring. In the above-mentioned PNIPAM-*co*-AAc microgel the electrostatic repulsions between charged carboxylic groups rival with the attractive forces between the hydrophobic polymer chains when the environmental conditions are such that the temperature is above the LCST of PNIPAM and the pH is above the pK_s of acrylic acid. The balance between attractive and repulsive interactions depends on the molecular composition of the polymer, which cannot be controlled in a random co-polymerization.

This drawback of co-polymerization can be overcome if regions of different sensitivity are spatially separated in the macromolecule. This spatial separation demands for a superior polymer structure on a length scale of at least several nanometers. Due to the spherical shape of the microgels, core-shell structures are well qualified for such an advanced macromolecular architecture.

Jones and Lyon have been the first who reported on microgels with a core-shell structure.[17] They investigated PNIPAM based microgels where either the core or the shell were co-polymerized with acrylic acid, thus introducing a pH sensitivity to these regions of the microgel. These particles exhibit very interesting properties. The incorporated acrylic acid shifted the LCST to higher temperatures such that a temperature dependent multi-step volume phase transition appears at a high pH. Core and shell networks of these particles interpenetrate in a thin layer at the core-shell interface which acts as a mechanical connection between core and shell and influences the behaviour of the entire particle.

1.2 Temperature-Sensitive Core-Shell Microgels

The approach used in this work is based on the combination of thermosensitive polymers with different LCSTs. To the best of our knowledge, only few studies have been reported in the literature using microgels that are sensitive to different quantities of a single stimulus. In contrast to multi-stimuli responsive microgels with orthogonal stimuli, these particles are very promising candidates for the application in environments where the sensitivity to such stimuli is limited due to interference. This work focuses on structural changes induced by temperature as temperature variations play an important role in every-day life. Furthermore, temperature changes are physical stimuli that are easily utilized by external controls. In comparison to chemical stimuli they exhibit the great advantage that they are reversible without any effects on the material composition.

It has been mentioned before that co-polymerization of monomers with either hydrophilic or hydrophobic character can shift the LCST towards higher or lower tempertures.[15] However, this method suffers from two major drawbacks. First, the LCST can only be shifted in a limited temperature range without overweighting the native properties of the polymer. The second disadvantage is that such modified polymers reveal broad and undefined transitions.

Taking all this into account in conjunction with the benefits of spatially separated differently sensitive domains, there is hope that a combination of two native thermoresponsive polymers with different LCSTs in core-shell morphology might lead to the desired properties.

The core-shell microgels in this work are based on PNIPAM and poly-*N*-isopropyl*meth*acrylamide (PNIPMAM). PNIPMAM has been chosen for several reasons: The LCST of PNIPMAM is 44 °C in aqueous media and PNIPMAM reveals chemical similarity to PNIPAM, as its molecular structure differs from PNIPAM only in an additional methyl group in the polymer backbone. The structures of PNIPAM and PNIPMAM repeating units are shown in Fig. 1-3.

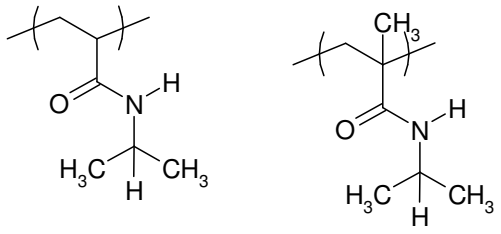

poly-*N*-isopropylacrylamide
LCST=34°C

poly-*N*-isopropylmethacrylamide
LCST=44°C

Fig. 1-3: Repeat units of PNIPAM and PNIPMAM.

The difference in the LCSTs of PNIPAM and PNIPMAM is large enough to observe distinct transitions, which do not overlap. On the other hand, both transitions can be observed under gentle experimental conditions. Furthermore, the combination of these two polymers is very interesting for biomedical applications since the human body temperature is exactly in the middle of the two LCSTs.

One might expect the LCST of PNIPMAM to be lower than that of PNIPAM due to the presence of the hydrophobic methyl group in the backbone,[18] however, the demixing temperature of PNIPMAM is higher. The explanation for this can be found in conformational reasons: The methyl group induces a sterical hindrance such that the hydrophobic groups cannot approach in an optimal orientation.[19]

Core-shell microgels composed of these temperature sensitive polymers are expected to exhibit two volume phase transitions at temperatures assigned to the LCSTs of core and shell, respectively. Increasing the temperature from below the PNIPAM core LCST to a temperature between the LCSTs of the two polymers, the solvent quality of water will change from good to poor for the core, while still being good for the PNIPMAM shell polymer. The polymer-polymer interaction will gain weight for the chains in the core and it will collapse. When the temperature is further increased above the shell's LCST, the shell will collapse in a second step (Fig. 1-4).

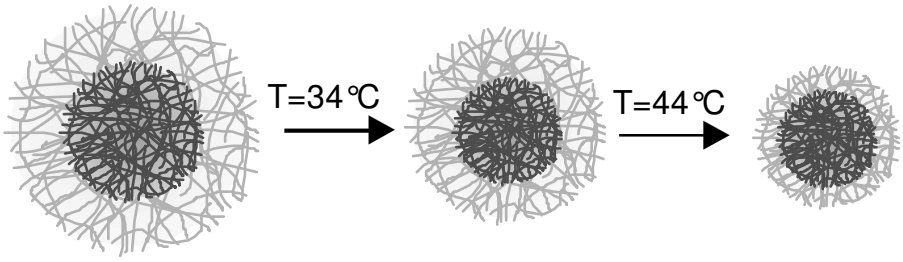

Fig. 1-4: Two-step particle collapse of a PNIPAM core-PNIPMAM shell microgel at temperatures assigned to the LCST of core and shell.

In general, doubly temperature-sensitive core-shell microgels enhance the versatility of the widely used PNIPAM microgels.

Although the volume phase transition is fully reversible, PNIPAM microgels aggregate on macroscopic scales when the temperature is increased above the LCST in a concentrated dispersion. The redispergation of these aggregates requires some effort in time or even mechanical work. The presence of a shell with a LCST higher than that of the core leads to colloidally stable dispersions above the core's LCST as depicted in Fig. 1-5.

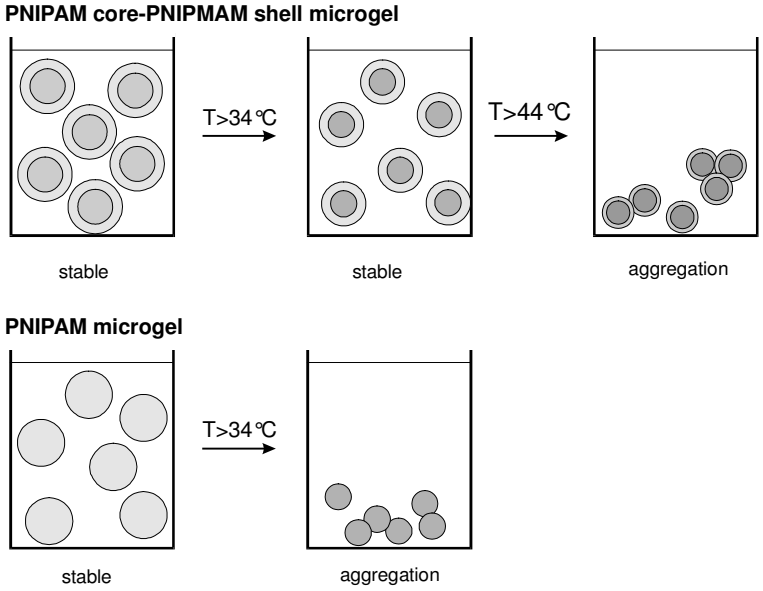

Fig. 1-5: Colloidal stability of PNIPAM and PNIPAM core-PNIPMAM shell microgels in aqueous dispersion at different temperatures.

1.3 Aim of this Work

The aim of this work was to investigate the structure of doubly temperature-sensitive core-shell microgels. The influence of the polymer network morphology and the external temperature stimulus on the internal and overall particle structure should be explored employing light and neutron scattering, data modelling and thermal analysis.
The work subdivides into five parts:

I) A synthesis route and purification method had to be developed to prepare core-shell microgels composed of PNIPAM and PNIPMAM with well-defined compositions. A two-steep seed-and-feed polymerization with intermediate purification steps of the products was to be employed in order to remove by-products of the polymerization reactions and to control the composition.
In order to investigate the influence of the shell composition on the thermal response of the PNIPAM core-PNIPMAM shell particles, the amounts of monomer and cross-linker present during the shell polymerization were varied.

II) In a previous work done in our group a form factor model was developed to describe small-angle neutron scattering (SANS) profiles of PNIPAM microgel particles.[20] The model allowed for obtaining real space information on the particle structure by calculating radial volume fraction profiles.
In order to obtain structural information on the core-shell microgels a new form factor model had to be developed accounting for the superior architecture of core-shell microgels. Special interest needed to be given to the shape of the interfaces between core and shell and at the particle surface.

III) Once a form factor model had been derived to describe the internal structure of the core-shell microgels, it was employed to analyse SANS data of various samples taken at temperatures below the PNIPAM core LCST (25 °C), in between the core and shell LCST (39 °C), and above the shell's LCST (50 °C).
One whould expect that the swelling of core and shell mutually influence at the different temperatures corresponding to the different swelling states. The mutual influence of core and shell should be regarded as opposing forces at the core-shell interface. In order to quantify the

opposing forces, two series of core-shell microgels were planned to be investigated, where the shell thickness, i.e., the shell/core mass ratio, and the shell cross-linker content were to be varied.
The radial density profiles obtained from the data analysis were supposed to give a clearer picture of the internal structure of these particles and were to be compared to results from dynamic light scattering (DLS).

IV) An "inverse" core-shell system was to be prepared and investigated by means of SANS and DLS.
This core-shell system consists of a PNIPAM core and shell of PNIPMAM. In comparison to the other core-shell microgels, the composition of these particles is such that the core should be swollen and the shell still be collapsed at a temperature between the LCSTs.
A similar situation with opposing forces between the swollen core and the collapsed shell at temperatures between the LCSTs should be observed as for the PNIPAM core-PNIPMAM shell particles. If the collapsed PNIPAM shell could restrict the core swelling, this should be directly observable by DLS. Exploring the internal structure, the core-shell form factor would probably need to be modified due to peculiarities of these particles.

V) In the last part of this work the swelling and the forces occurring at the core-shell interface were to be examined by means of thermal analysis (DSC).
In principle these data should reveal two distinct transitions according to the LCSTs of the two components and correlate with the core/shell mass composition. If core and shell swelling mutually influence each other and the swollen shell exerts an expanding force on the collapsed core at temperatures between the LCSTs, this should affect both the transition temperatures as well as the transition heats.
These data were to be compared to SANS results and should reveal a very clear picture of the internal structure of the doubly temperature-sensitive core-shell microgel particles.

2 Doubly Temperature Sensitive Core-Shell Microgels

Abstract. We report on synthesis and characterisation of doubly temperature sensitive core-shell microgels. These core-shell microgels are composed of a core of chemically cross-linked poly-(*N*-isopropylacrylamide) (PNIPAM) and a shell of cross-linked poly-(*N*-isopropylmethacrylamide) (PNIPMAM). PNIPAM exhibits in water a lower critical solution temperature (LCST) of ca. 34 °C, the LCST of PNIPMAM is ca. 45 °C. Solution properties were investigated by means of dynamic light scattering (DLS), optical transmission, and small-angle neutron scattering (SANS). Core-shell microgels of this composition display a temperature dependent two-step shrinking behavior. The influences of the content of the cross-linking agent *N*,*N*'-methylenbisacrylamide (BIS) and of the thickness of the PNIPMAM shell on the thermosensitive response of the PNIPAM/PNIPMAM core-shell microgels were investigated. Core-shell microgels with a thick shell do not show a size transition at the PNIPAM LCST anymore. The volume transition is adjustable by varying the cross-link density of the shell. The swelling behaviour of the core-shell microgels is compared to that of pure PNIPAM and PNIPMAM. Additionally, an inverse system consisting of a PNIPMAM core and a PNIPAM shell was prepared and investigated by DLS.

2.1 Introduction

Environmentally sensitive microgels attract attention because of their versatility to many fields as, e.g., drug delivery,[1] catalysts[2] and chemical separation. The probably most studied responsive polymer is cross-linked poly-(N-isopropylacrylamide) (PNIPAM).[3,4,5]

Aqueous PNIPAM solutions display phase separation upon heating with a lower critical solution temperature LCST of ca. 34 °C. Microgels are internally cross-linked spherical particles swollen by the solvent with a typical size in the range of 50-1000 nm. PNIPAM microgels shrink upon heating with a sharp transition at the LCST. Since monodisperse PNIPAM microgels are readily accessible via emulsion polymerization, they can be

considered as model systems for colloid science [6] and the influence of various parameters, e.g. cross-link density,[7] co-monomers,[8,9] solvent composition,[10] salt effects,[11] etc. on the particles´ properties has been investigated.

Recently Lyon and co-workers demonstrated that the versatility can be enhanced when core-shell microgels with different properties of core and shell, respectively, are prepared.[12,13,14] They synthesized PNIPAM core-shell microgels where either core or shell consisted of a copolymer of PNIPAM with acrylic acid (AAc). Incorporation of AAc shifts the LCST to higher temperatures and furthermore introduces a pH-sensitivity. These core-shell microgels are multi-responsive.

In this contribution we report on a different approach, namely the preparation of core-shell microgels based on PNIPAM as core and poly-(*N*-isopropyl*meth*acrylamide) (PNIPMAM) as shell polymer, the LCST of which is ca. 45 °C. An inverse system with a PNIPMAM core and a PNIPAM shell was also prepared, which exhibits interesting features. Pure PNIPMAM microgels behave similar to PNIPAM microgels. The influence of cross-link density on the thermosensitivity of PNIPMAM was investigated in detail by Duracher and co-workers.[15,16]

The enhanced variety of material properties enables advances in pharmaceutical and cosmetic applications, filters and immobilisation. The objective of our study was to explore the possibility to control the temperature dependent size and colloidal stability of core-shell microgels via the variation of thickness and cross-link density of the PNIPMAM shell.

2.2 Experimental Section

Materials. NIPAM and NIPMAM monomers and BIS were purchased from Aldrich. NIPMAM monomer was recrystallized from cyclohexane. Sodium dodecylsulfate (SDS) and the initiator potassium peroxodisulfate (KPS) were purchased from Merck Eurolab and used as received. Water for all purposes was ion-exchanged to a resistance of 18.2 MΩ/cm (Milli-Q) and filtered through a 0.2 µm filter.

PNIPAM core synthesis. PNIPAM core microgel particles were prepared via free radical emulsion polymerisation as reported previously. Polymerisation was performed in a 1 L reaction vessel equipped with a mechanical stirrer, reflux condenser, thermometer and gas inlet. 11.80 g NIPAM, 0.225 g BIS and 0.225 g SDS were dissolved in 0.6 L water at 70 °C and nitrogen purged for at least 1 h. Polymerization was initiated with 0.45 g KPS dissolved in 5 ml water and carried out for 6 h under nitrogen stream and constant stirring at 400 rpm.

The dispersion was passed through glass wool in order to remove particulate matter and dialyzed against deionised water for 30 days to a conductance < 0.01 mS. For details see ref.[6]
PNIPMAM shell synthesis. PNIPMAM shell synthesis was performed using core particles as nuclei for subsequent emulsion polymerization. A core solution was heated to 70 °C and purged with nitrogen. A separately prepared mixture of NIPMAM monomer, BIS and SDS was added after 1 h and the mixture was purged with nitrogen for 1 h. Shell polymerization was initiated with KPS solved in 5 ml of degassed water, for details see Tab. 2-1. The synthesis proceeded for 6 h at constant stirring at 200 rpm. The product was passed through glass wool and dialyzed in the same way as the core particles.

Tab. 2-1: Experimental conditions for core-shell microgel syntheses.

sample	core solution	shell solution				
	PNIPAM [g/mL]	NIPMAM [g]	BIS [g]	KPS [g]	SDS [g]	water [mL]
CS005	0.0238	1.19	0.143	0.023	0.0103	50
CS006	0.0119	1.19	0.143	0.023	0.0103	50
CS008	0.0025	1.19	0.143	0.023	0.0103	50
CS009	0.0238	0.571	0.0686	0.0011	0.0048	30
CS010	0.0238	0.476	0.0303	0.0092	0.0040	25
CS011	0.0238	0.476	0.0178	0.0092	0.0041	25
INV001	0.0199 (PNIPMAM)	0.493 (NIPAM)	0.0353	0.0124	0.0052	25

Dynamic light scattering. Particle sizes were determined by dynamic light scattering (DLS). Light scattering experiments on the highly diluted samples (Milli-Q water) were carried with an ALV goniometer equipped with an avalanche photodiode. The samples were allowed to equilibrate for 20 min at each temperature. Temperature programs have been run both directions, increasing and decreasing temperature. Temperature dependent size changes are completely reversible, so only data of heating direction will be shown. Scattered light was detected at 90 ° with an integration time of 120 s and computed with a digital ALV 5000E autocorrelator using ALV Software (version 5.3.2). Particle sizes were calculated by cumulant fits. In other experiments particles tend to form colloidal crystals, polydispersity can be assumed to be less than 10 %.

Optical transmission. A METTLER Phototrode DP550 (λ=550 nm) was used for transmission measurements on samples of ca. 0.5 wt%. Output voltage was received by a common multimeter (METEX 3640D) and transmitted to a personal computer. Transmission was measured at temperature increments of 0.5 °C with equilibration times of 2 min. Transmission data were normalized to initial transmission at T=25 °C.

Small angle neutron scattering. SANS experiments were carried out at the Institut Laue-Langevin, Grenoble, France, on the D11 beam line. The data were collected using a two dimensional detector with detector settings at 2, 10, 36 m to cover a maximum q-range of $0.002<Å^{-1}<0.15$ at 6 Å neutron wave length. Data were background corrected and water normalized with ILL provided software GRASP (version 3.25).

2.3 Results

Two series of core-shell microgels were synthesized using the same PNIPAM microgel as core. One series of core-shell microgels with different PNIPMAM shell thickness was prepared. In the second series the cross-link density in the shell was modified. Since both PNIPAM and PNIPMAM are thermosensitive polymers a general size decrease with temperature is observed. However, the characteristic swelling behaviour depends on the thickness and the cross-link density of the shell as will be shown below.

Fig. 2-1 shows the temperature dependent hydrodynamic radius R_h of four core-shell microgels with different shell thickness of 14, 19, 28 and 41 nm as well as of the PNIPAM core. The cross-linker content of the shell was 9.0 mol% BIS.

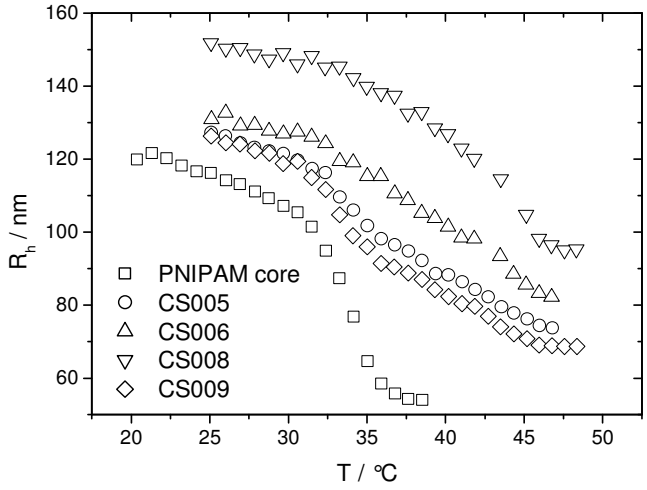

Fig. 2-1: Hydrodynamic radius vs. temperature of core-shell microgels with different shell thickness at a shell cross-linker content of 9.0 mol%. The parent PNIPAM core is shown for comparison.

Two features are noticed. i) The particle size increased with increased amount of PNIPMAM shell in both the collapsed and swollen state. Taking into account that the syntheses were performed at 70 °C, where the PNIPAM core is collapsed, we find a linear growth of shell volume with the amount of shell monomer present during synthesis. ii) The temperature sensitivity strongly depends on the thickness of the PNIPMAM shell. Samples CS005 and CS009 that have a low PNIPMAM content show two regions. Up to 35 °C they display a sharp decrease in particle size corresponding to the PNIPAM core collapse. A less pronounced decrease at temperatures to 45 °C indicates the PNIPMAM shell collapse. At high PNIPMAM (CS008) content, i.e. with a thick shell, the first transition is no longer observed and the core-shell particle behaves similar to a pure PNIPMAM microgel.

Similar behavior was observed when the cross-link density in the PNIPMAM shell was varied. Cross-linker contents of 3.0, 5.0 and 9.0 mol% were employed. Fig. 2-2 demonstrates the influence of the shell cross-linker content on the core-shell particles swelling behavior. Sample CS009 with 9.0 mol% cross-linker was already shown in Fig. 2-1. Shell thicknesses at 47 °C are between 9-15 nm.

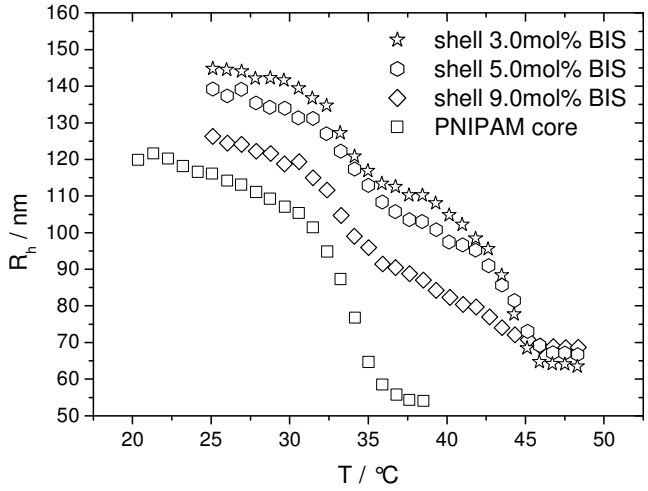

Fig. 2-2: Hydrodynamic radius vs. temperature of core-shell microgels with different shell cross-linker content. The parent PNIPAM core is included again

These samples reveal two transitions with a pronounced intermediate plateau. The particle size in the totally collapsed state at 48 °C is nearly identical for the three samples. The particles swell with decreasing temperature, and lower shell cross-link density leads to larger hydrodynamic radii.

Transmission measurements were carried out complementary to dynamic light scattering in order to characterize the samples at concentrations of ca. 0.5 wt%. Fig. 2-3 shows transmission data of core-shell microgels with different shell thickness.

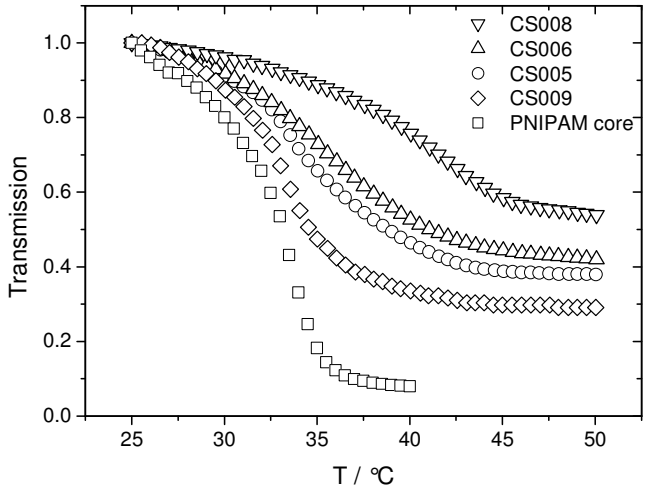

Fig. 2-3: Optical transmission data of core-shell microgels with varying shell thickness and PNIPAM core.

The optical transmission of the core-shell systems at 25 °C increased with increasing shell thickness. Fig. 2-3 the relative optical transmission is shown, thus the relative change in transmission was smaller with increasing shell thickness.

The general trend is very similar to what was found in DLS for highly diluted samples. The behavior changes from PNIPAM-like to PNIPMAM-like with increasing shell thickness. However, a smooth transition is observed in all cases, whereas the hydrodynamic radius revealed a two-step process for the same samples (see Fig. 2-1).

In Fig. 2-4 transmission data for core-shell microgels with varied shell cross-linker contents are shown. The two-step process is now observable with the samples that have cross-link density of 3.0 and 5.0 mol%, respectively.

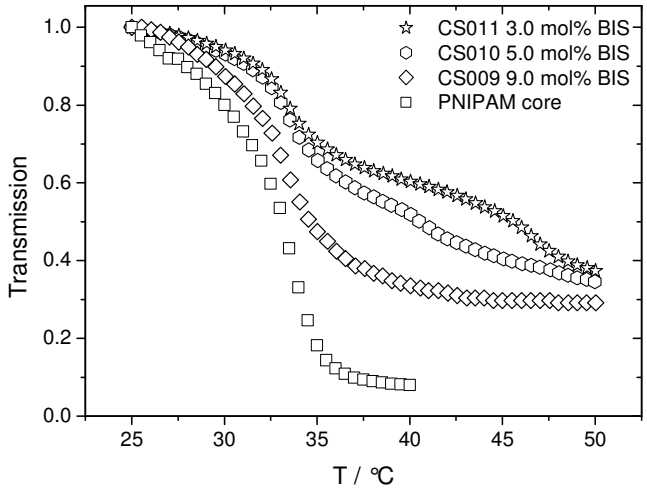

Fig. 2-4: Transmission data of core-shell microgels with shell cross liner content varied from 3.0 to 9.0 mol%.

2.4 Discussion

The results clearly show that the swelling behavior of thermosensitive core-shell microgels can be controlled by mass and cross-link density of the PNIPMAM shell.

A swelling ratio $\alpha = \left(\frac{R_h(T)}{R_{h,T>48°}} \right)^3$ can be defined where the temperature dependent particle size is normalized by the value above 48 °C, i.e. in the collapsed state. Fig. 2-5 and Fig. 2-6 show the swelling ratios for the two series of varied shell thickness and varied shell cross-link content, respectively.

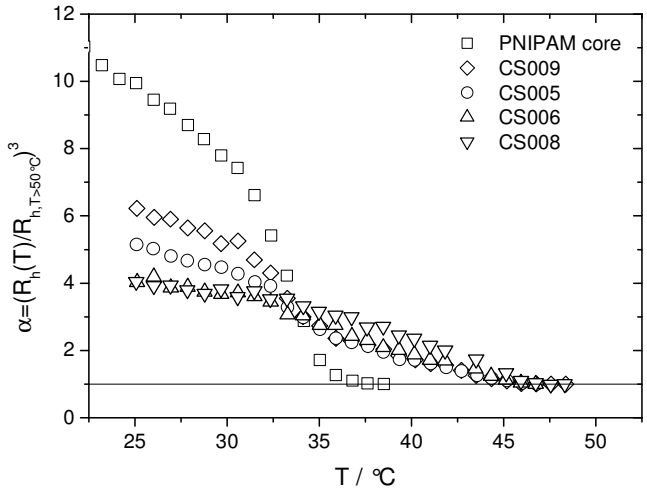

Fig. 2-5: Temperature-dependent swelling ratios α of core-shell microgels with different shell thickness. The PNIPAM core is shown for comparison.

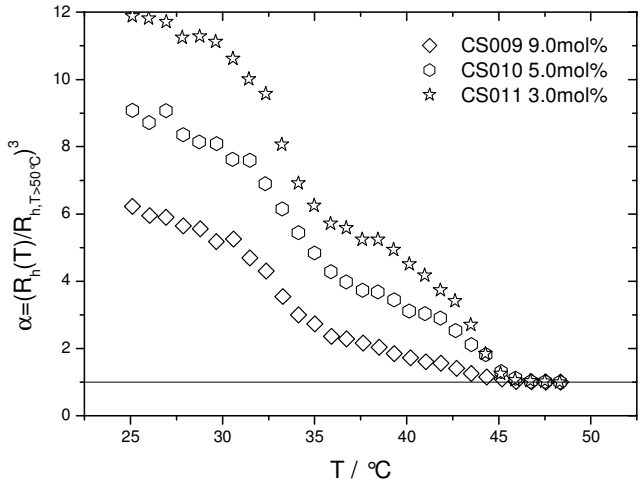

Fig. 2-6: Swelling ratios α of core-shell microgels with varied shell cross-link density.

Significant differences between the samples shown in Fig. 2-5 are found only at temperatures below the core-LCST, i.e. in the good solvent limit, when both the shell and core are strongly

swollen. A smaller shell thickness leads to a higher swelling ratio of the entire particle. However, at temperatures above the core LCST but below the shell LCST, i.e. 34-44 °C, differences are hardly observed. A series of pure PNIPMAM microgels was prepared with same cross-link densities as were applied in core-shell particles and investigated for a quantitative comparison with PNIPAM core and core-shell microgels. Fig. 2-7 shows swelling ratios of pure PNIPMAM microgels with 3.0, 5.0 and 9.0 mol% cross-linker content.

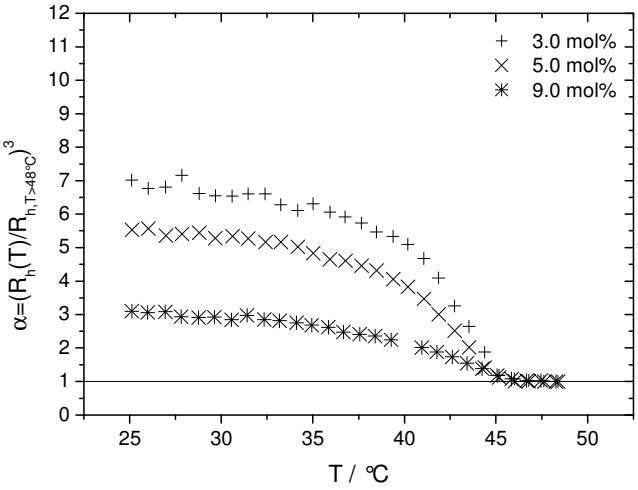

Fig. 2-7: Swelling ratios of pure PNIPMAM microgels with same cross-link densities as employed in core-shell particles.

Swelling ratios of 3 to 7 at 25 °C are found for pure PNIPMAM microgels. The swelling ratio increases with decreased cross-link density as is known for PNIPAM microgels.[17] However, pure PNIPMAM particles swell less thancompared to pure PNIPAM particles with the same cross-linker content.[18] Comparing the swelling ratios of core-shell particles with different shell thickness with the 9.0 mol% cross-linked PNIPMAM and the parent PNIPAM core at 25 °C, we find values between these boundaries. The swelling ratio is bigger than the swelling ratio of a pure PNIPMAM microgel with same cross-linker content, even for particles with a thick shell, i.e. CS008. This effect is due to the core contribution to the entire particle volume. When the shell thickness is decreased, the swelling ratios at temperatures below 34 °C

increase. A growing influence of the core to the particles swelling behavior is observed; below 34 °C the expanding core presses the shell outwards. But this expansion is limited by a mechanical stress in the shell. So the swelling ratio of the parent pure PNIPAM cannot be reached. The balance between expansion of the core and mechanical stress in the shell is an effect of the shell thickness. When a specific shell thickness is exceeded, the influence of the core is not longer observable.

Fig. 2-6 shows swelling ratios of core-shell microgels that have different shell cross-link densities, and the expected behavior is found. At temperatures between 34 and 44 °C the shell swells depending on the cross-link density. Below 34 °C the core swells and presses the shell outwards.

For a more detailed discussion we will employ a simple model to calculate a particle size at 37.5 °C (where the intermediate plateau is found) from particle sizes at 48 °C and the known swelling ratios of the shell. Synthesis was performed at 70 °C where water is a poor solvent for both PNIPAM and PNIPMAM. Hence, the collapsed state should be taken as the reference state for the particles (index 0). The difference of the particle sizes at a temperature above the shell LCST is $R_{CS}^0 - R_C^0 = \Delta R$, where R_{CS}^0 and R_C^0 are the radii of the core-shell microgel and the core in the reference state. From ΔR we can calculate the shell volume V_s^0 in the collapsed state. A shell volume for any temperature between 34 and 44 °C can now be calculated by multiplying the shell volume V_s^0 by the swelling ratio $\alpha(T)$ of a pure PNIPMAM microgel with the same cross-link density: $V_S(T) = \alpha(T) \cdot V_S^0$. The particle radius can be calculated from the sum of core and shell volume: $R_h(T) = \left(\frac{3 \cdot (V_C^0 + V_S(T))}{4\pi} \right)^{\frac{1}{3}}$ and the results are shown in Fig. 2-8.

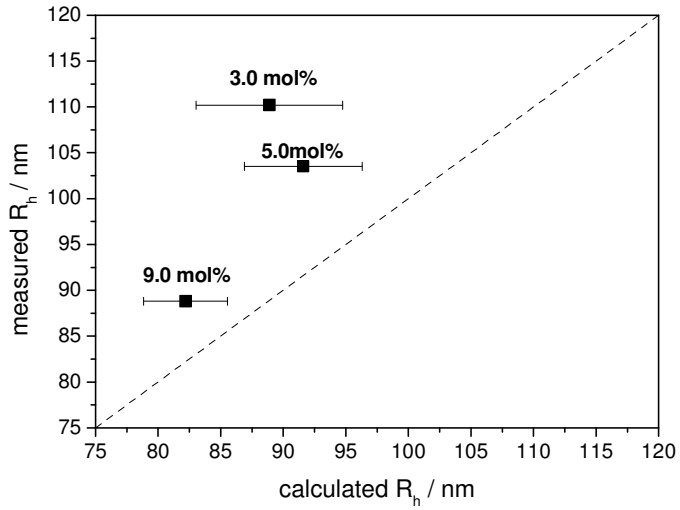

Fig. 2-8: Comparison of calculated and measured particle sizes of core-shell microgels at 37.5 °C with different shell cross-link densities.

In all cases the measured particle size is found to be larger than the calculated radius. That demonstrates that both core and shell do not swell independently, but influence each other.

Ballauff and co-workers have investigated core-shell particles with a rigid sphere polystyrene core and a thermosensitive PNIPAM shell.[19] Using SANS and SAXS techniques they could show that the swelling process is restricted due to the fixation of the network on the polystyrene surface. The network can only expand along the surface normal direction. Swelling in the two other directions is limited by spatial constraint. In our samples the shell is attached to a swellable network. We explain the bigger experimental radius that the shell avoids the constraint by widening the shell sphere. The core is collapsed but since it is only lightly cross-linked, the forces which would restrain the shell are weak. Thus the shell will mechanically expand the collapsed core. One could suspect that the core in those samples which have a thick PNIPMAM shell is almost fully expanded at temperatures above the PNIPAM LCST.

Preliminary small angle neutron scattering measurements on sample CS010 were performed at D11 instrument at the ILL, Grenoble. The concentration was 0.2 wt% in D_2O. In Fig. 2-9 SANS data for three different temperatures are shown. The sample was investigated at a temperature where both core and shell are swollen (32 °C), a temperature where the core is

expected to be collapsed (39 °C), and a temperature where both core and shell are collapsed (50 °C).

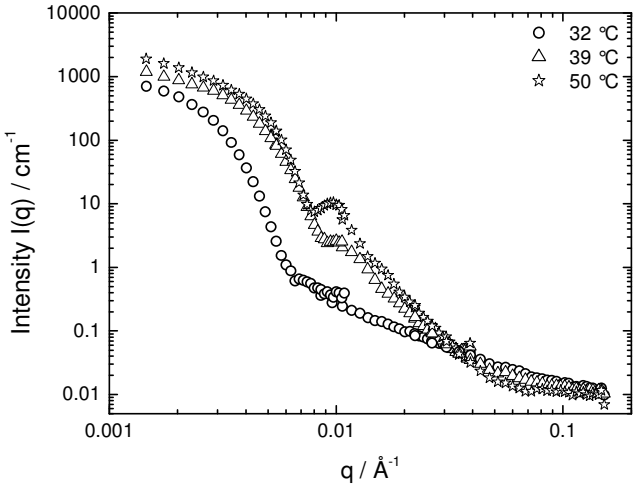

Fig. 2-9: Small-angle neutron scattering spectra of sample CS010 below core LCST (T=32 °C), between core and shell LCST (T=39 °C) and above shell LCST (T=50 °C). The form factor minimum shifts towards lower q with increasing temperature.

At 32 °C the scattering intensity at high q is found to be proportional to the scattering vector $q = |\vec{q}| = \frac{4\pi}{\lambda} \cdot \sin\left(\frac{\Theta}{2}\right)$ with $I(q) \propto q^{-1.33}$, almost the same scattering exponent was found for pure PNIPAM microgels by Kratz et al.[20] When the temperature is increased to 39 °C a particle form factor with a minimum at ~0.009 Å^{-1} is observable and the scattering exponent at high q is -3.2. For T=50 °C Porod-scattering with $I(q) \propto q^{-4.1}$ is found in the same manner as for pure PNIPAM microgels[21,22] which is characteristic for scattering of a phase separated structure with sharp interfaces. However, the form factor minimum shifts to lower q values with increasing temperature at which at first sight suggests an increasing particle size. This is contradictory to DLS data that unambiguously revealed that the hydrodynamic radius decreases with temperature. At 39 °C $I(q) \propto q^{-3.2}$ is observed in the high q regime and one can suppose that scattering is dominated by a partially collapsed core. This suggests that the

intensity minimum characterizes the core. At 50 °C the shell collapses as well and the apparent particle size increases as scattering occurs on the shell surface. So the minimum will shift towards lower *q*. This model suggests strong differences of local segment density in core and shell, respectively, at different temperatures. Thus a direct modelling of the SANS data should provide detailed information on segment densities, and therefore on the temperature dependent swelling of core and shell. Such data analysis is in progress and will be presented elsewhere.[23]

Finally, an inverse core-shell microgel (sample INV001) with a PNIPMAM core (7.0 mol% cross-linker) and a PNIPAM shell (5.0 mol% cross-linker) was prepared and investigated by DLS, Fig. 2-10 shows the temperature dependent hydrodynamic radius.

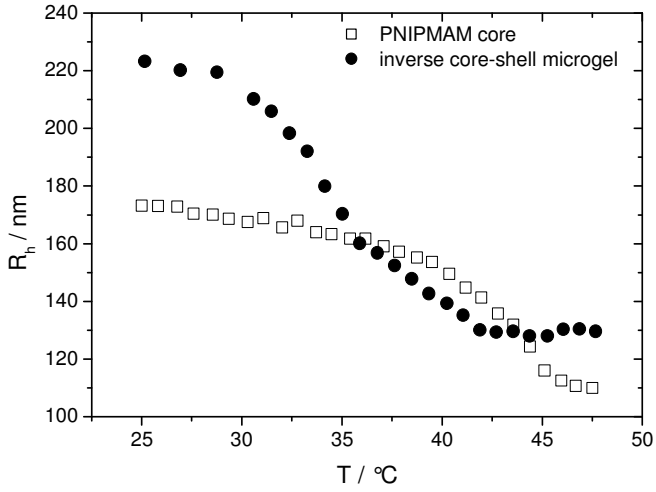

Fig. 2-10: Hydrodynamic radii vs. temperature of inverse core-shell microgel and parent PNIPMAM microgel.

The inverse system displays interesting features. In the collapsed state (where synthesis was performed) the radius of the inverse core-shell microgel is 19 nm bigger as compared to the PNIPMAM core. At intermediate temperatures of 34-44 °C, however, the hydrodynamic radius of the core-shell system is smaller than that of the core. Obviously the collapsed PNIPAM shell strongly restricts the swelling of the PNIPMAM core, so that the core cannot

expand to its native volume. This results in an overall particle size smaller than the parent core. Below the PNIPAM LCST, both core and shell swell and the core-shell system has again a larger radius as compared to the core. This behavior is in good agreement with what was discussed above with PNIPAM-core-PNIPMAM-shell systems and nicely demonstrates the mutual influencing of core and shell swelling.

2.5 Conclusions

Doubly thermosensitive core-shell microgels consisting of a PNIPAM core and a PNIPMAM shell have been prepared and investigated by dynamic light scattering, optical transmission and small angle neutron scattering. An inverse core-shell microgel where the core shrinks at higher temperatures than the shell was prepared as well. The results demonstrate that shell thickness and cross-link density of the shell control the thermosensitive behavior of the entire particle and that core and shell influence each other. Thus it is possible to have a rational synthesis of thermosensitive microgels that display one or two distinct volume transitions as a function of temperature. SANS data reveal interesting information on segment densities at different temperatures.

PNIPAM-PNIPMAM particles are colloidally stable in concentrated solution until the PNIPMAM LCST is reached. The inverse system becomes colloidally unstable above the PNIPAM LCST as is known from core-shell particles with a rigid core. However, the thermosensitivity of the PNIPMAM core in the core-shell microgel allows altering the structure even in the flocculated state, which will provide e.g. interesting ageing phenomena. This will be explored in the future.

Acknowledgement. The financial support of the Deutsche Forschungsgemeinschaft (DFG) and the Fond der Chemischen Industrie is thankfully acknowledged. We thank the ILL, Grenoble, France, and especially P. Lindner for beam time at the D11 instrument.

3 Structure of Multiresponsive 'Intelligent' Core-Shell Microgels

Abstract. A doubly temperature-sensitive core-shell microgel composed of two temperature sensitive polymers with different LCSTs in the core and shell has been studied by small-angle neutron scattering (SANS). The application of a novel universal form factor model in the analysis of the SANS data reveals that the radial density profile at temperatures above the LCSTs of both polymers can be well described by a two box-profile with narrow interfaces. At temperatures between the LCSTs the radial density profile reveals that the core in the core-shell microgel has larger dimensions than the naked core. Thus the swollen shell pulls the core apart. At temperatures below both LCSTs, however, the shell restricts the core swelling and the core is found to be smaller than in its native state. This clearly demonstrates the mutual influence of core and shell swelling.

3.1 Introduction

Environmentally responsive microgels have been subject of great interest in the past years due to their versatile applications. Such microgels are sometimes termed ‘intelligent’ since their properties can be tailor made to react in a specific way to the environment. The most intensively studied thermosensitive polymer is poly-*N*-isopropylacrylamide (PNIPAM) that exhibits a lower critical solution temperature (LCST) of 34 °C.[1,2] Chemically crosslinked PNIPAM microgels reveal a drastic particle size decrease upon heating in aqueous solution. The responsive characteristics can be modified either by co-polymerization or advanced polymer architecture and especially core-shell microgels have been investigated recently.[3,4] Such an advanced microgel architecture can give rise to unique particle properties since one can assume that core and shell de-/swelling mutually influence.[5,6,7] Indeed, dynamic light scattering experiments (DLS) probing the hydrodynamic size of the entire particle as well as

fluorescence studies[8,9] probing the core-shell interface have demonstrated a mutual influence of core and shell swelling.

3.2 Results and Discussion

Scattering experiments can provide more detailed information of the internal structure of the entire microgel.[10,11,12] In this contribution, we present small-angle neutron scattering (SANS) results on doubly temperature sensitive microgels realized by a core-shell structure of two thermosensitive polymers with different LCSTs. Recently, we reported emulsion polymerization and properties of PNIPAM-core-PNIPMAM-shell microgels, where PNIPMAM is poly-*N*-isopropylmethacrylamide with a LCST of 44 °C.[7] These particles show a two-step shrinking process of hydrodynamic radius R_h upon heating in aqueous solution (Fig. 3-1). The transitions at 34 °C and 44 °C are assigned to core and shell collapse, respectively. In the analysis of the SANS data, a new general form factor model is employed for describing the particles with core-shell morphology.

Experimental scattering curves at three temperatures corresponding to the fully collapsed (50 °C), partially collapsed (39 °C) and fully swollen (25 °C) state are plotted in Fig. 3-2.

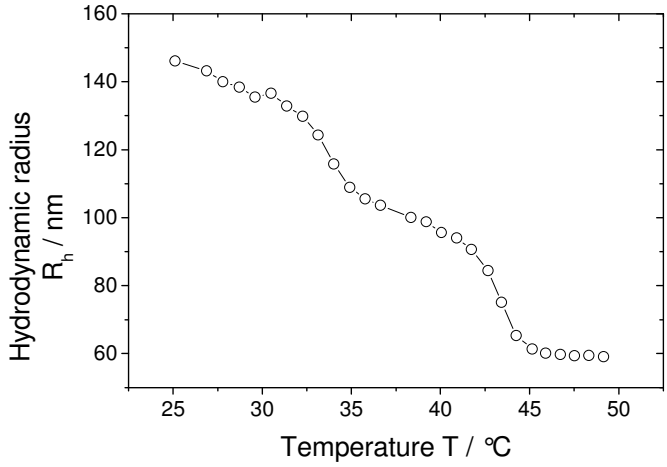

Fig. 3-1: Temperature dependence of the hydrodynamic radius R_h of a PNIPAM-core-PNIPMAM-shell microgel in D_2O. Mass ratio core/shell = 1:0.7, cross-link density in core: 1.4, in shell: 5 mol%.

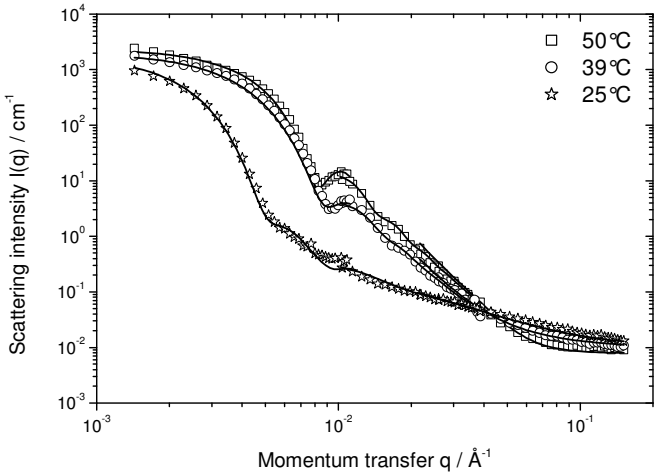

Fig. 3-2: Experimental SANS scattering profiles at 25, 39, and 50 °C. Lines show the fits. Note the shift of the minimum towards higher q-values with decreasing temperature from 50 to 39 °C.

Experimental details are given elsewhere.[13] Porod scattering ($I(q) \sim q^{-4}$) is observed at 50 °C in the intermediate q-range of q =~0.02-0.06 Å^{-1} indicating presence of a sharp interface, whereas the slope is slightly smaller at 39 °C. Counterintuitive on first sight is the shift of the minimum towards higher q-values with decreased temperature from 50 to 39 °C, indicating a particle size decrease contradictory to DLS results.

The radial (scattering length) density distribution of homogeneous particles with the radius R is well described by a box profile. Microgels have a graded interface due to a faster consumption of cross-linker molecules than of monomer during synthesis.[10,14] Consequently, the structure of core-shell microgels has to be described by a profile with two boxes of widths W_{core} and W_{shell}, a graded outer surface and an additional interface accounting for interpenetration of core and shell polymer networks as depicted in Fig. 3-3.

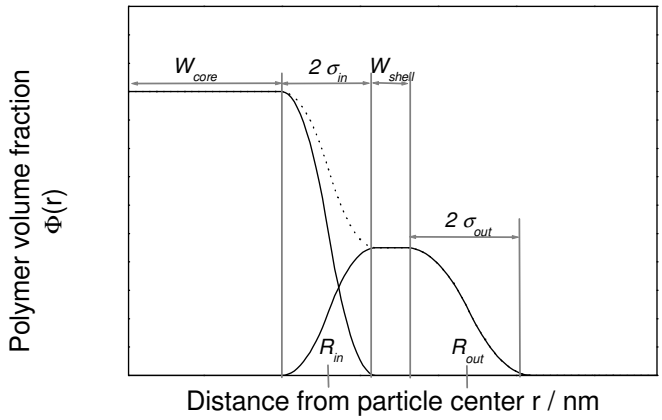

Fig. 3-3: Schematic density profile used to model scattering data from core-shell systems. The core is characterized by a box with width W_{core} and an interface with a width of 2 σ_{in} accounting for core and shell interpenetration. The shell is described by a box of width W_{shell} and surface profile of 2 σ_{out}. The dotted line shows the total density profile.

The scattering amplitude of a core-shell particle can be described by:

$$A(q) = \Delta\rho_{shell} V_{shell} \Phi(q, R_{out}, \sigma_{out}) + (\Delta\rho_{core} - \Delta\rho_{shell}) V_{core} \Phi(q, R_{in}, \sigma_{in}) \qquad (3\text{-}1)$$

where $\Delta\rho_{shell}$ and $\Delta\rho_{core}$ are the excess scattering length densities of shell and core, respectively. V_{shell} and V_{core} are the partial volumes of the polymer in the shell and in the core, respectively, and $\Phi(q,R,\sigma)$ is the normalized Fourier transformation of a particle with half-width radius R and with a width of the interface given by σ. If the radial profile is described with a symmetric form based on a parabolic shape:

$$\rho(r) = 1 \qquad r \le (R - \sigma) \qquad (3\text{-}2a)$$

$$\rho(r) = 1 - \frac{1}{2}\frac{\left[(r - R) + \sigma\right]^2}{\sigma^2} \qquad (R - \sigma) < r \le R \qquad (3\text{-}2b)$$

$$\rho(r) = \frac{1}{2}\frac{\left[(R - r) + \sigma\right]^2}{\sigma^2} \qquad R < r \le (R + \sigma) \qquad (3\text{-}2c)$$

$$\rho(r) = 0 \qquad r > (R + \sigma) \qquad (3\text{-}2d)$$

the Fourier transformation can be done analytically leading to:

$$\Phi(q,R,\sigma)=\frac{1}{V_n}[\left(\frac{R}{\sigma^2}+\frac{1}{\sigma}\right)\frac{\cos(q(R+\sigma))}{q^4}-\frac{3\sin(q(R+\sigma))}{q^5\sigma^2}$$
$$+\left(\frac{R}{\sigma^2}-\frac{1}{\sigma}\right)\frac{\cos(q(R-\sigma))}{q^4}-\frac{3\sin(q(R-\sigma))}{q^5\sigma^2}+\frac{2\cos(qR)}{q^5\sigma^2}+\frac{6\sin(qR)}{q^5\sigma^2}] \qquad (3\text{-}3)$$

where $V_n=(R^3/3+R\sigma^2/6)$ and $V=4\pi V_n$ is the volume of a particle with the radial profile $\rho(r)$ (Eqn. 3-2). The parameters R_{in} and R_{out} in the expression for the amplitude are related to the parameters W_{core} and W_{shell} in fig. 2 by $R_{in}=W_{core}+\sigma_{in}$ and $R_{out}=W_{core}+2\,\sigma_{in}+W_{shell}+\sigma_{out}$. Similar profiles were considered by Kerker[15] using Lorenz-Mie theory for light scattering and some examples of form factors were calculated numerically. Our calculations are performed within Rayleigh-Debye theory and result in relatively simple closed expressions (Eqn. 3-3). The model includes the following additional features: (i) polydispersity of the size in terms of Gaussian distribution, (ii) a Lorentzian to describe the polymer-like scattering from the internal structure of microgels, (iii) smearing of the model expression due to the instrumental resolution, and (iv) incoherent background scattering.[16]

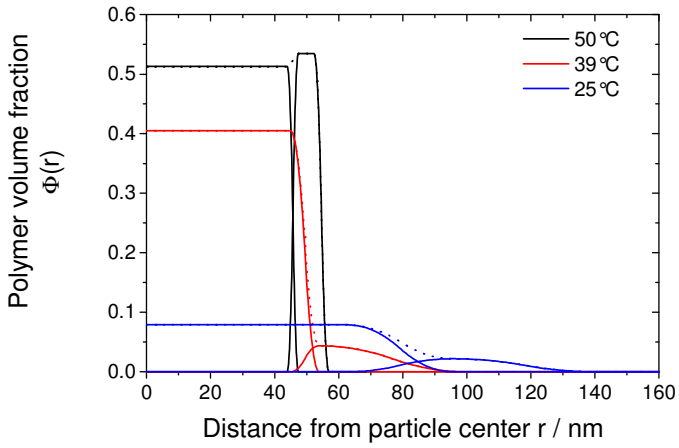

Fig. 3-4: Radial density profiles of a core-shell microgel at 25, 39, and 50 °C. Dotted lines represent the total of core and shell profiles.

The analysis of SANS data provides the radial density profile, see Fig. 3-4. At 50°C the microgel structure is described by two boxes of similar volume fractions of 51 and 53 %, a narrow interface and relative size polydispersity of 8%. The total radius is in good agreement with DLS results. As the temperature is above the LCSTs of both polymers, core and shell are both in a fully collapsed state. Significant changes are observed at 39 °C, where the temperature is between the LCSTs of core and shell polymer. The shell is found to be highly swollen with a low volume fraction of 4.4 % and a fuzzy surface of 2 σ_{out}=46 nm. The interface σ_{in} has increased from 1.7 to 4.4 nm and the core volume fraction has decreased to 41 %. When the temperature is further decreased, also a highly swollen core with a volume fraction of 8 % and a broad σ_{in}=16 nm is observed.

Decreasing the temperature below 44 °C, leads the shell to swell in radial and tangential directions. The radial growth directly contributes to an increase of particle size, whereas swelling in the tangential directions leads to mechanical strains at the core-shell interface. As the shell is interpenetrated with the collapsed but flexible core network, these strains can be released by stretching the core and core/shell interface leading to increased core dimensions (characterized by R_{in} and σ_{in}) as compared to 50 °C. At temperatures below 34 °C, the dimensions of the core in the core-shell system are smaller as compared to the naked core (i.e. without shell). The size of the pure core microgel was determined independently and was found to be $R_i+2\sigma_{in}$=122 nm[13] This clearly demonstrates that in the core-shell microgel at 25°C the shell restricts full swelling of the core. Thus compared to the naked core, the core of the core-shell particles is expanded at intermediate temperature and compressed at low temperature due to the swelling properties of the shell.

From the scattering point of view the change of temperature can be regarded as a contrast variation. At the intermediate temperature Fig. 3-4 shows the volume fraction of the shell decreased by an order of factor 10 at 39 °C. As the contrast changes in the same manner, the scattering profile is mainly determinated by the scattering from the core, which is smaller than the entire particle at 50 °C. Thus we can explain the shift of the minimum to high-q.

The use of the SANS technique thus provides a more detailed insight into the internal structure of ‘intelligent’ PNIPAM-core-PNIPMAM-shell microgels than is possible by DLS. The analysis of SANS data from microgels with different compositions provides quantitative information on the mutual influence of core and shell swelling and will be reported

elsewhere.[13] The particle properties can be controlled by the core-shell mass ratio as well as by the cross-link density in core and shell.[7]

3.3 Conclusions

In conclusion a novel universal form factor has been introduced which is very well suited for analyzing scattering data of core-shell/core-corona systems. The simple form used for the radial profile allows the form factor expressions to be calculated in analytical form. The model is quite general as it allows analysis of both core-shell particles with diffuse and sharp interfaces. In the case of the doubly thermosensitive microgel investigated in this study, detailed information on the mutual influence of the temperature dependent swelling of core and shell is obtained.

Acknowledgement. We gratefully acknowledge financial support by the DFG. We thank the ILL, Grenoble, France, for beam time at D11 and especially P. Lindner for local support.

4 Influence of Shell Thickness and Cross-Link Density on the Structure of Temperature Sensitive Poly-*N*-Isopropylacrylamide – Poly *N*-Isopropyl-methacrylamide Core-Shell Microgels investigated by Small-Angle Neutron Scattering

Abstract. Swelling properties of doubly temperature sensitive core-shell microgels consisting of two thermosensitive polymers with lower critical solution temperatures (LCTS) at, respectively, 34°C in the core and 44 °C in the shell have been investigated by small-angle neutron scattering (SANS). A core-shell form factor has been employed to evaluate the structure, and the real space particle structure is expressed by radial density profiles. By this means, the influences of both shell/core mass composition and shell cross-linker content on the internal structure have been revealed at temperatures above, between, and below the LCSTs. Higher shell/core mass ratios lead to an increased expansion of the core at temperatures between the LCSTs, whereas a variation of cross-linker in the shell mainly effects the dimensions of the shell. The influence on the core structure was interpreted as resulting from an elastic force developed from the swollen shell. At temperatures below the core LCST, the core cannot swell to its native size (i.e., in the absence of a shell) because the maximum expanded shell network prohibits further swelling. Thus, depending on temperature the shell either expands or compresses the core.

4.1 Introduction

Materials composed of chemically cross-linked polymers that are sensitive to external stimuli have been used in a wide variety of applications such as, e.g., catalysis,[1] drug delivery,[2]

sensors,[3] chemical separation,[4] biomolecule immobilization,[5] colloidal crystals,[6] and micro-optics.[7]

Poly-*N*-isopropylacrylamide (PNIPAM) is the most widely investigated temperature-sensitive microgel system[8] and shows structural changes upon heating above the lower critical solution temperature (LCST) in aqueous solution.[9] The temperature sensitive properties of PNIPAM can be extended to react on further stimuli as e.g. ionic strength,[10] solvent composition,[11] pH,[12] radiation,[13] and selective reaction[14] by copolymerization with monomers that show sensitivity to one of those stimuli.

The versatility of multi-responsive microgels enhances the number of potential applications. A particular approach of introducing multi-sensitivity is the spatial separation of two different polymers that are each responsive to a single stimulus. These systems allow better control and may react differently from a random copolymer.

Lyon and co-workers introduced multi-responsive microgels with a core-shell morphology preparing PNIPAM core-PNIPAM-*co*-acrylic acid shell microgels that are sensitive to temperature and pH.[15] Our group recently presented core-shell microgels composed of two temperature sensitive polymers, PNIPAM and poly-*N*-isopropylmethacrylamide (PNIPMAM) with LCSTs of 34 and 44 °C, respectively, in either core or shell.[16] These particles seem promising candidates for biomedical and cosmetic applications, since the human body temperature is between the LCSTs of both polymers. Furthermore, a multi-temperature sensitivity has the advantage that temperature variations can be controlled more rapidly than, e.g., ionic strength or pH changes and can be reversed easily.

Detailed knowledge of the internal microgel structure is important for their application in fields where special properties are demanded as, e.g., protein adsorption. Scattering methods such as small-angle neutron scattering (SANS), small-angle X-ray scattering (SAXS), as well as dynamic (DLS) and static light scattering (SLS), are powerful tools to explore the structure of macromolecules and have been applied to microgels.[17,18,19,20,21] However, scattering intensity profiles are often investigated in the high-q regime only (where $q = (4\pi/\lambda)\sin(\Theta/2)$) is the modulus of the scattering vector for a wavelength of λ and scattering angle Θ). Thus, the applied model equations will not sufficiently describe the structure of the entire particle.

Stieger et al. have been the first to apply a direct modeling approach to describe SANS data of PNIPAM microgels over a wide q-range.[22] They convoluted a homogeneous sphere form factor with a Gaussian, obtaining density profiles that gradually decreased at the surface, to

describe the surface fuzziness at temperatures below the LCST. This particle structure agrees with studies revealing that the cross-linker is consumed more rapidly than the monomer.[23] The same model was applied to SLS data of PNIPAM microgels, and it was demonstrated that a stepwise addition of cross-linker during the synthesis leads to a more homogeneous structure.[24] Boyko et al. combined a hard sphere form factor with the form factor of a randomly branched polymer to describe SANS data of temperature sensitive poly-*N*-vinylcaprolactam-*co*-*N*-vinylpyrrolidone microgels.[25]

The structure of polystyrene core-PNIPAM shell colloid particles was investigated by Ballauff´s group by means of SAXS and SANS.[26,27] They found that at high temperatures the PNIPAM shell has a rather compact structure described by a box profile, whereas at temperatures below the LCST, the PNIPAM shell has to be described by a fuzzy profile. These studies further suggested that the swelling of PNIPAM grafted to a solid surface is limited because of spatial constraints.

The mutual influence of core and shell swelling was observed with core-shell systems where both core and shell consist of swellable polymer networks.[16,28,29] In comparison to the core-shell systems reported by Ballauff, spatial constraints can be released by the deformation of the flexible core network. Experiments by Lyon and co-workers employing fluorescence resonance energy transfer techniques (FRET) revealed that swelling properties of the core are affected by the shell and the phase transition temperature of the core shifted toward higher temperatures as the shell thickness increased. This technique also allows for a calculation of interface thickness.[30,31]

Our group recently established a form factor model to describe scattering data and analyze the structure of microgel particles with core-shell morphology.[32] The model accounts for an interpenetrating layer of core and shell network and a graded particle surface. Here, we report on the application of small-angle neutron scattering combined with direct data modelling to evaluate the internal structure of doubly temperature sensitive core-shell microgels with different compositions. Two series of PNIPAM core-PNIPMAM shell microgels have been investigated: (i) The thickness of the PNIPMAM shell was varied at constant shell cross-linker content in the first series; (ii) in the second series, the shell cross-linker content was varied at constant shell thickness. The form factor analysis provides detailed information on the influence of shell thickness and cross-linker content on the internal structure and the mutual influence of core and shell swelling that hardly can be provided by other techniques.

4.2 Experimental Section

N-Isopropylacrylamide (97 %) and *N*-isopropylmethacrylamide (97 %) monomers were purchased from Sigma-Aldrich and recrystallized twice from cyclohexane (p.a. quality, Aldrich). Surfactant sodium dodecyl sulfate (SDS), initiator potassium peroxodisulfate (KPS), and cross-linker *N*,*N´*-methylene-*bis*-acrylamide (BIS, 99.95 %) were used without further purification. Water for all purposes was of Milli-Q quality with a resistance of >18.2 MΩ/cm and filtered through a 0.2 µm filter. Heavy water (D_2O, 99.9 %) was purchased from Deutero GmbH and used as received.

The synthesis of the core-shell microgel particles has been described in detail previously.[16] In brief, the synthesis was done in a two-step seed-and-feed emulsion polymerization in a reaction vessel equipped with a reflux condensor, mechanical stirrer, and nitrogen inlet. A separately prepared mixture of shell monomer and cross-linker was added to the solution of purified core particles at 70 °C. The initiator KPS was dissolved in 10 ml of degassed water at room temperature. After 30 min of extensive nitrogen purging, the initiator solution was added. A low concentration of surfactant (0.08-0.10 g/l) was present to prevent particle coagulation. The amount of initiator was chosen as 1 mol% of the reacting monomer. After 6 hours at 70 °C under a slight nitrogen stream then reaction mixture was cooled down to room temperature under stirring. Tab. 4-1 gives details on the synthesis conditions.

Tab. 4-1: Synthesis recipes for the preparation of PNIPAM core-PNIPMAM shell microgels in water at 70 °C.

sample	core solution		shell solution			
	PNIPAM core [g]	water [ml]	NIPMAM [g]	BIS [g]	BIS [mol%]	water [ml]
CS-5/0.23	0.370	25	0.185	0.0118	5.0	25
CS-5/0.69	8.140	550	8.140	0.5192	5.0	550
CS-5/1.42	0.185	25	0.370	0.0236	5.0	25
CS-5/2.50	4.070	550	12.210	0.7789	5.0	550
CS-3/0.54	0.370	25	0.370	0.0138	3.0	25
CS-7/0.77	0.370	25	0.370	0.0337	7.0	25
CS-9/0.79	0.370	25	0.370	0.0443	9.0	25

All samples are based on the same PNIPAM core, which has a molar cross-linker content of 1.4 % BIS. Specifications of the shell composition are given in the sample name scheme, for example, CS-5/0.69, where the first number denotes the molar percentage of cross-linker monomer in the shell (omitting the units) and the second number gives the relative mass ratio m_{shell}/m_{core} after purification (see below), where m_{shell} is the mass of the shell and m_{core} is the mass of the core.

Ultra-centrifugation is highly preferable to the common dialysis purification procedure, because low molecular weight water-soluble polymers are removed. The samples were purified by repeated ultra-centrifugation, decantation of the supernatant, and redispersion in deionized water. A Beckman-Coulter LM-55 ultra-centrifuge with a Ti 70.1 rotor was used for the centrifugation at 25 °C. Aliquots of the transparent supernatant of three centrifugation cycles were merged and dried at 70 °C for 3 days. The transparent solution became turbid at higher temperatures, whereas the supernatant of a fourth centrifugation cycle did not become turbid, indicating sufficient removal of low molecular weight polymer. Aliquots of the microgel fraction were freeze-dried. From the weight ratio of soluble low molecular mass polymer and the microgel fraction, core-shell mass ratios were calculated and listed in Tab. 4-3.

Dynamic light scattering experiments have been performed with a modified ALV goniometer setup (LSI, Switzerland) at a laser wavelength of 632.8 nm. The samples were highly diluted in heavy water (c<0.01 wt%) to prevent multiple scattering and filtered through a 1.2 µm filter to remove dust. The scattered light was detected at a scattering angle of 90°, and hydrodynamic radii $R_h(T)$ have been calculated using second-order cumulant fits via the Stokes-Einstein equation. Heating and subsequent cooling cycles have been performed. The particle size changes are fully reversible in the given time scales. For the sake of clarity, only data of heating runs are shown.

Measurements of apparent specific polymer densities of PNIPMAM polymer were performed with an oscillating-tube densitometer DMA 5000 (Anton Paar, Graz) in the temperature range 20-50 °C on PNIPMAM samples with 5 and 7 mol% BIS at concentrations from 1 to 5 wt% in heavy water. The densitometer was calibrated using water and air at 20 °C. The influence of cross-linker content was found to be <0.5 %, which is within the experimental error. Density data of 1.4 mol% cross-linked PNIPAM were taken from a previous study performed on the same instrument.[22]

SANS experiments were performed at the D11 beam line at the Institut Laue-Langevin (ILL) in Grenoble, France. A neutron wavelength of 6 Å with a spread of $\Delta\lambda/\lambda$=9% was used. The data were collected on a ^{3}He detector with 64×64 pixels of 10×10 mm^2 size. The maximum accessible *q*-range was covered by three detector-sample distances of 2.5, 10.0, and 36.7 m. The incoherent scattering of water at detector distances of 2.5 and 10.0 m was used for absolute intensity calibration. ILL provided software GRAS$_{ANS}$P (v. 3.85) was used for absolute calibration, background correction, and azimuthal averaging following standard procedures at the ILL. The microgels were investigated at mass concentrations of 0.2 wt% in D_2O. The temperature was adjusted to ±0.1 °C.

4.3 Theory and Data Analysis

Small-angle neutron scattering experiments give an intensity distribution *I(q)* in reciprocal space as a function of momentum transfer *q*, and data analysis has to be performed to obtain real space information.[33]

A convenient way to express the scattering intensity distribution of a sample is the introduction of the differential scattering cross section $d\sigma(q)/d\Omega$, as it does not depend on the transmission and form of the sample. In general, the differential scattering cross-section may be expressed for a dispersion of spherically symmetric particles by

$$\frac{d\sigma}{d\Omega} = nP(q)S(q) \qquad (4\text{-}1)$$

where *n* is the number density of particles. *P*(*q*) is the particle form factor that describes the structure of the particle, and *S(q)* is the structure factor. *P(q)* is normalized so that $P(0)=\Delta\rho^2 V_{polymer}^2$, where $\Delta\rho$ is the scattering contrast of the polymer and $V_{polymer}$ volume of the polymer within the particle. The structure factor accounts for the interference of scattering from different particles. In the present paper, we present only data obtained at high dilution (0.2 wt%); hence, interparticle correlations can be neglected and *S(q)=1*.

Generally, the scattering contrast is the difference of the scattering length density of the polymer and the surrounding solvent $\Delta\rho = \rho_{polymer} - \rho_{solvent}$. ρ can be calculated from the

molecular mass of one repeat unit accounting for polymer composition (molar fraction x of cross-linker monomer) and the apparent specific density ρ_d at the given temperature by

$$\rho_{polymer} = (1-x)\frac{\rho_d}{M_{monomer}} N_A \sum_i b_{i,monomer} + x\frac{\rho_d}{M_{crosslink}} N_A \sum_i b_{i,crosslink} \qquad (4\text{-}2)$$

with $M_{monomer}$ and $M_{cross\text{-}link}$ the molecular weight of, respectively, the repeat and cross-linker units, N_A Avogadro´s number, and b_i the bound coherent scattering length of each nucleus.[34] Microgel particles are expected to have an inhomogeneous structure with a fuzzy surface due to faster consumption of cross-linker molecules during the earlier stages of the synthesis.[23] As a consequence, our model of the structure of core-shell microgels employs a profile like the one shown in Fig. 4-1, with a graded outer surface characterized by σ_{out}, and an interface between core and shell characterized by σ_{in}. The inner part of the core is described by a box of the width W_{core} and the central part of the shell by a box of width W_{shell}. The central portions may have different densities depending on the swelling state of the particles.

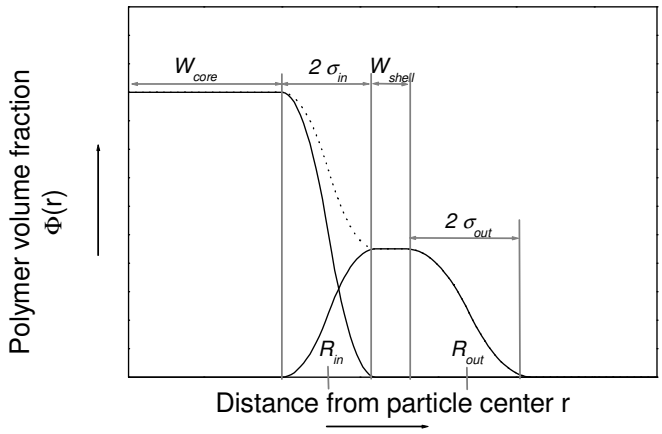

Fig. 4-1: Schematic illustration of the internal structure of core-shell microgels. W_{core} and W_{shell} describe the widths of central core and shell boxes. The interpenetration layer of core and shell is characterized by $2\sigma_{in}$ and σ_{out} denotes the half-width of the outer surface. The dotted line represents the total of core and shell.

The radial density profile $\rho(r)$ of a particle with a graded surface can also be expressed by the half-width radius R and the interface half-width of σ. We used a parabolic shape

$$\rho(r) = 1 \qquad r \le (R-\sigma) \tag{4-3a}$$

$$\rho(r) = 1 - \frac{1}{2}\frac{\left[(r-R)+\sigma\right]^2}{\sigma^2} \qquad (R-\sigma) < r \le R \tag{4-3b}$$

$$\rho(r) = \frac{1}{2}\frac{\left[(R-r)+\sigma\right]^2}{\sigma^2} \qquad R < r \le (R+\sigma) \tag{4-3c}$$

$$\rho(r) = 0 \qquad (R+\sigma) < r\,. \tag{4-3d}$$

The width of the central part is given by $W=R-\sigma$, and the volume of the particles is $V=4\pi V_n$, where $V_n=(R^3/3 + R\sigma^2/6)$. The Fourier transformation of this profile can be calculated analytically and the normalized Fourier transformation $\Phi(q,R,\sigma)$, i.e. with $\Phi(q=0,R,\sigma)=1$, is

$$\begin{aligned}\Phi(q,R,\sigma) = \frac{1}{V_n}\Bigg[&\left(\frac{R}{\sigma^2}+\frac{1}{\sigma}\right)\frac{\cos\left(q(R+\sigma)\right)}{q^4} + \left(\frac{R}{\sigma^2}-\frac{1}{\sigma}\right)\frac{\cos\left(q(R-\sigma)\right)}{q^4} \\ &- \frac{3\sin\left(q(R+\sigma)\right)}{q^5\sigma^2} - \frac{3\sin\left(q(R-\sigma)\right)}{q^5\sigma^2} + \frac{2\cos(qR)}{q^5\sigma^2} + \frac{6\sin(qR)}{q^5\sigma^2}\Bigg]\end{aligned} \tag{4-4}$$

Thus, the scattering amplitude of a core -shell particle can be expressed by

$$A(q) = \Delta\rho_{shell} V_{shell} \Phi_{shell}(q, R_{out}, \sigma_{out}) \quad + \quad (\Delta\rho_{core} - \Delta\rho_{shell}) V_{core} \Phi_{core}(q, R_{in}, \sigma_{in}) \tag{4-5}$$

In this expression, $R_{in}=W_{core}+\sigma_{in}$ and $R_{out}=W_{core}+2\sigma_{in}+W_{shell}+\sigma_{out}$. For spherically symmetric objects, the form factor is the squared scattering length amplitude $P(q)=A^2(q)$. To account for scattering due to concentration fluctuations inside the microgel, a Lorentzian function $I_L(q) = I_L(0)/[1+q^2\xi^2]$ is added to $P(q)$. The average correlation length in the network is described by ξ. $I_L(q)$ contributes significantly only in the high-q regime. However, a very accurate determination of ξ from SANS data is difficult because of the high incoherent background in the high-q regime and statistical errors.[22,27] Finally, a constant background I_{back} is included to correct for residual incoherent scattering.

Particle size polydispersity was described by a normalized Gaussian number distribution

$$D = \left(R, \langle R \rangle, \sigma_{poly}\right) = \frac{1}{\sqrt{2\pi\sigma_{poly}^2 \langle R \rangle^2}} \exp\left(-\frac{\left(R - \langle R \rangle\right)^2}{2\sigma_{poly}^2 \langle R \rangle^2} \right) \tag{4-6}$$

with $\langle R \rangle$ as the average particle radius, and σ_{poly} denotes the relative particle size polydispersity. The influence of polydispersity was included by scaling all dimensions of the particles by $R/\langle R \rangle$.

The SANS experiments have a finite experimental q-resolution, since scattering vectors q are distributed around the nominal $\langle q \rangle$ and are also probed for a particular nominal setting. The finite collimation of the neutron beam, the wave length spread, and the finite resolution of the detector contribute to the experimental smearing and can each be approximated by a Gaussian function[35] so that the experimental smearing can be expressed by a combined resolution function

$$R(\langle q \rangle, q) = \frac{q}{\sigma_{smear}^2} \exp\left[-\frac{1}{2}\left(q^2 + \frac{\langle q \rangle^2}{\sigma_{smear}^2} \right) \right] I_0\left(\frac{\langle q \rangle q}{\sigma_{smear}^2} \right) \tag{4-7}$$

that describes the distribution of scattering vectors q around $\langle q \rangle$ by means of σ_{smear}, which was evaluated for each experimental setting (wavelength, collimation, detector distance) by fitting an attenuated direct beam profile with a Gaussian. The resolution function is merged to the model to account for experimental smearing.

Incorporation of all above-mentioned contributions leads to the model expression for the scattering intensity distribution:

$$I^{\mathrm{mod}}(q) = n \int_0^\infty \int_0^\infty R\left(\langle q \rangle, q\right) D\left(R, \langle R \rangle, \sigma_{poly}\right) \left[A^2(q) + I_L(q) \right] dR\, dq + I_{back} \tag{4-8}$$

where the number density is given by

$$n = c \left[\int_0^\infty \left[m_{core}(R) + m_{shell}(R) \right] D(R, \langle R \rangle, \sigma_{poly})\, dR \right]^{-1} \tag{4-9}$$

where c is the polymer concentration per volume of sample and the R dependence of the mass and core has been expressed explicitly. Note that $m_{core}=\phi_{core}\cdot\rho_{core}\cdot V_{core}$, with ϕ_{core} the volume fraction of polymer in the core, ρ_{core} the partial specific mass density of the polymer in the core and V_{core} the volume of the core. Similar expressions are valid for the shell.

The model was fitted to the experimental data using a least-squares routine to a reduced χ^2 criterion. The Fourier transformation of the scattering amplitude using volume fractions instead of scattering length densities gives the radial volume fraction profiles in real space.

The model was formulated so that the mass of the shell and the core could be fixed at certain values. This was used extensively in the data analysis in order to reduce the number of free fit parameters in the model; see further discussion below.

4.4 Results and Discussion

Core-shell microgels composed of PNIPAM which exibits a LCST of 34 °C in the core, and PNIPMAM with a LCST of 44 °C in the shell, show distinct changes in particle size at temperatures corresponding to the transitions of core and shell polymers. (All experiments were performed with D_2O as solvent; in H_2O, the transition temperatures are slightly lower.) In Fig. 4-2, the influences of shell thickness (i.e., the relative mass ratio m_{shell}/m_{core}) and the degree of cross-linking in the shell on the thermal response in aqueous solution (D_2O) are illustrated. The core-shell particles are all based on the same core, which is shown as reference.

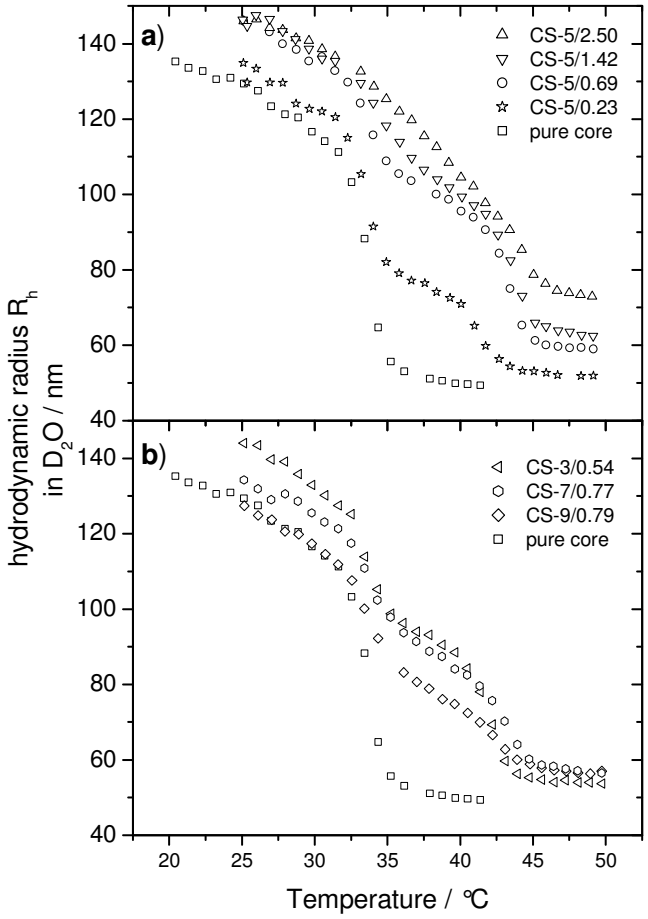

Fig. 4-2: Dynamic light scattering results for core-shell microgels and the parent core with: (a) varying shell thickness samples at constant cross-linker content, samples CS-5/0.23, CS-5/0.69, CS-5/1.42 and CS-5/2.50; (b) varying shell cross-linker content, samples CS-3/0.54, CS-7/0.77, CS-9/0.79.

The influence of the core-shell mass ratio can be directly observed at temperatures above the shell LCST (Fig. 4-2a). The particle sizes increase as the relative shell mass increases from 0.23 to 2.50. At lower temperatures, the solvent quality changes from poor to good for the shell polymer, and at 44 °C, a distinct transition is found. With further decreased temperature below 34 °C, the PNIPAM core starts swelling, and a second transition is found. The polymerization of the shell proceeds at 70 °C onto the fully collapsed core, and one can calculate a linear growth of the shell volume with the relative shell mass at temperatures

above the shell's LCST from the hydrodynamic radii by $V_{shell} = \frac{4}{3}\pi\left(R^3_{core-shell,T>44°C} - R^3_{core,T>34°C}\right)$ as shown in Fig. 4-3.

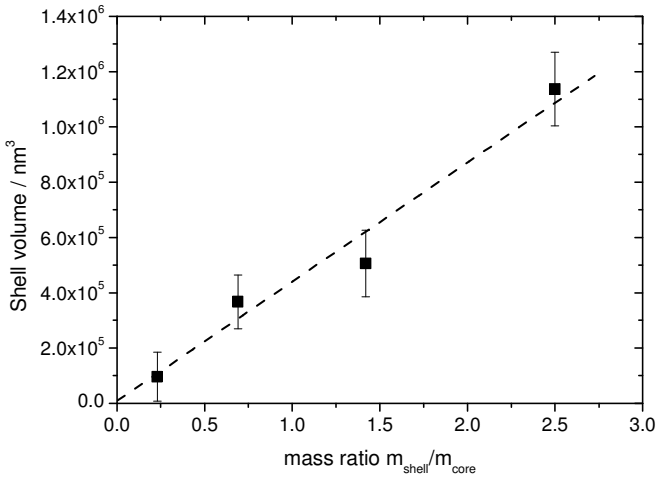

Fig. 4-3: Volume of the shell in core-shell particles with varied core-shell mass ratios calculated from hydrodynamic radii at 50 °C assuming an experimental error of 3 %. The linear dependency indicates the homogeneous structure of the shell.

This linear growth of the shell volume with the mass implies a rather homogenous and compact structure of the shells at this temperature.

Similar behavior is found when the shell cross-linker density is varied from 3 to 9 mol%. The more pronounced changes in particle size at 34 and 44 °C with lower shell cross-linker content are due to the fact that less cross-linked networks exhibit a larger swelling ratio at lower temperatures.[16] The shell's influence on the core's swelling is obvious with sample CS-9/0.79, which exhibits a slightly smaller hydrodynamic radius at 25 °C than the parent core. The little size differences at high temperatures in Fig. 4-2b are caused by the different extent of incorporation of chains into the particle. It has been shown that lower cross-linker densities lead to a higher fraction of so-called water-soluble polymer,[36] which is removed by ultra-centrifugation purification.

SANS is a powerful technique to investigate internal structural changes of core-shell microgels, whereas DLS only provides information on the total hydrodynamic particle size. SANS experiments were carried out at three temperatures: 50, 39, and 25°C. These temperatures correspond to the states where (a) both core and shell are collapsed, (b) the shell is swollen and the core is collapsed, and (c) both core and shell are swollen. The fully collapsed state of core and shell can be regarded as the native state of the particles, since synthesis proceeds at 70 °C, i.e., at a temperature well above the LCSTs of both core and shell. A large *q*-range (0.001-0.2 $Å^{-1}$) was employed in this study, which allows obtaining information about the internal as well as the overall structure of the core-shell microgel particles. Parameters obtained from the fitting procedure are summarized in Tab. 4-2; the uncertainties are similar to those obtained previously.[22] The data will be discussed in detail in the following sections.

Tab. 4-2: Summary of the parameters describing the structure of core-shell microgel particles obtained from the modelling procedure.

sample	T	Φ_{core}	W_{core}	σ_{in}	Φ_{shell}	W_{shell}	σ_{out}	σ_{poly}	R_{SANS}	R_h
	°C	%	nm	nm	%	nm	nm	%	nm	nm
CS-5/0.23	50	51.3	44.0	1.7	53.4	0.1	1.7	8.2	51	52
	39	45.9	44.0	3.4	3.3	0.9	8.1	7.4	68	73
	25	9.0	39.7	27.5	1.9	0.7	21.4	12.8	127	135
CS-5/0.69	50	51.3	43.9	1.7	53.4	4.9	2.3	7.8	57	59
	39	40.5	45.0	4.4	4.4	1.2	16.3	9.9	88	99
	25	7.9	62.8	16.4	2.2	2.3	21.0	12.6	140	146
CS-5/1.42	50	51.3	43.7	1.9	53.4	10.1	2.0	8.7	62	63
	39	37.9	43.9	6.5	7.0	2.9	17.6	11.0	95	102
	25	8.6	58.1	15.6	4.5	1.2	25.6	9.8	142	146
CS-5/2.50	50	51.3	43.7	2.1	53.4	20.3	2.0	8.0	72	73
	39	31.8	54.1	5.8	9.7	15.8	8.9	6.9	99	110
	25	9.6	64.2	10.2	7.4	3.1	24.5	11.0	137	145
CS-3/0.54	50	51.3	43.9	1.0	52.0	3.2	2.1	7.7	53	54
	39	44.3	45.7	2.3	3.3	0.6	15.3	10.0	82	90
	25	9.1	59.1	16.2	2.2	2.1	22.4	15.1	138	143
CS-7/0.77	50	51.3	43.5	1.9	50.1	4.9	2.1	10.7	56	57
	39	40.5	45.0	4.4	6.7	4.1	14.5	10.7	87	87
	25	8.0	62.5	16.2	2.8	0.1	18.1	13.2	131	134
CS-9/0.79	50	51.3	44.1	1.7	50.6	5.9	1.6	8.9	57	57
	39	38.8	45.2	4.9	8.1	3.6	8.3	9.1	75	76
	25	8.2	65.8	12.5	2.7	3.9	14.0	13.3	123	127

4.4.1 Influence of Shell/Core Mass Ratio

4.4.1.1 Behavior at high temperature: LCST (core) < LCST (shell) < T

Fig. 4-4 shows the SANS scattering data and fits obtained at high temperature, i.e., in the fully collapsed state for the core-shell microgel series with varying shell thicknesses.

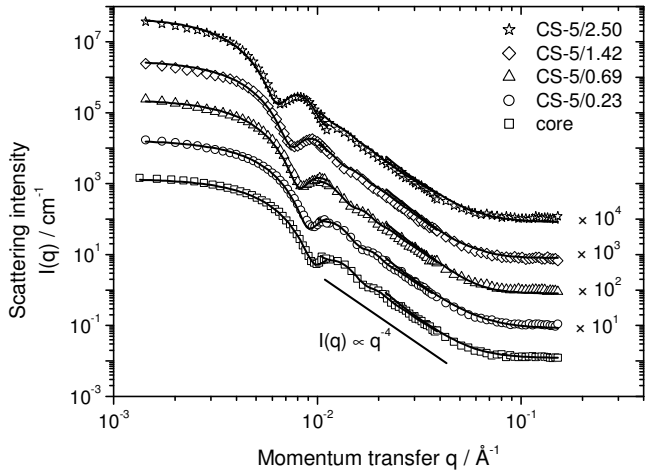

Fig. 4-4: SANS scattering profiles of the parent PNIPAM core and core-shell microgels with varied shell thicknesses, i.e., relative shell mass, at 50 °C. The lines represent fits according to the model equation. The shift of the form factor minima to lower *q* values indicates the increased particle size with larger shell mass.

Particle form factor minima up to second order indicate that the particle polydispersity is quite small. From the fitting procedure, the polydispersities were determined for all microgels to be around 8 %. In the intermediate *q*-range (0.01-0.04 Å^{-1}), the slope of the scattering profiles $I(q) \propto q^{-4}$ indicates the presence of a sharp surface (Porod scattering). A shift of the form factor minimum toward lower *q*-values is observed with increasing mass ratio m_{shell}/m_{core}, i.e., increased shell thickness and total particle size in agreement with DLS data.

The modelling of SANS data in the fully collapsed state is straightforward and is performed in two steps. The analysis of the pure core without a shell reveals a box-like density profile with a volume fraction Φ_{core} of 51 % and a narrow surface. The width (W_{core}) of the core was 43.0 nm with a sharp surface defined by a half-width of σ_{in}=2.7 nm. When the shell is polymerized at 70 °C, core and shell form an interpenetrating network, which can be assumed to be identical for all samples regardless of the thickness of the shell. Furthermore, we can assume that the core structure at this temperature is not altered by the presence of the shell. To obtain the volume fraction of the collapsed PNIPMAM in the shell, a homo-PNIPMAM microgel with the corresponding cross-linker content of 5 mol% was analyzed independently and in the same way as the PNIPAM core[37] and revealed a polymer volume fraction of 53 %; thus close to the core volume fraction. Then, the PNIPMAM volume fraction was used as a fixed parameter in the data evaluation. The width of the shell and the outer surface remain the two parameters to fully describe the core-shell microgels in the collapsed state. Fig. 4-5 displays the radial density profiles obtained. The structure of the core-shell particles can be well-described by two-box profiles with a narrow core-shell interface and a sharp outer surface. The width of the core-shell interfaces for the different samples is $2\sigma_{in}$=3.4-4.2 nm and slightly smaller than the surface thickness of the collapsed pure core, which is 5.4 nm. The width of the outer surface $2\sigma_{out}$=3.4-5.2 nm is similar to that of the pure core.

The width of the shell W_{shell} increases with higher ratios m_{shell}/m_{core} from 1.2 nm with sample CS-5/0.23 to 20.3 nm for the sample with the thickest shell CS-5/2.50. The total particle sizes nicely agree with the hydrodynamic radii measured by DLS (Tab. 4-2).

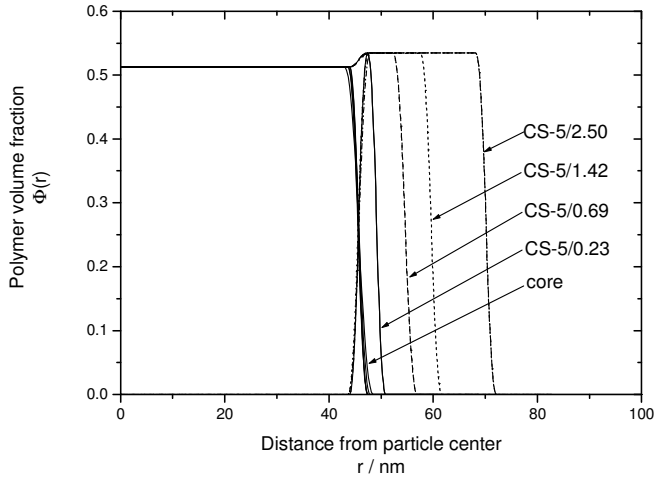

Fig. 4-5: Density profiles of samples with varied shell thicknesses at 50°C where core and shell are in the collapsed state. The profiles describe two boxes with a narrow interface and sharp outer surface. Increased shell/core mass ratios lead to wider shell boxes. The core profiles show only minimal deviations from the pure core profile (bold line).

Masses of core and shell can be calculated from the radial density profiles by

$$m_{core} = N_A \rho_{core} V_{core} = N_A \rho_{core} 4\pi \int_{r=0}^{R_{inner}+\sigma_{inner}} \Phi_{core}(r)\, r^2 dr \qquad (4\text{-}10)$$

and

$$m_{shell} = N_A \rho_{shell} V_{shell} = N_A \rho_{shell} 4\pi \int_{r=R_{inner}-\sigma_{inner}}^{R_{outer}+\sigma_{iouter}} \Phi_{core}(r)\, r^2 dr\,, \qquad (4\text{-}11)$$

respectively, where ρ_{core} and ρ_{shell} are the polymer partial specific densities. Tab. 4-3 lists the calculated ratios and compares them to those found by gravimetrical analysis (experimental section: ultra-centrifugation). Good agreement is found for the determination of the mass composition with these two independent methods.

Tab. 4-3: Mass composition of core-shell microgels from synthesis and SANS data analysis.

sample	shell/core mass ratio m_{shell}/m_{core}	
	by gravimetric analysis	by SANS
CS-5/0.23	0.23	0.26
CS-5/0.69	0.69	0.75
CS-5/1.42	1.42	1.31
CS-5/2.50	2.50	2.75
CS-3/0.54	0.54	0.49
CS-7/0.77	0.77	0.71
CS-9/0.79	0.79	0.74

4.4.1.2 Behavior at intermediate temperature: LCST (core) < T < LCST (shell)

Pleštil investigated scattering profiles from block copolymer micelles in a selective solvent, which exhibits good solvent conditions for one block and bad conditions for the other.[38] The insoluble blocks formed a dense core, which was surrounded by a corona of swollen soluble blocks. Simulations and evaluation of experimental data revealed that the scattering profiles in an intermediate *q*-range are insensitive to scattering contributions from the swollen corona if its excess scattering amplitude is low in comparison to that of the dense core. The so-called bare-core approximation can be applied to the core-shell microgels at temperatures between the LCSTs, because the positions of the form factor minima are mainly determined by the dimensions of the core. At temperatures between 34 and 44 °C, the swollen PNIPMAM shell has a lower volume fraction and exhibits less neutron scattering contrast; thus, the temperature variation can be regarded as contrast variation, by which core and shell scattering are separated at the intermediate temperature.

Furthermore, we can assume that the mass of the core is not affected by the apparent mass loss at lower temperatures, which occurs because of dangling polymer chains on the particle surface that are not detected by neutron scattering.[21,22] Thus, we can introduce the constraint in the model that the core mass is preserved.

In Fig. 4-6, scattering data and fits at 39 °C are presented. A slight shift of the form factor minima to lower *q* with increased shell mass is found with sample CS-5/0.23, CS-5/0.69, and CS-5/1.42 indicating slightly increased dimensions of the dense PNIPAM core. Obviously, the scattering profile of sample CS-5/2.50 is more affected by contributions from the shell in the range q=0.015-0.04 $Å^{-1}$, and an even stronger shift to lower *q* is observed.

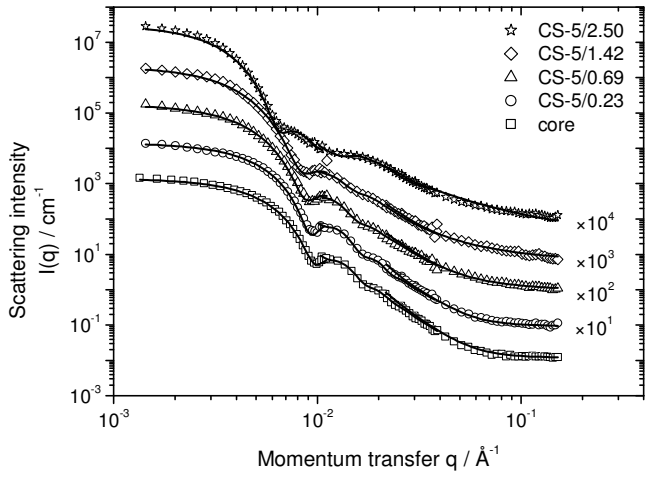

Fig. 4-6: Scattering profiles of core-shell microgels with varied shell/core mass ratios taken at 39 °C. Samples CS-05/0.23, CS-5/0.69, and CS-5/1.42 exhibit a slight shift of the form factor minima toward lower *q* compared to the pure core indicating increased dimensions of the core. The scattering profile of CS-5/2.50 is more affected from contributions of the shell in the intermediate *q* range.

The scattering profiles reveal a steeper slope in the low *q* range (q=0.002-0.008 Å^{-1}) with increased core-shell mass ratio indicating a bigger radius of gyration. This intuitively agrees with the DLS results, as a thicker shell is more swellable than a thinner one. Furthermore, one observes that the slope of the scattering profiles in the intermediate *q*-range from 0.01 to 0.04 Å^{-1} becomes less steep with higher shell mass. Thus, there are only small contributions from swollen shell ($I(q) \propto q^{-2}$) to the scattering profile in this regime.

The swelling of the shell polymer network proceeds in tangential and radial directions. The swelling in radial direction directly leads to an increase of the shell thickness. Swelling in the tangential directions influences the core, as it leads to a mechanical stress at the core-shell interface;[27,30,32] in other words, the core-shell interface is pulled outward. The force which is developed from the swollen shell to stretch the core increases with the shell mass.[39] This stress is released by expanding the flexible core and core-shell interface. The core dimensions

will be increased until equilibrium between the force exerted by the shell and the resisting elastic force developed in core is reached.

Radial density profiles obtained from SANS curves at 39 °C are displayed in Fig. 4-7.

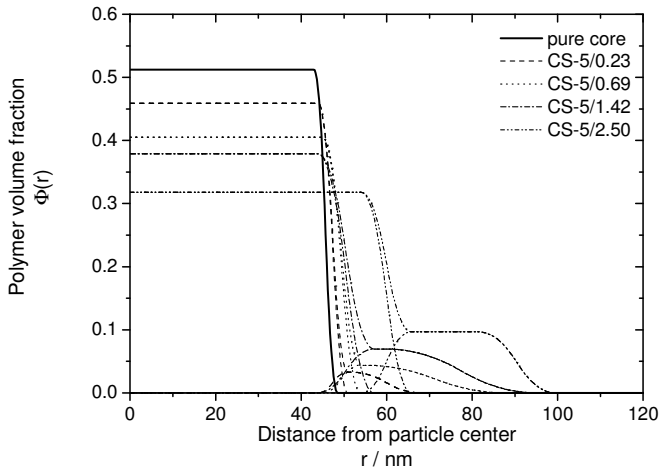

Fig. 4-7: Density profiles at 39 °C. The PNIPAM core has a compact structure, but its dimension is increased because of the influence of the swollen shell. The effect increases with higher shell masses. Dotted lines represent the total polymer density distribution.

Generally, the density profiles reveal that the structure can be described by a dense box profile for the core and a highly swollen shell. The dimensions of the core (described by R_{in}) grow from 47.4 to 59.9 nm as the shell mass increases, and the width of the interface increases from $2\sigma_{in}$=6.8 nm at the sample with the thinnest shell to 11.8 nm at the sample with the thickest shell. The polymer volume fraction of the core decreases from 45.9 % to 31.8 % in the same order. One observes that the volume fraction of the shell increase from 3.3 % to 9.7 % as the shell mass increases. The thickness of the shell as given by $\sigma_{in}+W_{shell}+2\sigma_{out}$ increases from 20.5 to 39.4 nm.

The sample with the highest shell mass (CS-5/2.50) reveals a much broader box in the shell profile. This may explain why this sample shows a much larger stretching of the core. From a chemical point of view, one may assume a much higher cross-linker gradient in the shell than in the core, so that in the case of thin shells (low shell mass) only a narrow layer of highly

cross-linked polymer close to the core-shell interface is present, and the fuzzy surfaces of the these sample mainly consist of only loosely cross-linked polymer chains. Only the cross-linked layers in the shell close to the core-shell interface will develop the force, which expands the core. Thus, samples CS-5/0.23, CS-5/0.69 and CS-5/1.42 show small expansions of the core as the shell mass increases, but in comparison to sample CS-5/2.50 the deformations are rather small. Because of a much higher shell/core mass ratio, CS-5/2.50 provides a much broader layer of highly cross-linked polymer in the shell and will consequently develop a stronger expanding force than the other samples. Calorimetric measurements revealed that the core transition is shifted to higher temperatures when the swollen shell restrains the core to collapse. The temperature shift increases with the mass of the shell.[39]

4.4.1.3 Behavior at low temperature: T < LCST (core) < LCST (shell)

The scattering data at 25 °C (Fig. 4-8) show fewer details compared to higher temperatures. One finds a shift of the form factor minimum to lower q values with higher shell masses. On first glance, this could be interpreted in terms of an increased particle size, but DLS data (Fig. 4-2a) reveal that the samples CS-5/0.69, CS-5/1.42, and CS-5/2.50 have similar hydrodynamic radii at this temperature. Furthermore, the form factor minima become more pronounced. With sample CS-5/2.50, even the third minimum was observed (Fig. 4-8).

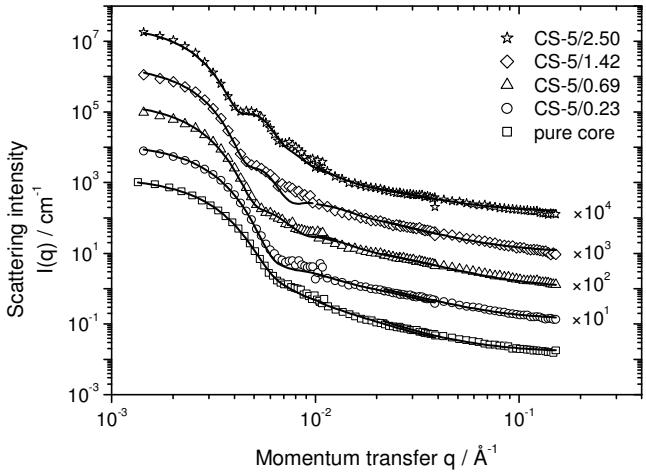

Fig. 4-8: Scattering profiles at 25 °C. The shift of the first minimum with higher shell masses indicates increased particle sizes, but the samples CS-5/0.69, CS-5/1.42, and CS-5/2.50 show similar hydrodynamic radii at this temperature.

The analysis of the low-temperature SANS data requires additional assumptions, since the bare-core approximation which was used at 39 °C is not longer valid; both core and shell are highly swollen and do not have significantly different scattering contrast. Therefore, the mass of the core in the core-shell particles at 25 °C was fixed to the value independently obtained for the pure core at 25 °C.

The density profiles obtained from the fitting are shown in Fig. 4-9 and two important observations were made.

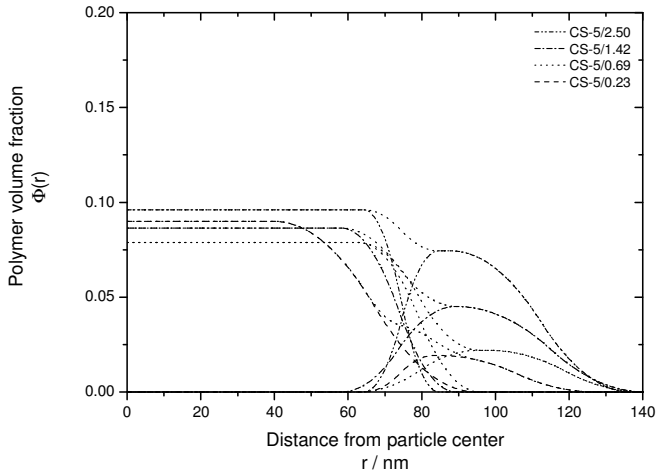

Fig. 4-9: Density profiles at 25 °C. The presence of the shell reduces the dimensions of the core compared to its native size (122 nm). The volume fraction in the shell increases with the shell/core mass ratio.

The volume fraction of the shell increases with higher shell masses, and the particle sizes correlate with the hydrodynamic radii from DLS. The observed low-q shift may be explained with the development of the polymer volume fraction in the shell as the shell mass increases. There is only a very small contribution to the scattering from the highly swollen shell with sample CS-5/0.23, which has the lowest shell mass. The contributions from the shell gain more weight as the volume fraction increases with higher shell masses. For the apparently larger particles, a shift to lower q values is found. The total density profiles of all samples smoothly decay similarly to the profiles of pure core microgels in the fully swollen state.
More remarkable is the fact that the dimensions of the core are significantly reduced to about 80-90 nm compared to the naked core where $R_i+2\sigma_i$ was found to be 122 nm. The situation at 25 °C is opposite to what happens at temperatures just below the shell's LCST. At 34 °C, the core begins to swell and pushes the shell in the radial direction, and an opposite force is developed in the shell due to the elasticity of the network. The cross-links in the shell close to the core-shell interface limit the core swelling. Even stronger forces from the core cannot lead to further size increase when the shell network is expanded to a maximum extent. The cross-linker content is similar in all shells, so that one may understand why the reduced core swelling is almost independent of the shell mass.

It should be noted that application of a symmetric interpenetration fails in the case of sample CS-5/0.23, which has the lowest shell mass, and an asymmetric profile needs to be employed to fit the data. For this sample, the shell is slightly displaced outward resulting in a shallow minimum in the polymer volume fraction between the core and shell. This could indicate that, for a very small shell, the attachment of the shell primarily occurs at the dangling chains of the core, leading to a poorer connection of the shell to the core, which is observed as a low polymer concentration at the core-shell interface.

In Fig. 4-10, the density profiles of sample CS-5/1.42 for all evaluated temperatures are shown. In comparison to the structure obtained at 50 °C, where core and shell are collapsed, one observes a large difference in the volume fractions of core and shell. Although the temperature is well above the core LCST, the size of the core is increased because of the force developed in the swollen shell, which expands the core. The 25 °C profile shows low polymer volume fractions in the core and the shell and smoothly decays from the particle center in a similar manner observed for PNIPAM microgels well below the LCST.

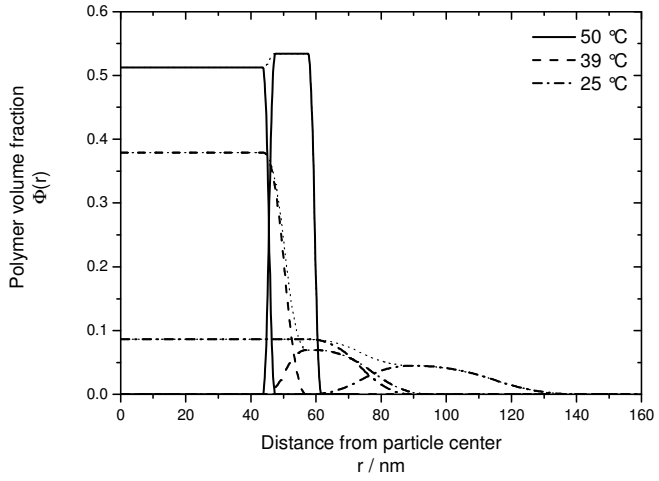

Fig. 4-10: Radial density profiles of sample CS-5/1.42 at temperatures 50, 39, and 25 °C. At the intermediate temperature, the core reveals increased dimensions due to expanding forces developed by the swollen shell.

4.4.2 Influence of Cross-Linker Content in the Shell

A second series of PNIPAM core-PNIPMAM shell microgels has been investigated. The three samples of this series have a nearly constant mass ratio m_{shell}/m_{core} of 0.54, 0.77, and 0.79, respectively, but differ in the amount of cross-linker in the shell. Cross-linker concentrations of 3, 7, and 9 mol% have been employed in samples CS-3/0.54, CS-0.77, and CS-9/0.79. Dynamic light scattering reveals smaller particle sizes at lower temperatures when the cross-linker content is increased, because a higher degree of cross-linking reduces the swelling properties.[16]

4.4.2.1 Behavior at high temperature: LCST (core) < LCST (shell) < T

The scattering profiles of samples CS-3/0.54, CS-7/0.77, and CS-9/0.79 in comparison with the parent core are shown in Fig. 4-11. The core-shell particles with constant mass ratios and varied concentrations of cross-linker in the shell do not significantly differ in size at this temperature. The minimum at $q \approx 0.007$ Å^{-1} of sample CS-3/0.54 is only slightly shifted to higher q-values compared to the other samples with higher cross-link density in the shell. The small size differences are caused by the difference in the extent of incorporation of chains into the particle; it has been shown that lower cross-linker densities lead to a higher fraction of linear polymer chains.[36] The free polymer chains had been removed by ultra-centrifugation.

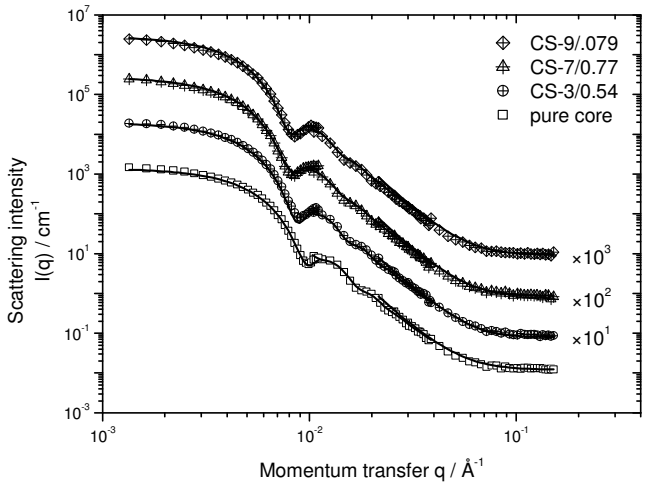

Fig. 4-11: SANS data at 50 °C: Core-shell microgels with varied shell cross-linker content. The form factor minimum of sample CS-3/0.54 is slightly shifted toward higher *q*-values compared to the two other samples indicating a smaller particle size due to lower polymer conversion during synthesis.

The SANS analysis proceeded in the same manner as with the series with different shell thicknesses. On the basis of the density profile of the parent core and the volume fractions of fully collapsed PNIPMAM microgels with comparable cross-linker densities, which have been investigated separately,[37] the width and surface fuzziness of the shell have been fitted by the model equation, and the results are also summarized in Tab. 4-2, and the radial density profiles are displayed in Fig. 4-12.

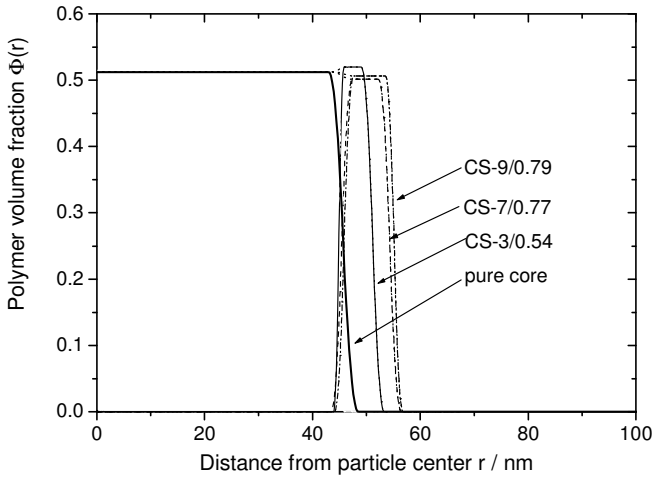

Fig. 4-12: Density profiles of core-shell microgels with varying shell cross-linker content from 3 to 9 mol% at 50 °C. The structures are-well described by a profile of two boxes with narrow interfaces.

Similar to the first core-shell series, the density profiles are well described by a two-box profile with a narrow interpenetrating layer between core and shell and a sharp outer surface. The widths of the core-shell interface $2\sigma_{in}$ and of the shell surface $2\sigma_{out}$ range between 2-3.8 nm and 3.2-4.2 nm, respectively. These parameters are comparable to what was found for the first series. Polydispersities of 7-11 % were obtained from the fits and slightly increase at lower temperatures to ca. 15 %. One should note that the polymer volume fraction of the shell (50.6-52.0 %) in the collapsed state is not significantly influenced by the cross-linker density.

4.4.2.2 Behavior at intermediate temperature: LCST (core) < T < LCST (shell)

On first glance, the scattering profiles at 39 °C (Fig. 4-13) of these samples look very similar, and only a slight shift of the form factor minima is observed with higher shell cross-linker contents. The slope in the intermediate q-range (q=0.01-0.04 Å^{-1}) is a little more flat than compared to the pure core, indicating again that there are small contributions from the swollen shell to the scattering profile.

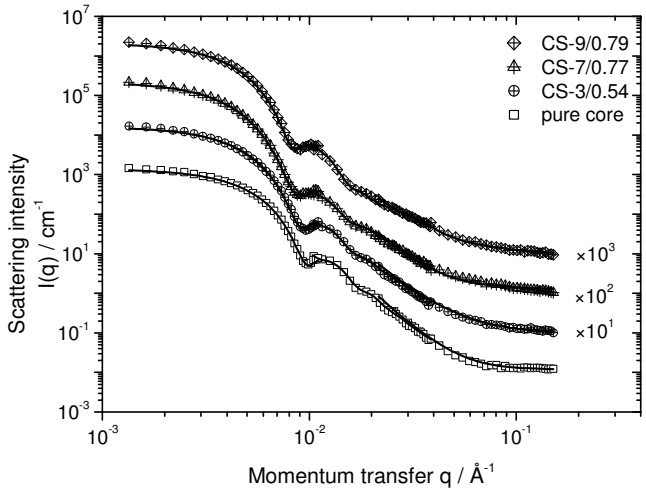

Fig. 4-13: Scattering profiles of core-shell microgel with varied shell cross-linker content at 39 °C. The profiles look similar with a slight shift of the form factor minima to smaller *q*-values indicating an increase in the size of the core.

Fig. 4-14 shows the radial density profiles obtained from the fitting procedure. In comparison to the naked core, the core sizes are increased to a similar extent as that found for sample CS-5/0.69, which has a comparable core-shell mass composition.

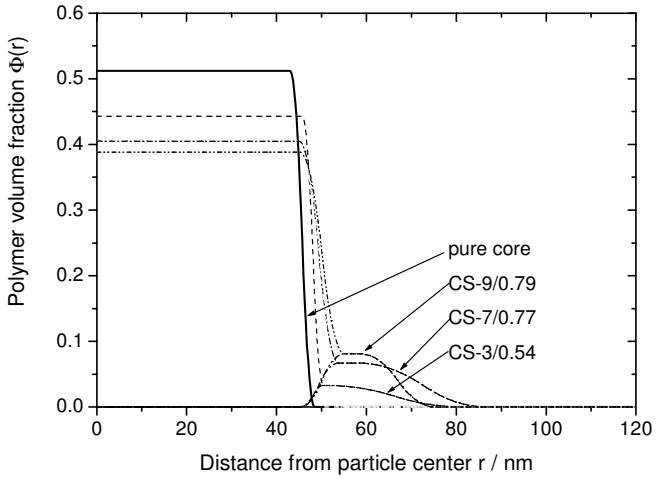

Fig. 4-14: The density profiles obtained from the fitting procedure at 39 °C reveal slightly increased size of the core due to the presence of the swollen shell. The thickness of the shell increases with lower cross-linker contents (CS-7/0.77 and CS-9/0.79).

The fits give similar values for the width of the core W_{core} (45.0-45.7 nm), but the thickness of the core shell interface $2\sigma_{in}$ broadens from 4.6 to 9.8 nm from sample CS-3/0.54 to CS-9/0.79. Obviously, a more highly cross-linked shell can develop a stronger force to expand the shell. Although more highly cross-linked gels are less swellable, one can assume that the efficiency of how the force from the shell is exerted onto the core depends on the degree of cross-linking. The force transmission of a loosely cross-linked shell is less effective. However, one has to keep in mind that the force transmission will also become weaker at overly high cross-linker densities when the shell's ability to swell is small.

The shell profiles of samples CS-7/0.77 and CS-9/0.79 demonstrate the influence of the shell cross-linker content on the total particle size. The shell volume fraction of sample CS-9/0.79 is 8.1 %, a little higher than that found for CS-7/0.77 with 6.7 %. As the cross-linker gradient of the shell in CS-7/0.77 is higher than in CS-9/0.79, the outer regions of the shell in this sample will consist of more loosely cross-linked chains, which increase the total size, whereas the shell profile of sample CS-9/0.79 reveals a more compact structure. Sample CS-3/0.54 cannot directly be compared to the others, because the relative shell mass is not exactly the same. In comparison with the other samples, the molar cross-linker content is very low. These

two facts lead to a more loosely cross-linked gel and more linear chains in the shell, and the polymer volume fraction is only 3.3 %. In accordance with the previous discussion for the other series, the shell in this sample will develop the weakest force to expand the core.

The 39 °C data demonstrate the validity of the bare-core approximation as the position of the form factor minimum is mainly determined by the size of the (dense) core independently from the thickness of the swollen shell.

4.4.2.3 Behavior at low temperature: T < LCST (core) < LCST (shell)

The low-temperature scattering data also agree with the results from the first series. The radial density profiles calculated from data at 25 °C (Fig. 4-15) reveal similar structures to what has been found for the core-shell series at this temperature.

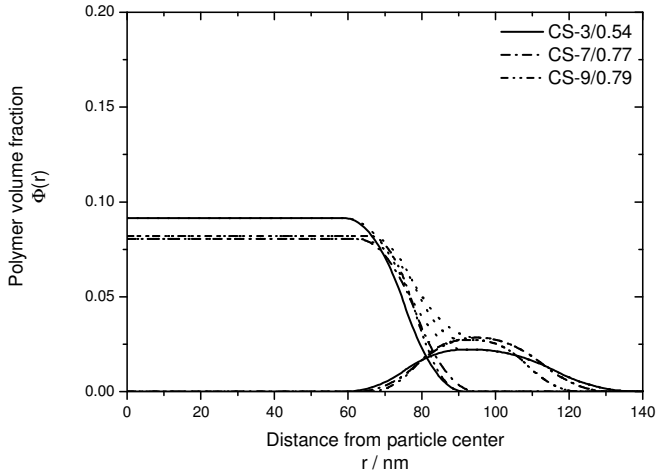

Fig. 4-15: Density profiles of samples with varied shell cross-linker content at 25 °C. The increase of particle size has to be contributed to the larger swelling ability when the cross-linker content in the shell is reduced.

The core reveals a reduced size compared to its native size at this temperature in the absence of a shell. It seems that the cross-linker density of the shell does not significantly influence the extent of core compression. One could argue that less cross-linked shells are more flexible

because the elastic modulus increases with the number of cross-links in the network, and so, one should expect larger a core size for the least cross-linked shell.

The increased hydrodynamic particle sizes as measured by DLS (Fig. 4-2b) are correlated with the shell properties. Less cross-linked shells reveal a higher ability to swell, and there are more linear chains in the outer regions of the shell, which contribute to the hydrodynamic size. In Fig. 4-15 a more slowly decaying shell surface is observed with lower shell cross-linker content.

4.5 Conclusions

A core-shell form factor model was employed for the evaluation of small-angle neutron scattering data of core-shell microgels composed of the temperature-sensitive polymers poly-*N*-isopropylacrylamide and poly-*N*-isopropylmethacrylamide with different LCSTs in the core and the shell. The influence of shell thickness and cross-linker content in the shell on the internal structure was investigated at temperatures well above the LCST of both polymers, between these temperatures, and below them. At high temperatures, the radial structure is well-described by a profile of two boxes with a sharp outer surface and narrow interface between core and shell. At temperatures between the two LCSTs, the core profile can still be regarded as a box but with increased dimensions and a broadened core-shell interface, because the swollen shell develops a force, which *expands* the core. This expanding force increases with the shell/core mass ratio. Investigation of the shell cross-linker content at this temperature shows slightly increased core dimension with higher cross-linker densities in the shell. It was shown that both shell mass and cross-linker content lead to an expanded core. But a significantly expanded core was found only in the presence of a moderately cross-linked shell with a big mass. Below the core LCST, the dimension of the core was found to be *smaller* than in the absence of a shell. The polymer network in the cross-linked shell prevents the core from swelling to its native size. The effect of core compression at this temperature is rather independent of shell mass and cross-linker content, because only a thin layer of the shell network close to the core/shell interface is responsible for this effect.

Acknowledgement. Financial support by the Deutsche Forschungsgemeinschaft (DFG) and by the Danish Natural Science Research Council is gratefully acknowledged. We thank Bente Olsen, University of Aarhus, for performing the density measurements.

5 Temperature-Sensitive Core-Shell Microgel Particles with Dense Shell

5.1 Introduction

Polymeric nanoparticles with core-shell morphology offer promising properties for applications in biomedical as well as technical fields.[1,2,3,4,5] Block-copolymers, which self-assemble into micelles belong to this type of particles. In the micelles the insoluble blocks form a dense core, which is surrounded by a corona of the soluble blocks.[6,7] Micellar structures, however, lack an intermolecular connection of the unimers and thus may dissolve as function of e.g. salt concentration, mechanical forces or simple dilution, which limits their application as smart materials. However, block-copolymer micelles with improved stability against dilution could be synthesized by covalently cross-linking core or shell.[8,9,10,11] Other approaches employed dendrimers or hyperbranched polymers.[12,13,14] Particles with even more sophisticated properties can be obtained when environmentally responsive polymers are incorporated. Using these, nanoparticles with spatial separation on colloidal length scales of regions with different sensitivities can be prepared.[15,16,17,18]

Systems with core-shell (or core-corona) morphology mostly display a density profile that decays from the particle center to its periphery. Core-shell nanoparticles where the shell has a denser structure compared to the core might provide superior properties useful for many applications, as e.g. in controlled release or sensors.

Dendrimers originally have been assumed to possess a structure with a rather open interior region that is surrounded by a denser shell, as the number of end groups grows exponentially with the dendrimer generation.[19] However, the presence of a dense shell would be observed only under very distinct conditions[20] and usually dendrimers have a dense core and a monotonically decaying density profile as was demonstrated by means of neutron scattering investigations and computer simulations.[21,22]

Recently, multi-responsive core-shell microgels have been introduced and investigated by various experimental techniques as e.g. fluorescence spectroscopy, calorimetry and small angle neutron scattering (SANS). This has revealed the mutual influence of core and shell on the temperature dependent swelling. However, the systems were characterized by having a shell density, which is lower compared to that of the core.[23,24,25,26]

In this contribution we present a core-shell microgel consisting of poly-*N*-isopropylacrylamide (PNIPAM) in the shell and poly-*N*-isopropylmethacrylamide (PNIPMAM) in the core. Both polymers display a lower critical solution temperature (LCST) in aqueous solution; in D_2O the transition temperatures are ca. 34 °C for PNIPAM and 44 °C for PNIPMAM, whereas in H_2O the transition temperatures are slightly lower. As a consequence the particle size of the core-shell microgel decreases upon heating in two steps. These doubly temperature sensitive microgel particles are expected to have a denser shell when the temperature is in between the two LCSTs such that the shell is collapsed but the core is swollen.

The microgel structure has been analyzed by means of SANS and dynamic light scattering (DLS). A core-shell form factor, which has been successfully applied for the analysis of SANS data from core-shell microgels with PNIPAM core and PNIPMAM shell,[25,26] was used in order to fit the experimental data. For the current application, modifications of the form factor were required to allow for different widths of the various interfaces of the particles. Radial density profiles revealing the real space structure have been calculated by Fourier transformation of the scattering amplitude which was obtained from fitting the form factor model to the SANS data.

5.2 Experimental Section

Core-shell microgels were prepared in two steps. PNIPMAM core particles were synthesized in a similar fashion as PNIPAM microgels via surfactant aided radical precipitation polymerization[27,28] and served as nuclei for the subsequent polymerization of the PNIPAM shell. A mixture of 0.5 g NIPAM monomer, 9.6 mg cross-linker monomer *N*,*N´*-methylenbiscarylamide (1.4 mol% with respect to total monomer) and 5.1 mg surfactant SDS in 25 ml water was added to 25 ml of the core solution (0.5 g microgel) and the polymerization was initiated with 12.1 mg of potassium peroxodisulfate. For experimental details see ref.[17,26] Hydrodynamic radii were determined by DLS from highly diluted samples

(c<0.01 wt%) in heavy water with an ALV goniometer setup at a laser wavelength of 632.8 nm and at a scattering angle of 90°. SANS measurements were carried out at the D11 facility of the Institut Laue-Langevin (ILL), Grenoble, France, on a 0.2 wt% sample at detector distances 2.5, 10.0, and 36.7 m to cover the q-range from 0.0015 to 0.2 $Å^{-1}$. Data were corrected for background scattering and calibrated on absolute scale by incoherent water scattering according the standard procedures at the ILL.

5.3 Theory

An expression for the scattering form factor was developed that allows describing the radial scattering length density distribution of core-shell microgels. A schematic picture of the model's radial density profile is displayed in Fig. 5-1. The center parts of core and shell with homogeneous density are described by W_{core} and W_{shell}. The microgel surface is fuzzy due to the inhomogeneous spatial distribution of cross-links within the particle.[29] A profile with a fuzzy surface can be expressed by a parabolic shape with half width radius R and interface width σ:

$$\rho(r) = 1 \quad r \le (R-\sigma) \tag{5-1a}$$

$$\rho(r) = 1 - \frac{1}{2}\frac{\left[(r-R)+\sigma\right]}{\sigma^2} \quad (R-\sigma) < r \le R \tag{5-1b}$$

$$\rho(r) = \frac{1}{2}\frac{\left[(R-r)+\sigma\right]^2}{\sigma^2} \quad R < r \le (R+\sigma) \tag{5-1c}$$

$$\rho(r) = 0 \quad (R+\sigma) < r\,. \tag{5-1d}$$

The width of the central part is given by $W=R-\sigma$ and the volume is $V=4\pi(R^3/3 + R\sigma^2/6)$. The normalized Fourier transformation of this profile can be expressed analytically as:

$$\begin{aligned}\Phi(q,R,\sigma) = \frac{4\pi}{V}\Bigg[&\left(\frac{R}{\sigma^2}+\frac{1}{\sigma}\right)\frac{\cos\left(q(R+\sigma)\right)}{q^4} + \left(\frac{R}{\sigma^2}-\frac{1}{\sigma}\right)\frac{\cos\left(q(R-\sigma)\right)}{q^4} \\ &- \frac{3\sin\left(q(R+\sigma)\right)}{q^5\sigma^2} - \frac{3\sin\left(q(R-\sigma)\right)}{q^5\sigma^2} + \frac{2\cos(qR)}{q^5\sigma^2} + \frac{6\sin(qR)}{q^5\sigma^2}\Bigg]\end{aligned} \tag{5-2}$$

The model was further modified such that the interpenetration at the core/shell interface is not necessarily symmetric. This allows having a "depletion" zone between core and shell, i.e. a region with a lower polymer volume fraction than in the centers of core and shell. The core part of the particle has radius R_{core}, interface width σ_{core}, volume $V_{core}=4\pi(R_{core}^3/3 + R_{core}\sigma_{core}^2/6)$, and scattering length density $\Delta\rho_{core}$. The outer dimensions of the shell are given by R_{out} and the width of the outer surface profile is σ_{out}. The inner dimensions of the shell are characterized by $R_{shell\text{-}in}$ and the width of the inner interface is $\sigma_{shell\text{-}in}$. With this the volume of the shell is $V_{shell}=4\pi[(R^3_{out}/3 + R_{out}\sigma^2_{out}/6)-V_{shell\text{-}in}]$, with $V_{shell\text{-}in}=4\pi[R^3_{shell\text{-}in}/3 + R_{shell\text{-}in}\sigma^2_{shell\text{-}in}/6]$ and the scattering length density is $\Delta\rho_{shell}$. One can calculate the parameter D, which describes the 'displacement' of the core and inner shell interface and it is this parameter that makes it possible to have a displacement of the centers of the two interface profiles. One has $D = R_{shell\text{-}in}-R_{core}$.

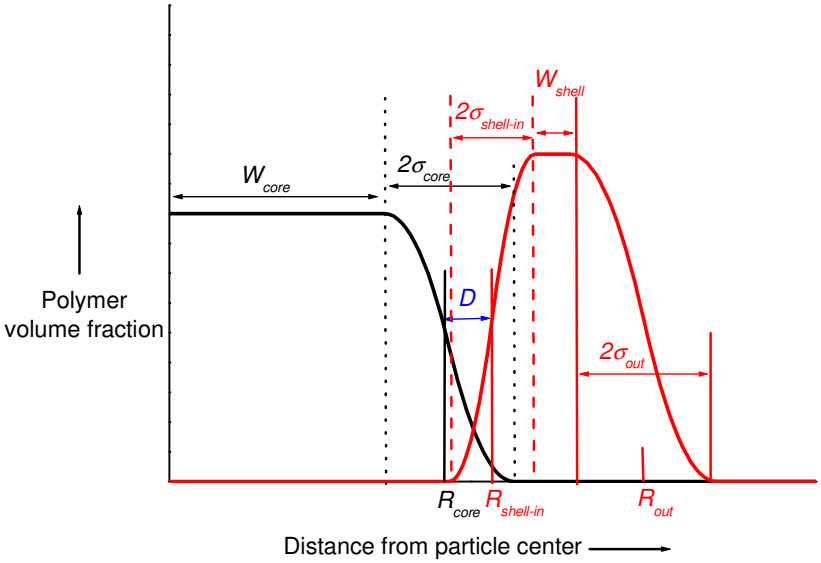

Fig. 5-1: Schematic representation of the radial density profile in core-shell microgel with a 'displaced' core-shell interface.

Using these definitions, the scattering amplitude of a core-shell particle with an asymmetric interface can be expressed as:

$$A(q) = \Delta\rho_{shell} V_{shell} \Phi(q, R_{out,} \sigma_{out}) - \Delta\rho_{shell} V_{shell-in} \Phi(q, R_{shell-in}, \sigma_{shell-in}) + \Delta\rho_{core} V_{core} \Phi(q, R_{core}, \sigma_{core}) \quad (5\text{-}3)$$

The half width radius of the core is $R_{core}=W_{core}+\sigma_{core}$ and the half width radius of the particle is $R_{out}=R_{core}+D+\sigma_{shell\text{-}in}+W_{shell}+\sigma_{out}$. The resulting form factor is given by the squared scattering length amplitude $P(q)=A^2(q)$. Polydispersity was included in the model using a Gaussian size distribution; a relative size distribution of ca. 10% (typical of such microgels) was obtained thus the sample can be considered as very monodisperse. Finally the model expression was convoluted by the resolution function, which describes instrumental smearing.[30] The model expression was fitted to the experimental data using least-square methods.[31]

5.4 Results and Discussion

Fig. 5-2 displays the influence temperature on the hydrodynamic radius (in D_2O) of the PNIPMAM core-PNIPAM shell microgel and, for comparison, of the parent PNIPMAM core. Two distinct transitions are observed for the core-shell microgel.

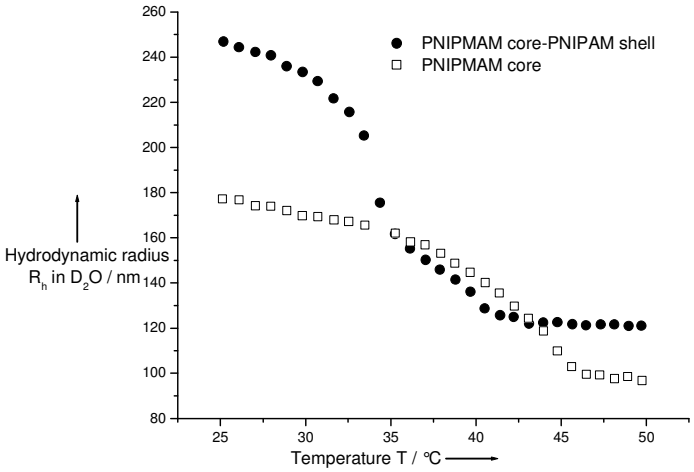

Fig. 5-2: Hydrodynamic radii of the PNIPMAM core-PNIPAM shell microgel and of the parent PNIPMAM core. The core-shell particle is smaller than the core in the intermediate temperature range from 35-41 °C.

The collapsed state at high temperatures can be regarded as a reference state since the synthesis proceeded at 70 °C, which is well above the core LCST and thus the shell is polymerized onto the collapsed core microgel. At temperatures above 45 °C the core-shell particle has a radius that is 13 nm larger as compared to the parent core. A continuous increase of the particle size is observed for the naked core when the temperature is decreased below the LCST of PNIPMAM. However, in the case of the core-shell microgel, the transition is shifted by 4 °C towards lower temperatures and only a slight increase of the hydrodynamic radius is observed when lowering the temperature. The core-shell microgel is smaller as compared to the naked core at temperatures between 35 and 41°C.

Although DLS can just provide information on the overall particle size, it is obvious that the presence of the shell significantly alters the swelling behavior of the core. When the temperature is further decreased below the LCST of PNIPAM a large increase in the hydrodynamic radius is observed and the size of the fully swollen core-shell microgel particle is larger than that of the parent core.

Differential scanning calorimetry and SANS experiments with core-shell microgels that consist of a PNIPAM core and a PNIPMAM shell have shown that a swelling shell exerts an elastic force on the collapsed core that expands the core and shifts the collapse temperatures

to higher values.[18] With the inverse core-shell microgel with a PNIPMAM core and a PNIPAM shell discussed here, the situation is opposite: at intermediate temperatures the collapsed shell restricts the core to a more compact structure as it prohibits the swelling of the core.

SANS can provide much more detailed information on the structure of colloidal particles in solution. SANS data obtained with the core-shell microgel are shown in Fig. 5-3; lines represent fits by the model. Fig. 5-4 displays the calculated radial density profiles and Tab. 5-1 summarizes structural parameters obtained from these fits.

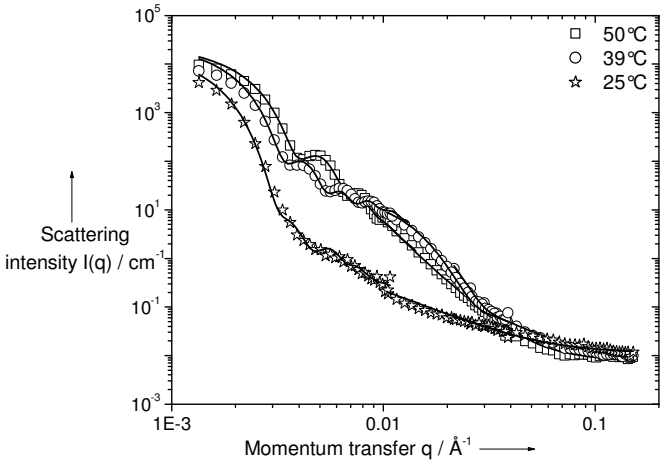

Fig. 5-3: SANS scattering data taken at 25, 39, 50 °C and fit lines according to the model.

At high temperatures, i.e. above both LCSTs, both core and shell are collapsed and the structure is well described by a density profile consisting of two boxes with a narrow interface and a sharp surface with a total width of 3-4 nm. In the high temperature case, the model could fit the data with a reduced number of parameters and especially D=0 and $\sigma_{shell\text{-}in}=\sigma_{core}$, i.e. a symmetric interface between collapsed core and collapsed shell describes the data. The polymer volume fractions in core and shell are similar at ca. 50 %. The parameter $R_{SANS}=R_{core}+D+\sigma_{shell\text{-}in}+W_{shell}+2\sigma_{out}$ gives the radius at which the shell density goes to zero. R_{SANS} can be compared directly to the hydrodynamic radius R_h determined by dynamic light scattering and very good agreement is observed.

Tab. 5-1: Structural parameters obtained from the analysis of SANS data with the model.

T °C	W_{core} nm	σ_{core} nm	Φ_{core} %	$\sigma_{shell\text{-}in}$ nm	D nm	W_{shell} nm	σ_{out} nm	Φ_{shell} %	R_{SANS} nm	R_h nm
50	95	1.5	50	1.5	-	15	2.0	51	117	121
39	72	28	41	10	13	1.2	9.8	53	144	143
25	80	45	15	23	3	1.1	46	4.7	244	247

At 25 °C, both core and shell networks are swollen. The density profile still shows a change in the segment density between core and shell, however, the profile decays constantly from the center to the periphery, as it is common and expected for microgels in the swollen state.[32,33]

Most interesting is the density profile obtained at 39 °C. The dimensions of the core are increased due to the swelling of the PNIPMAM at this temperature and the water content in the core increased. Nevertheless, the dimensions of the core at 39 °C (128 nm) are still reduced as compared to the pure, naked core at 39 °C, which were determined from SANS measurements to be 148 nm (not shown in the plot). More important, however, the density of the shell is *higher* than the density inside the core. At this temperature D_2O is already a good solvent for the PNIPMAM core but still a poor solvent for the PNIPAM shell. Apparently, the thermodynamic hydration forces that lead to the swelling of the core are not sufficient to expand the PNIPAM network in the shell. Consequently, a structure is obtained with a shell that is *denser* as compared to the core.

The total density profiles shown in Fig. 5-4 provide further information on the particle morphology. At the intermediate temperature of 39 °C a density minimum is observed at ca. 108 nm. At this temperature, the experimental SANS data could only be fitted with an asymmetric interface between core and shell, i.e. $D \neq 0$ and $\sigma_{core} \neq \sigma_{shell\text{-}in}$; this leads to a minimum of the total density.

Static light scattering and SANS investigations of simple (i.e. not core-shell) PNIPAM and PNIPMAM microgels showed that the cross-link density near the particle surface is lower than in the center of the particle when the particles are prepared in a batch polymerization.[32,33,34] This inhomogeneous distribution of cross-links is caused by different reaction kinetics of cross-linker and monomer.[29] Such an inhomogeneous cross-link density is

also present in the core of the core-shell microgels investigated in this study. Thus the network in the outer region of the PNIPMAM core near the core-shell interface can swell stronger as compared to the network in the center of the core. It is at first glance surprising that the core is now swollen in such a way that it has an inhomogeneous density. However, one should keep in mind that the swelling is a result of the systems tendency of maximizing the conformational entropy of the polymer strands between cross-links. Swelling is a more effective way of increasing the entropy in the outer region with low cross density (long strands) compared to that of the more cross-linked (short strands) core center and this is valid also with the gel encapsulated in a constraining shell. The pressure of the swollen core on the collapsed PNIPAM shell leads to a lateral stretching of the shell and a slight increase in the maximum density in the shell compared to what is found at the higher temperature.

An interpenetrating network of core and shell material is formed when the shell is formed on the collapsed core. Referring to results from fluorescence experiments by Lyon and coworkers,[23,24] we can assume that this interpenetration layer does not penetrate strongly into the core. Consequently, the core network close to the core-shell interface, but not yet inside the interpenetrating network region, is characterized by long strands that can swell strongly at 39 °C. This leads to the segment density minimum shown in Fig. 5-4.

The density profile at the particle surface, i.e. the outer profile of the shell, at 39 °C does not decay as strongly as at 50 °C, although the PNIPAM chains at the shell surface should still be in the collapsed state. This could indicate that the surface is slightly rough. As already mentioned above, the swelling core exerts a lateral stretching force on the shell at the core-shell interface, which can lead to some buckling of the shell. Since a scattering experiment provides averaged information, the slightly smeared surface profile could be caused by a locally rough surface. At 25 °C the particle surface profile is characterized by a broad decay as it is known from pure PNIPAM microgels.

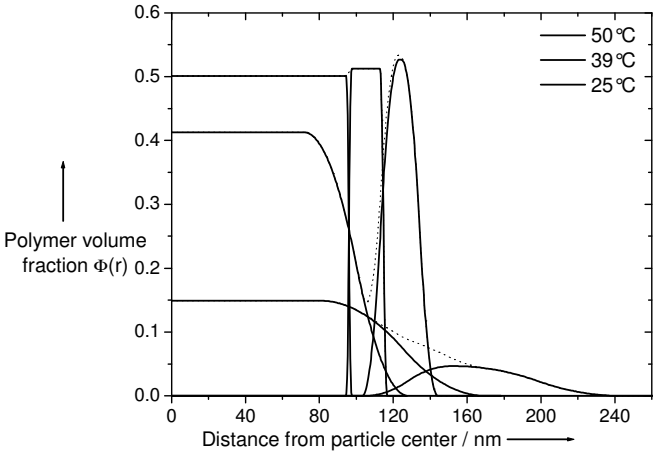

Fig. 5-4: Radial density profiles calculated from the modelling procedure at 25, 39, and 50 °C. At the intermediate temperature the shell reveals a higher density than the swollen core.

The data presented here demonstrate that different temperature sensitive polymers can be combined in core-shell microgels in order to tailor and control the density profile in different regions of the particle. The change of density ratio of core and shell with temperature can lead to different uptake and release properties, as compared to core-shell microgels with different chemical functionalities in core and shell, respectively. Adding further shells, as e.g. grafted chains, can be used to design even more sophisticated nanoparticles.

5.5 Conclusions

In conclusion, we present a doubly temperature sensitive core-shell microgel, which at intermediate temperatures reveals a shell with a higher segment density than the core. The temperature dependence of the hydrodynamic radius already demonstrated that the shell restricts the core swelling at temperatures between the LCSTs of core and shell. More detailed information is obtained from small-angle neutron scattering. A new form factor model was developed that describes experimental scattering curves at different temperatures. This analysis provides radial density profiles, which clearly show that the shell is denser than the core at intermediate temperatures. Due to the pronounced temperature sensitivity of core and shell polymers, such core-shell microgels display unique properties that can be tailored via the

synthesis and which can be useful in many different applications as e.g. encapsulation of active ingredients. In addition the form factor model developed here can be applied very generally to particles with core-shell morphology and displaced interfaces.

Acknowledgement. Financial support by the Deutsche Forschungsgemeinschaft (DFG) is gratefully acknowledged. We thank the Institut Laue-Langevin (ILL), Grenoble, France, for beam time at the D 11 instrument and Dr. Peter Lindner for local support.

6 Mechanics versus Thermodynamics: Swelling in Multi-Temperature Sensitive Core-Shell Microgels

Abstract. The thermal transition of a thermo-responsive microgel of poly-*N*-isopropylacrylamide is shifted from 34°C to higher temperatures when it is embedded in a shell of temperature-sensitive poly-*N*-isopropylmethacrylamide with a transition temperature of 44°C. The magnitude of the shift depends on the shell-core mass ratio. A very thick shell induces an additional third transition between the two temperatures due to strong mechanical forces exerted on the core. The temperature shift can be interpreted in terms of a "chemo-mechanical" model.

6.1 Introduction

The incentive to prepare multifunctional nanomaterials has inspired various synthetic approaches in the last year and several different approaches, where different chemical functionalities are incorporated at different positions within the molecule, have been explored, as e.g. dendrimers, hyperbranched polymers or cross-linked micelles.[1,2,3,4,5]

A second field of research concerns stimuli-responsive nanomaterials. Here thermosensitive microgels, often based on poly-*N*-isopropylacrylamide (PNIPAM) which exhibits a lower critical solution temperature (LCST) of ca. 32 °C in H_2O (and ca. 34 °C in D_2O), have been intensively investigated in the past years and found application in numerous fields.[6] More advanced polymer architectures can lead to materials with superior properties and e.g. core-shell microgels responsive to two external stimuli (temperature and pH) have been introduced by Lyon and co-workers.[7,8]

Multiresponsive core-shell microgels can display unique behavior since the two domains, core and shell, respectively, are mechanically linked. Indeed it has been observed that the degree of swelling of core and shell region is mutually influenced.[9,10,11,12] However, it is not clear whether such a mechanical connection can lead to qualitatively different properties.

In this contribution we report on the thermal behavior of aqueous (D_2O) solutions of core-shell microgels composed of temperature-sensitive PNIPAM core and a temperature-sensitive shell of poly-*N*-isopropylmethacrylamide (PNIPMAM), the latter exhibits a LCST of ca. 44 °C. These particles combine the two above-mentioned concepts: two polymers with different temperature sensitivity are combined in spherical core-shell morphology. The mutual influences can be controlled via the core/shell mass ratio.

6.2 Experimentals

Thermal measurements were carried out with a Perkin-Elmer Pyris 1 DSC. Stainless steel pans with silicon rubber gaskets were used as sample holders and a pan with 30 mg of heavy water was used as reference. The sample environment was rinsed with a nitrogen flow during the measurement. Approximately 30 mg of a 6 wt% microgel dispersion in D_2O was used per measurement. D_2O was used as solvent for comparability with small-angle neutron scattering results. The study was carried out over a temperature range from 25 to 55 °C with a constant heating rate of 2 K min^{-1}. For all samples at least two heating and one cooling run were performed and all transitions are fully reversible and appear in each heat-cool cycle. Several heating-cooling rates (0.5, 1, 2, 5, 10 and 20 K min^{-1}) were employed for sample CS-5/0.69 and an influence of the rate on the transitions was only observed for rates ≥10 K/min. The errors in calculating the enthalpies were determined from the peaks in repeated cycles and were <5%, in most cases <1%. The sample names in Tab. 6-1 reflect the composition of the particles. The core-shell samples are all based on the same PNIPAM core with a molar cross-linker content of 1.4%. The pure PNIPMAM microgel and the PNIPMAM shell have a cross-linker content of 5 mol% denoted by the first number in the name. The second number refers to the particle composition given by the mass ratio m_{core}/m_{shell}. Synthesis, removal of soluble polymer chains via ultracentrifugation and sample preparation are described elsewhere.[11,12]

6.3 Results and Discussion

Core-shell microgel particles composed of a poly-*N*-isopropylacrylamide (PNIPAM) core and shell of poly-*N*-isopropylmethacrylamide (PNIPMAM) with a wide range of core/shell mass compositions have been investigated in this study. In aqueous solution these particles show a two-step shrinking behavior corresponding to the LCSTs of core and shell polymer.

Fig. 6-1 shows the baseline-corrected and normalized DSC thermograms of four PNIPAM core-PNIPMAM shell microgels with core/shell mass ratios of 1:0.23, 1:0.69, 1:1.42, and 1:2.50. All core-shell samples are based on the same PNIPAM core. The core-shell microgels exhibit, generally, two peaks, which correspond to the shrinking processes of the core at low and shell at high temperature, respectively.

With increased amount of PNIPMAM in the shell, i.e., increased shell thickness, one observes a shift of the core's transition peak towards higher temperatures from 32.5 to 33.8 °C. The peak temperatures of the shell transition stay fairly constant at 44.5 °C, except in the case of a very thin shell where the peak transition is reduced to 41.8 °C. This observation will be explained further below.

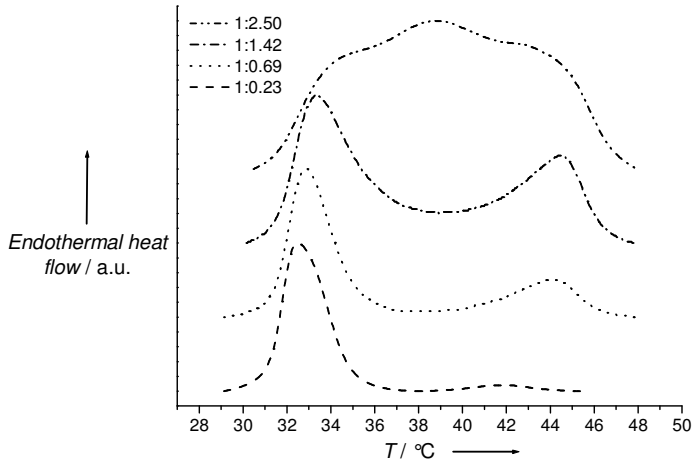

Fig. 6-1: Normalized DSC thermograms of PNIPAM core-PNIPMAM shell microgels with core/shell mass ratios of 1:0.23, 1: 0.69, 1:1.42 and 1:2.50, recorded at a heating rate of 2 K min^{-1}.

A general kinetic function was employed to deconvolute the DSC signals and allowed characterizing each peak by its enthalpy and peak temperature assuming a weighted superposition of each thermal process.[13] Peak temperatures and calorimetric heats of the thermal transitions of the core-shell particles as well as of the pure core and shell materials are listed in Tab. 6-1.

Tab. 6-1: Peak temperatures and calorimetric heats of core-shell microgels and pure core and shell material.

sample	mass ratio	core transition		shell transition	
		T / °C	ΔH_{PNIPAM} / kJ mol^{-1}	T / °C	$\Delta H_{PNIPMAM}$ / kJ mol^{-1}
pure core-1.4/0	1:0	32.5	5.38	-	-
CS-5/0.23	1:0.23	32.5	5.32	41.8	1.20
CS-5/0.69	1:0.69	32.8	4.94	44.3	2.61
CS-5/1.42	1:1.42	33.3	4.82	44.5	2.12
CS-5/2.50	1:2.50	33.9	2.47	44.5	2.01
CS-5/2.50	1:2.50	38.7	9.23	-	-
pure shell-5/1	0:1	-	-	43.0	5.04

The enthalpy values of the different transitions correlate very well with the variation in the samples' composition i.e. the shell/core mass ratio. For three samples the transition enthalpy of the PNIPAM core component are found to be 4.8-5.3 kJ mol^{-1} (i.e. per mol NIPAM repeating unit) and agree to data found in the literature for similar systems.[14,15] This indicates that the thermal transition of the PNIPAM component in these core-shell microgels, as measured by DSC, is not altered qualitatively by the presence of the other component. On the other hand, the enthalpy of the PNIPMAM transition as shell material in the core-shell microgels was always significantly smaller than compared to the enthalpy obtained for a pure PNIPMAM microgel with the same cross-linker content. Apparently, the swelling behavior in a shell is different; this will be discussed further below.

Most important, however, is the case of the core-shell microgel with the highest amount of shell component, i.e. with the thickest shell: Here a third peak appears at an intermediate temperature without any evident relation to the two polymer components. Fig. 6-2 demonstrates that all three peaks were also observed upon cooling; all transitions were fully reversible and appeared in each heat-cool cycle. With respect to the above-mentioned peak shifts this third thermal transition cannot be considered as an overlap of two distinct peaks of core and shell, respectively.

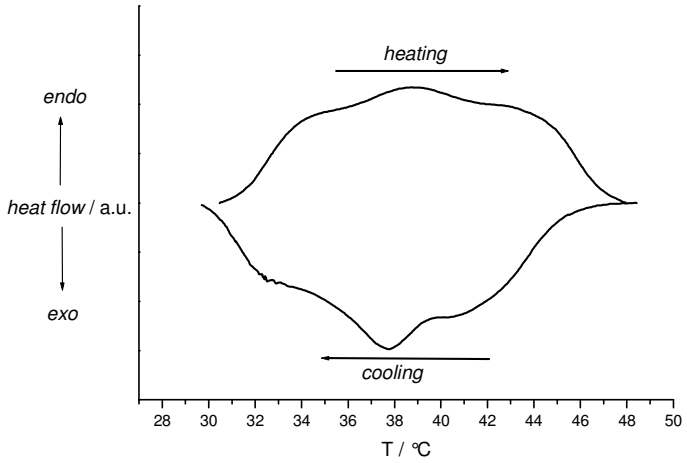

Fig. 6-2: DSC heating and cooling curve for PNIPAM core-PNIPMAM shell microgel sample CS-5/2.5 with core/shell mass ratio of 1:2.50 recorded at 2 K min^{-1}.

The influence of the composition on the core transition can be interpreted with a rather simple mechanical model.

The core-shell microgels are considered as spherical particles with a total radius *R*. Each particle is composed of a PNIPAM core of radius *r* and a PNIPMAM shell of thickness *d*. The total particle volume is denoted as V_{CS} and the volume of the core as V_C . We can assume that the densities of PNIPAM and PNIPMAM are very similar so that one can express the core-shell mass ratio as (Eqn. 6-1)

$$\frac{m_C}{m_S} = \frac{r^3}{R^3 - r^3} = \frac{1}{a} \tag{6-1}$$

with *a* being the relative amount of the PNIPMAM shell and the radius *r* of the PNIPAM core is thus given as (Eqn. 6-2)

$$r = \frac{R}{\sqrt[3]{1+a}} \tag{6-2}$$

Upon heating from a temperature below the core LCST, the core shrinks and expels water through the water permeable PNIPMAM shell and the heat signal recorded by DSC is directly proportional the shrunken dimension of the core $x=r_0 - r$ with r_0 the core radius at 25°C. Core and shell are connected by an interpenetrating network layer. Assuming this interaction of core and shell, the temperature shift may be understood as being caused by an elastic force developed in the shell, balancing the thermodynamic force and thus decreases the shrinking force in the core.

The total shrinking force F_c, that is acting in the core, is temperature dependent and can be expressed by Eqn. 6-3

$$F_C = k_C \cdot T \tag{6-3}$$

where k_C is a material constant of the core. This force drives the shrinking process in the core at elevated temperatures and is related to elastic properties of the PNIPAM network. Being an elastic force one may apply Hook's Law (Eqn. 6-4) for the core sphere of radius r_0:

$$\frac{F_C}{S_C} = \frac{k_C \cdot T}{4 \cdot \pi \cdot (r_0 - x)^2} = -E_C \cdot \frac{x}{r_0} \tag{6-4}$$

where $S_C=4\pi(r_0-x)^2$ is the surface on which the force is applied. When a PNIPMAM shell, which retains the core from collapsing, is present, one may write for the same shrinkage (Eqn. 6-5):

$$\frac{F_{CS}}{S_{CS}} = \frac{k_{CS} \cdot T'}{4 \cdot \pi \cdot (r - x)^2} = -E_{CS} \cdot \frac{x}{r} \tag{6-5}$$

The subscript *CS* denotes a material constant for the core-shell microgel and T' is the peak temperature shift due to the shell. The peak temperature shift caused by the elastic force of the shell is now readily inferred as the difference of the two temperatures above (Eqn. 6-6), calculated at x_p the core shrinkage at the peak temperature:

$$\Delta T_p = 4 \cdot \pi \cdot x_p \cdot \left[\frac{E_C}{k_C} \cdot \frac{(r_0 - x_p)^2}{r_0} - \frac{E_{CS}}{k_{CS}} \cdot \frac{(r - x_p)^2}{r} \right] \tag{6-6}$$

In Fig. 6-3 the experimental and calculated shifts ΔT_P of the core (PNIPAM) peak temperature are shown and very good agreement is observed. The thicker the shell, the stronger is the elastic force and the higher is the transition temperature of the core.

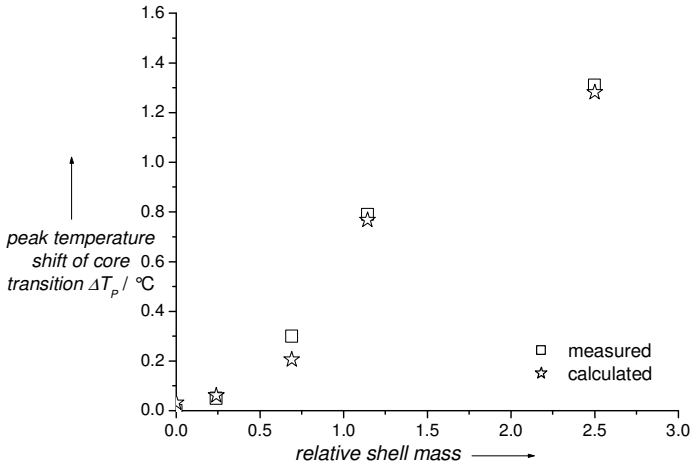

Fig. 6-3: Shifts of the core (PNIPAM) peak temperatures as measured by DSC and calculated from the elastic model compared to the pure core. Thicker shells lead to stronger elastic forces and higher transition temperatures.

The simple elastic model also accounts for the behavior of the second peak. For a very thin shell, its thickness cannot sustain itself against the shrinking force of the core and the core collapse leads to an earlier shrinkage of the shell due to confined geometry. Consequently, the temperature of this peak is lowered to 41.7 °C. For all other samples the shell can resist the collapse of the core and the temperature of the shell shrinking process stays fairly constant at 44.5 °C.

The sample with the thin shell can be compared with systems where a thermosensitive polymer is attached to a rigid particle.[16,17] In such a case the rigid substrate reduces the mobility of the chains in the shell and the transition is shifted to higher temperatures. In our

case the core can be considered as an "active" substrate and the shrinking core shifts the transition of the shell material to lower temperatures.

However, the model *cannot* explain the appearance of a third peak in case of a very thick shell.

Our group recently established a form factor model to analyze small-angle neutron scattering data (SANS) from such core-shell microgels.[12] This model provides the polymer volume fraction in the core and shell as well as the core size and the shell's thickness. The analysis of SANS data taken at 39 °C, where the third peak is found, reveals the radial density profiles shown in Fig. 6-4. The SANS data provide additional information on the swelling behaviour of core and shell.

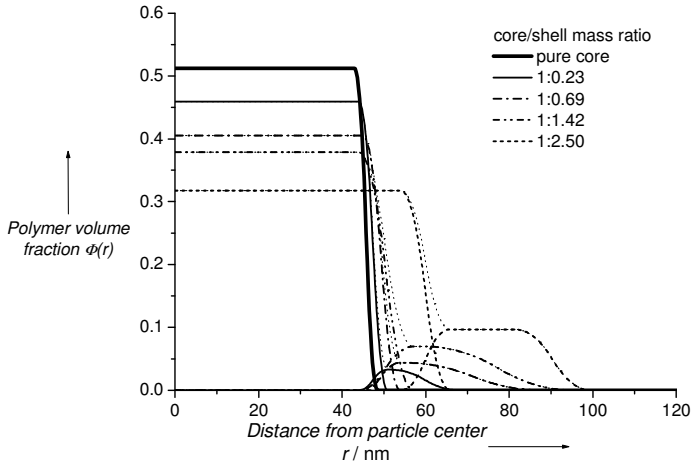

Fig. 6-4: Radial polymer volume fraction profiles of the PNIPAM core-PNIPMAM shell microgels and pure PNIPAM microgel at 39°C obtained from SANS.

The swelling properties of the shell material can be discussed in terms of the volume change when the temperature is reduced from 50 to 39°C. The form factor model described in ref.[12] enables one to calculate the shell volume at different temperatures taking into account the decay of the density profile at the particle surface. We find that the volume change in the PNIPMAM shell when the temperature is decreased from 50 to 39°C is much smaller than the volume change in a pure PNIPMAM microgel. Taking the volume change and enthalpy of the

pure PNIPMAM microgel as a reference allows comparing the ratio of experimental enthalpy values (i.e. ΔH per repeating unit in shell normalized by ΔH per repeating unit in pure microgel) with the ratio of volume changes in shell and pure microgel, respectively. These data are plotted in Fig. 6-5 and clearly show that the low enthalpy values that are found for the shell transition are correlated with the lower swelling ratio. Obviously, the PNIPMAM shell cannot swell as strong as a pure PNIPMAM microgel and consequently the heat flow is reduced.

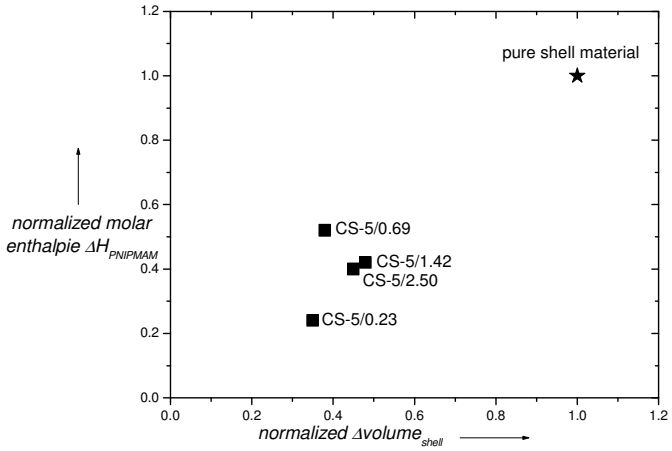

Fig. 6-5: Normalized enthalpy of the transition of shell component in core-shell microgels vs. normalized volume change of shell component. The experimental data of the pure PNIPMAM microgel were used for normalization.

The analysis of the SANS data provides also important information on the core's dimensions in the core-shell microgels. Compared to the pure PNIPAM microgel (bold line in Fig. 6-4), the core dimensions in the core-shell microgels with mass ratios up to 1:1.42 are only slightly increased. In agreement with the above-mentioned model, the core is the more expanded the stronger the elastic force from the shell is, i.e. the thicker the shell is. The sample with the thickest shell exhibits a rather *large, significant stretching* of the core.

The DSC analysis clearly shows that the third peak at intermediate temperature must be caused by additional molecular interactions. In principle these could come from the

interpenetrating network at the core-shell interface. However, Lyon et al. could demonstrate that the thickness of the interpenetrating network is rather limited[18] and furthermore should be identical for all samples. Thus, the third peak should be observed with all samples if it was caused simply by the interfacial region.

The experimental finding that the third peak in the DSC is only observed with the sample where the thick shell leads to a significant stretching of the core at intermediate temperature leads us to suggest that the additional thermal transition is caused by the breaking of hydrogen bonds between mechanically stretched chain segments. In other words, the conformations of the chains in the microgel network near the core-shell interface are altered when the elastic force in the shell overcompensates the thermodynamic force during the PNIPAM transition. These altered chain conformations will lead to the formation of different hydrogen bonds the breaking of which leads to the addition thermal transition.

6.4 Conclusions

In conclusion thermal characteristics of PNIPAM core-PNIPMAM shell microgels dissolved in D_2O have been investigated by DSC. DSC thermograms reveal two transitions assigned to the thermal transition of core and shell material. With increased shell thickness a shift of the core transition towards higher temperatures was observed and interpreted in terms of an elastic model. *Vice versa* a collapsing core can shift the transition of a thin shell to lower temperatures. An additional thermal transition is found in case of a very thick shell suggesting that the balance between the thermodynamic forces developed in the core material upon heating and the elastic force resisting a volume change of the shell leads to stretching of chain segments which allows additional hydrogen bonds to be formed. Thus an additional "chemo-mechanical" process is generated. Obviously, the competition between thermodynamic and elastic forces gives rise to *qualitatively* different behaviours thus demonstrating the unique properties of cross-linked, multiresponsive core-shell nanomaterials.

Acknowledgement. Financial support by the Deutsche Forschungsgemeinschaft (DFG) is gratefully acknowledged. The authors thank Dr. Heiko Huth, Institute of Physics, University of Rostock, for his support during the DSC experiments.

7 Summary and Outlook

7.1 Conclusions

The internal and overall structure of multi-temperature sensitive core-shell microgels was studied in the present work.

The particles consist of chemically cross-linked networks of two temperature sensitive polymers, namely poly-*N*-isopropylacrylamide (PNIPAM) and poly-*N*-isopropyl*meth*acrylamide (PNIPMAM), forming either the core or the shell. In aqueous solution these polymers exhibit lower critical solution temperatures (LCST) at 34 and 44 °C, respectively. Upon heating, the particles display two-step temperature induced structural changes. A first transition occurs when the LCST of PNIPAM is approached, the solvent quality of water changes from good to poor and the PNIPAM network undergoes a volume phase transition from a swollen to a collapsed state. Increasing the temperature further leads to the PNIPMAM network collapse when the LCST is reached. As both polymers are united in a single macromolecule though spatially separated in a centrosymmetric core-shell morphology, the temperature dependent swelling behaviour of core and shell is mutually influenced by opposing forces acting between core and shell.

The aim of this work was to explore the internal structure of these particles as a function of molecular structure, composition and the structure determining stimulus temperature.

I) The first steps were the synthesis of the core-shell microgels and the characterization by means of dynamic light scattering (DLS) and turbidity measurements.

The particles were prepared by a two-step seed-and-feed polymerization. Pre-existing PNIPAM core particles served as nuclei for the subsequent polymerization of the PNIPMAM shell. The amount of shell monomer and cross-linking monomer *N*,*N´*-methylenbisacrylamide (BIS) present during the shell polymerization were varied in order to investigate the influence of the shell thickness and the degree of cross-linking on the thermosensitive response of the

particles. The dispersions were purified by dialysis or ultracentrifugation. The latter allowed for the removal of low molecular weight by-products from the synthesis and for quantitative analysis of the core/shell mass composition.
Hydrodynamic radii as obtained by DLS revealed two distinct transitions of the particle size with increased temperature. It was observed for the core-shell microgel series with varied shell thickness, i.e. varied shell/core mass ratio, that the volume of the shell in the fully collapsed state linearly increased with the shell/mass ratio indicating a compact and homogeneous structure of the shell at this temperature. The particle size transition at 34 °C became less pronounced with thicker shells. The other series with a varied degree of cross-links in the shell exhibited more pronounced transitions both at 34 and 44 °C when the cross-linker content was decreased, since less cross-linked shells are more swellable. Small size differences at high temperatures above the shell LCST were associated with a reduced monomer conversation at lower cross-linker contents. Optical transmission measurements agreed qualitatively with the particle sizes, revealing transitions at temperatures assigned to the core and shell collapse.

II) Dynamic light scattering indicated mutual influence of core and shell swelling but did not yield information on the internal structure as it monitored only the entire particle size. Small-angle neutron scattering (SANS) on the other hand did provide both information on the entire particle as well as on the internal structure.
A core-shell form factor model was developed to analyze experimental SANS data. Due to the inhomogeneous distribution of cross-links throughout the particle, microgels (i.e. not core-shell particles) are described by a region of homogenous density in the interior and fuzzy surface at temperatures below the LCST. At high temperatures their structure was well described by a box-like profile with a sharp outer surface. Consequently, the new form factor model described the density profile of the core-shell microgels by two center parts of the core and the shell with homogeneous densities and a graded outer surface. Furthermore the model accounted for the interface between core and shell where both polymer networks interpenetrate. Real space information could be obtained from an analytical expression of the form factor calculating radial density distributions.
The radial density distribution at 50 °C was given by a profile of two boxes with similar densities and sharp interfaces according to the collapsed state of the core and the shell at this temperature. Decreased temperature below 44 °C led the shell to swell in tangential and radial

directions. The radial swelling directly contributed to an increase in particle size, whereas swelling in tangential directions led to strains at the core-shell interface, which could be released by stretching the core and core-shell interface. The scattering pattern at 39 °C, i.e. between the LCSTs, showed a low-q shift of the form factor indicating a particle size decrease which was contradictory to DLS results. The data analysis employing this model could explain this unexpected behaviour. The polymer density of the shell calculated from the model was about ten times smaller than that of the core. From the scattering point of view temperature changes could be regarded as contrast variation. Thus the scattering profile was dominated by the collapsed core that was smaller than the entire particle in the collapsed state at 50 °C. At 25 °C both core and shell network were highly swollen with solvent and a fuzzy outer surface was found. The particle sizes calculated from SANS were slightly smaller than observed by DLS due to dangling polymer chains at the particle surface that contributed to the hydrodynamics but could not be detected by SANS.

III) Once the form factor model was successfully established, it was employed to analyze the SANS data of two series of core-shell microgels. Both the influence of shell/core mass composition, i.e., the thickness of the shell in the collapsed state, and shell cross-linker content on the internal structure have been investigated by this means at temperatures above, between and below the LCSTs, respectively.
At high temperatures the radial structures were well described by a profile of two boxes with a narrow interface between core and shell and a sharp particle surface. The width of the box describing the shell increased with the mass of the shell revealing a proportional dependency of shell mass and volume as it was expected for a dense and homogeneous structure of the shell. At the intermediate temperature between the LCSTs, it was found that the dimension of the core was increased compared to its native state, i.e. without shell, at the same temperature. The influence on the core structure could be interpreted in terms of an elastic force developed in the swollen shell. This expansion force increased with the shell/core mass ratio. Consequently, thicker shells could exert a stronger force to the core. The influence of the shell cross-linker content at this temperature revealed only slightly increased core dimensions with higher cross-linked shell. The increase of both shell mass and cross-linker content led to an expanded core. However, a significant expansion was only observed in case of a moderately cross-linked shell with a very big mass.

At temperatures below the PNIPAM core LCST, the core could not swell to its native size and its dimensions were found to be smaller than in the absence of the shell. The shell polymer close to the core-shell interface was expanded to a maximum due to the presence of the cross-links and thus prevented further swelling of the core. The core compression was rather independent from the variation of the shell mass and cross-linking. Only a thin layer of the shell network close to the core-shell interface, which could be regarded as almost identical for all samples, was responsible for the restricted swelling of the core at the low temperature.

IV) An inverse core-shell microgel consisting of a PNIPMAM core and a PNIPAM shell was prepared and investigated in comparison to the PNIPAM core-PNIPMAM shell microgels by means of DLS and SANS.
These particles displayed two distinct transitions in particle size at temperatures according to the LCSTs of PNIPAM and PNIPMAM. In contrast to the other core-shell microgel, here first the shell collapsed at 34 °C followed by the transition of the core at 44 °C upon heating. The temperature dependency of the hydrodynamic radii already demonstrated a mutual influence of core and shell swelling. Particle sizes detected for the inverse core-shell system in the temperature range between the LCSTs were *smaller* than for the parent PNIPMAM core. Further it was observed that the PNIPMAM transition was shifted by 4 °C towards lower temperatures due to the compression of the core by the shell.
In order to fit the SANS data of these particles the core-shell form factor model was modified such that it allowed an asymmetric shape of the core-shell interface. The most interesting information was gained from the density profile at 39 °C. The analysis validated the core compression and further exhibited an inhomogeneous swelling of the core that was accredited to loosely cross-linked polymer chains near the core-shell interface, which did not interpenetrate with the shell network. The density profile at the particle surface decayed more smoothly than at 50 °C although the PNIPAM shell should still be collapsed. This indicated a slightly rough surface due to some buckling caused by a laterally exerted force from the core to the shell.

V) The thermo-chemical properties of PNIPAM core-PNIPMAM shell microgels were investigated in the last part of this work and compared to structural information obtained from the other methods of investigation.

DSC thermograms revealed two transitions attributed to the thermal transitions of the core and shell material. It was observed that the core transition shifted towards higher temperatures with increased shell/core mass ratios. Assuming a weighted superposition, the peaks were quantitatively evaluated and revealed a good agreement of the calorimetric heats and the sample composition in the case of moderate thick shells. The shift of core transition temperatures was interpreted in terms of an elastic model that balances the expanding forces from the shell and the forces, which lead to the collapse of the core above the LCST. In agreement with the structural information gained from SANS, thicker shells could exert stronger forces to the core, decreasing the shrinkage force of the core and thus increasing the transition temperature. A third thermal transition was found in the case of a very thick shell, where a significant expansion of the core was observed by SANS analysis, at a temperature not directly related to any of the components. This transition was explained by reorganized hydrogen bonds, which were formed by the stretching of chain segments close to the core-shell interface. The interaction of core and shell swelling could be regarded as a „chemo-mechanical“ process since the deformation of the core by external forces affects its thermodynamic properties.

The transition heats of the PNIPMAM shells were much smaller in comparison to a pure PNIPMAM microgel (i.e. without shell) with the same cross-linker content. The swelling properties were compared in terms of the volume changes from 50 to 39 °C. It was found that the volume changes in the PNIPMAM shells were smaller compared to the pure PNIPMAM microgel. The restricted swelling in the confined geometry of the shell explained the observed decrease of the transition heats.

7.2 Suggestions for Future Work

It has been demonstrated that core-shell microgels from PNIPAM and PNIPMAM have a much more complex internal structure than it was expected in the beginning of this work. Although detailed insight in the structure of the core-shell microgels has been gained in this work, some questions remain unanswered.
A few ideas for further investigations are presented in the following.

7.2.1 Contrast Variation SANS Experiments

Tokuhiro and co-workers reported on partially deuterated d^7-PNIPAM.[1] Using the deuterated NIPAM monomer for the preparation of core-shell microgels would allow SANS experiments where either the core or the shell would be "invisible" for neutrons due to contrast matching with the solvent.
The use of contrast variation in this work was limited because the scattering length densities of PNIPAM and PNIPMAM are very similar and would lead to unusual long acquisition times and results with only low resolution. Scattering profiles obtained from these samples could be analysed without significant modifications of the existing form factor model and could provide a direct experimental proof of the internal structure of the core-shell microgels obtained by the data modelling.

7.2.2 PNIPMAM Hollow Spheres

The analysis of DSC data and the comparison with SANS modelling results have shown that the swelling of the PNIPMAM shell in the core-shell particles is constrained. Further, smaller transition heats have been observed than expected from the particle mass composition due to the confinement of the shell when it is attached onto the core.
In recent publications the preparation of PNIPAM hollow spheres has been reported. These hollow spheres were prepared by grafting a cross-linked PNIPAM shell on silica particles and subsequently degrading the core using hydrofluoric acid.[2,3] An even more sophisticated approach was introduced by Nayak[4] and Zhang[5]. They prepared core-shell microgel systems where the core was degraded by the gentle use of oxidation cleavage of the cross-links in the core or by an enzyme. The hollow spheres exhibited larger particle sizes at temperatures below the LCST and slightly smaller sizes above the LCST compared to the core-shell particles, which indicates a higher ability to swell in the absence of the core. However, the authors did not present any thermographic data.

The preparation of PNIPMAM hollow spheres, especially based on Nayak´s approach, would be well suited to compare the thermochemical properties of identical (!) PNIPMAM shells in the presence and absence of the core and could provide more details on the restricted swelling of the shell. Data obtained from SANS and DSC experiments on the hollow spheres could be compared to the PNIPAM core-PNIPMAM shell particles presented in this work giving further insight to the restricted swelling in the confined geometry of a shell.

7.2.3 Spectroscopic Methods

Spectroscopic methods might lead to further insight into the states of swelling of the components at different temperatures.

Maeda and co-workers used Fourier transform infrared spectroscopy (FTIR) to monitor the changes of the hydration state of linear PNIPAM, PNIPMAM and other poly-alkylamides during the phase transition in water and heavy water, respectively.[6,7,8,9] They observed a shift of characteristic bands in the IR spectra during the phase transition and could also give a quantitative statement of the solvation of the carboxylic moieties in the side chains at different temperatures.

Similar investigations of microgel particles, and especially core-shell microgels can be expected to be much more challenging due to the presence of the cross-links in the polymer network and the heterogeneous composition in case of core-shell microgels.

As it is possible to distinguish distinct bands and assign them to different hydration states the appliance of this technique could be a very useful tool in order to obtain information on the degree of swelling of both the core and shell networks if the core-shell mass composition is known.

The groups of Schönhoff[10,11,12] and Starovoytoya[13,14] used ^{1}H NMR to monitor structural changes during the temperature induced phase transition of PNIPAM and PNIPAM/PNIPAM co-polymers, respectively. Both groups found that liquid state proton signals observed in the swollen state of the polymer broadened and decreased at elevated temperatures monitoring a decreased mobility in the collapsed polymer.

Starovoytoya reported on mixtures and random co-polymers of PNIPAM and PNIPMAM. She investigated the fraction of phase separated polymer by monitoring the –CH signal from the isopropyl side-chain and observed that for co-polymers a single transition occurred and the transition temperature shifted according to the polymer composition. However, for

mixtures of these polymers a two-step transition was found and each polymer phase separated at a temperature corresponding to its LCST. The amount of phase separated polymer at temperatures between both LCSTs agreed quantitatively with the mixture composition.
Schönhoff used a similar technique to explore the phase transition of PNIPAM chains adsorbed onto silica particles and found the phase transition temperature to be shifted to higher temperatures due to the restricted geometry of an adsorption layer on the surface.
Both approaches have shown that NMR techniques are suitable for the investigation of phase transition behaviour of temperature-sensitive polymers. Although the situation might be more complicated for mircogels than for linear polymers as mentioned above, a core-shell microgel can be regarded as somewhat in between a mixture and a co-polymer of PNIPAM and PNIPMAM. Thus, it should be possible to deduce information from the swelling states of the core and shell networks from measurements below, in between and above the LCST. The mutual influence of core and shell swelling could be proven if a deviation of the ratio of phase separated and swollen polymer from the core/shell mass composition would be found at the intermediate temperature.
The method presented by Schönhoff could be crucial to explain the low temperature shift of the shell transition found in this work for a core-shell microgel with a very thin shell. It should be mentioned at this point, that one has to keep in mind the experimental conditions when the temperature sensitive polymer is attached to the substrate. Adsorption at a temperature below the LCST onto a silica particle shifted its transition temperature to higher values because the polymer was confined in the swollen state. Attaching it to a collapsing core which can be regarded as an active substrate, however, forces it to the shrunken state and will decrease the temperature.

Fluorescence correlation spectroscopy (FCS) is currently established in our group. This technique would allow to monitor the temperature dependent compression and expansion of the core in a core-shell microgel in single molecule. It would require to immobilize to particle on a surface.
Core-shell microgels with a fluorescently labelled core have to be prepared specially for this purpose.[15,16] In order to get a sufficient resolution particle sizes of 1 µm or above are recommended. One would expect that the intensity of the fluorescence signal directly corresponded to the degree of swelling of the core. Further, the dimensions of the core could be deduced from this experiment. An even more exquisite approach comparable to the work

of Jones[17] could be done with a similar system where the core is labelled with a fluorescence donor and acceptor using fluorescence resonance energy transfer (FRET). In this case the fluorescence intensity would depend on the proximity of donor-acceptor pairs in the core and should correspond to the swelling state of the core.

7.2.4 Concentrated Core-Shell Microgel Dispersions

This work focused on the internal structure of temperature-sensitive core-shell microgels. Therefore most of the experiments were carried out in highly diluted suspensions where interparticle interactions can be neglected.

It has been demonstrated that the shell consists of a highly swollen and flexible network at temperatures below the LCST. The phase behaviour of highly concentrated dispersions of PNIPAM microgels and polystyrene core-PNIPAM shell particles has been investigated by rheology, scattering methods and model calculations revealing deviations from hard sphere behaviour.[18,19].

SANS experiments revealed that PNIPAM microgel particles interpenetrate and deform each other at very high volume fractions, i.e. reveal soft sphere behaviour.[20]

By surrounding a PNIPAM core with a PNIPMAM shell, particles are obtained which are colloidally stable at temperatures above the LCST of the core. The cores of the particles are highly attractive but the sterical stabilization of the shell prevents macroscopic phase separation. In general, the interaction potential can be tuned by varying the temperature. Studies of the colloidal phase behaviour of such systems seem to be interesting. The question arises whether the collapse of the core has a similar influence on the phase behaviour as the attractive depletion interaction in model hard sphere suspensions.

The extension of the core-shell form factor model accounting for particle-particle interaction by the incorporation of a structure factor, and analysis of SANS data obtained at higher concentrations would help to answer the question, whether the core is also compressed when the particles come in close contact. A soft sphere model for the structure factor would be preferable.

7.2.5 Investigation of the Interpenetrated Layer at the Core-Shell Interface

Another very important point worth investigating would be to gain further insight in the structure of the connecting layer between core and shell.

So far it has been regarded as an interpenetration of the different networks which can exert forces from the shell to the core. This interpenetration of two covalent networks gives a functional description but does not reveal a clear picture of its chemical nature. So far, only little work has been done on this topic.[15]

One might argue against a physical interpenetration that the outer region of the core mainly consists of loosely cross-linked chains which would not be able to form a permanent interpenetration. Thus, other mechanisms like entanglements of the core chains with the shell network or by-reactions during the shell polymerization as radical transfer would gain a more important role in this concern.

For this purpose smaller core-shell particles need to be prepared in order to increase the relative amount of interpenetrated network at the core/shell interface with respect to the total particle composition.

Several authors reported on the preparation and investigation of stimuli-sensitive microgels from interpenetrated networks (IPN) based on PNIPAM.[21,22,23,24] In contrast to the core-shell microgels, these particle consist of two polymer networks which completely interpenetrate in the entire particle. Their preparation requires different experimental conditions than the core-shell microgels. The parent polymer network needs to be swollen, i.e. the temperature is below the LCST, in order to allow the monomer molecules and oligomers to penetrate the network. The employment of UV polymerization or radial accelerators is well suited for polymerizations at room temperature.

The comparison of these materials with the core-shell microgels seems to be essential to gain further understanding of the chemical nature of the interpenetrated layer at the core/shell interface.

7.2.6 More Sophisticated Core-Shell Structures of Stimuli-sensitive Polymers

Finally one could think about the preparation of even more advanced core-shell structures.

Promising candidates are particles with two or more shells from temperature sensitive polymers with different LCSTs. One could imagine that the effects of mutual influenced core and shell swelling would be much more pronounced when the outer shell acts only on a thin layer of the intermediate shell which surrounds a rigid core. This could be realized for example by a polystyrene core-PNIPAM shell-PNIPMAM shell morphology. Also doubly temperature sensitive hollow spheres prepared by etching the core from these particles will promise interesting features.

Further, one could think about moving a step forward from temperature sensitivity to core-shell microgel structures that are multi-sensitive to different quantities of other stimuli. First attempts were presented by Plunkett who used a combination of two pH-sensitive polymers with different pK_a values in a core-shell morphology of rather large sizes of several hundred micrometers.[25] The response times of these particle on pH changes were rather slow. However, scaling the size down to the order of common microgels (< 1µm), one could expect similar effects upon pH changes as observed in this work.

Overall, there is an enormous potential for stimuli-sensitive core-shell microgels with respect to their application and characteristic properties. With this study great progress was made towards a thorough characterization of these particles.
I therefore believe that core-shell microgels with tuneable sensitivity to external stimuli will continue to be the subject of great interest and scientific work!

8 Experimental Section

8.1 Materials

8.1.1 Purified and Heavy Water

Ion-exchanged water with a specific resistance > 18.2 MΩ/cm (Milli-Q, Millipore) was used for all purposes and filtered through a 1.2 µm filter unless the use of heavy water is stated. Heavy water (D_2O, 99.9 %) was purchased from Deutero GmbH[1] (www.deutero.de) and used as received.

8.1.2 Chemicals

The monomers *N*-isopropylacrylamide (NIPAM, 97 %) and *N*-isopropylmethacrylamide (NIPMAM, 97 %) were purchased from Sigma-Aldrich (www.sigmaaldrich.com) and recrystallized before use (see below) before polymerization.

The radical initiator potassium peroxodisulfate (KPS, > 99.0 %), surfactant sodium dodecylsulfate (SDS, ≥ 99 %), and the cross-linker monomer *N*,*N*´-methylenbisacrylamide (BIS, ≥ 99.5%) were supplied from Sigma-Aldrich and used without purification.

8.1.3 Monomer Purification

The NIPAM and NIPMAM monomers were recrystallized from cyclo-hexane (Sigma-Aldrich) before they were used for the polymerization.

The recrystallization procedure was as follows: 50.0 g of either monomer was placed in a 500 ml round bottom flask equipped with a magnetic stirrer and reflux condenser. 200 ml of cyclohexane (Sigma-Aldrich) were added and heated to the boiling point (81 °C) for 10 min. The yellow coloured solution was then allowed to cool down slowly to room temperature. In a final step the supernatant was removed via vacuum filtration through a paper filter. This procedure was repeated once and the purified monomers were then dried in vacuum for one day. After this purification the monomers were obtained as pure white (NIPAM) and slightly

yellow crystals (NIPMAM), respectively. The purified monomers were stored in a sealed glass container in the fridge at +6 °C.

8.2 Sample Preparation

8.2.1 Synthesis

In general, PNIPAM and PNIPMAM microgels were prepared via free radical precipitation polymerization based on procedures given in the literature by Senff and Richtering for PNIPAM microgels[2] and Duracher et al. for PNIPMAM micgrogels.[3] The synthesis of core-shell microgels was carried out in a two-steep seed-and-feed polymerization introduced by Jones and Lyon.[4] Pre-existing core particles were used as seed for the subsequent polymerization of the shell.

The preparation of PNIPAM and PNIPMAM microgels will be described in detail below, the synthesis of PNIPAM core-PNIPMAM shell and the inverse PNIPMAM core-PNIPAM shell microgels in Chap. 8.2.1.2.

8.2.1.1 Synthesis of PNIPAM and PNIPMAM Microgels

PNIPAM and PNIPMAM core microgel polymerizations were performed at 70 °C in glas reaction vessel (250, 1000, or 5000 ml) equipped with a reflux condenser, a mechanical stirrer and a gas inlet. The temperature was controlled by an external thermometer in the silicon oil heating vat. The choice of the size of the reaction vessel depended on the batch size. Detailed information on the amounts of substances used for each polymerization are given in Tab. 8-1 below.

Ion exchanged water was filled into the reaction vessel, heated to 70 °C and purged with an intensive nitrogen stream for at least 30 min. Then the monomer (NIPAM or NIPMAM), the cross-linker BIS and the surfactant SDS were added and purged further with nitrogen, while the initiator KPS was dissolved in a few milliliters of degassed water using a magnetic stirrer. The initiator solution was added after 30 min and the polymerization was allowed to proceed at 70°C for 6 h under slight nitrogen bubbling and stirring at 200 rpm. Afterwards the dispersion was cooled to room temperature and purified either by dialysis or ultracentrifugation.

Tab. 8-1: Experimental conditions for PNIPAM and PNIPMAM microgel syntheses.

lab name	sample, reference	monomer [g]	BIS [mg]	BIS [mol%]	SDS [mg]	KPS [mg]	water [ml]
M71	PNIPAM core (Chap. 2)	11.805	225.0	1.4	225.0	450	600
M71SU	PNIPAM core (Chap. 3,4,6)	78.73	1512.0	1.4	1502.0	3011	4000
PM013	pure PNIPMAM (5mol%) (Chap. 2)	1.105	70.5	5.0	30.0	22.0	50
PM013SU	pure PNIPMAM (5mol%) (Chap. 3-6)	19.90	1269.1	5.0	540.8	540.8	900
PM014	pure PNIPMAM (3mol%) (Chap. 2)	1.105	41.4	3.0	30.0	22.0	50
PM016SU	PNIPMAM core (7mol%) (Chap. 2,4,5)	22.11	2017.0	7.0	600.1	440.0	1000
PM017	pure PNIPMAM (9mol%) (Chap. 2)	1.105	132.6	9.0	30.0	22.0	50

8.2.1.2 Synthesis of PNIPAM Core-PNIPMAM Shell and Inverse PNIPMAM Core-PNIPAM Shell Microgels

An amount of the core dispersion with known solid content (and if necessary additional deionized water) was placed in the glas reaction vessel (250 or 1000 ml) equipped with a reflux condenser, a mechanical stirrer, and a gas inlet and then heated to 70 °C under nitrogen bubbling for 30 min under external temperature control. The shell solution was prepared in a separate round bottom flask. Deionzed water was heated to 70 °C under reflux for at least 30 min. A few milliliters of the water were taken from the flask and cooled down to room temperature to dissolve the initiator. Shell monomer, cross-linker, and surfactant were dissolved in the round bottom flask and then added to the core dispersion. The merged solution was heated to 70 °C and purged with nitrogen for further 30 min before the dissolved initiator was added. The synthesis was carried out over 6 h and then slowly cooled down to room temperature.
Detailed information on the sample compositions are listed in

Tab. 8-2. PNIPAM core-PNIPMAM shell samples referred to in Chap. 2 are based on PNIPAM core M71, all others are based on PNIPAM core M71SU. PNIPMAM016SU is the parent core of the inverse PNIPMAM core-PNIPAM shell microgels.

Tab. 8-2: Experimental conditions and sample compositions of core-shell microgel syntheses.

lab name	sample, reference (chapter)	core solution			shell solution					shell/core mass ratio[4)]
		core [ml]	core [g]	water [ml]	monomer [g]	BIS [mg] / mol%	KPS [mg]	SDS [mg]	water [ml]	
PNIPAM core-PNIPMAM shell										
CS005	Ch. 2	50.0[1)]	1.19	0	1.19	143.0 / 9.0	23.0	10.3	50.0	1:1
CS006	Ch. 2	25.0	0.595	25.0	1.19	143.0 / 9.0	23.0	10.1	50.0	1:2
CS008	Ch. 2	12.5	0.298	37.5	1.19	143.0 / 9.0	23.0	10.2	50.0	1:4
CS009	Ch. 2	30.0	0.714	30.0	0.571	68.6 / 9.0	11.4	4.8	30.0	1:0.8
CS010	Ch. 2	25.0	0.595	25.0	0.477	30.3 / 5.0	9.2	4.0	25.0	1:0.8
CS011	Ch. 2	25.0	0.595	25.0	0.476	17.8 / 3.0	9.2	4.2	25.0	1:0.8
CS010SU	CS-5/0.69, Ch. 3,4,6	550[2)]	8.14	0	8.14	519.2 / 5.0	182.2	86.6	550	1:1
CS018SU	CS-5/2.50, Ch. 4,6	275	4.07	275	12.2	778.9 / 5.0	273.1	88.0	550	1:3
CS017	CS-5/1.42, Ch. 4,6	12.5	0.185	12.5	0.370	23.6 / 5.0	8.3	3.9	25.0	1:2
CS019	CS-5/0.23, Ch. 4,6	25.0	0.370	0	0.185	11.8 / 5.0	4.1	4.0	25.0	1:0.5
CS009SU-T	CS-9/0.79, Ch. 4	25.0	0.370	0	0.370	44.3 / 9.0	8.6	4.1	25.0	1:1
CS011SU-T	CS-3/0.54, Ch. 4	25.0	0.370	0	0.370	13.9 / 3.0	8.1	3.8	25.0	1:1
CS013SU-T	CS-7/0.77, Ch. 4	25.0	0.370	0	0.370	33.7 / 7.0	8.4	4.0	25.0	1:1
PNIPMAM core-PNIPAM shell										
INV001	Chap. 2	25.0[3)]	0.498	0	0.493	35.3 / 5.0	12.4	5.2	25.0	1:1
INV002	INV-1.4/0.79, Ch. 5	25.0	0.498	0	0.498	9.6 / 1.4	12.1	5.1	25.0	1:1

[1)] core solution solid content: 23.8 g/l, [2)] 14.8 g/l, [3)] 19.9 g/l, [4)] core-shell mass ratios calculated on the basis of synthesis recipes.

8.2.2 Purification

8.2.2.1 Dialysis

The PNIPAM core and PNIPAM core-PNIPMAM shell samples described in Chapter 2 were purified by dialysis using dialysis tubes with a pore size of 25-30 Å (Nadir, Roth GmbH). 40 cm long cuts of the tube were washed with deionized water for one day and then filled with the dispersion. The tubes were placed in a 5 l beaker with deionized water (Milli-Q quality) and a magnetic stirrer. The serum was replaced daily over a period of 30 day until the final conductance was < 0.01 mS (conductometer HI3292, Conmet 2).

The dispersions were concentrated before freeze drying by evaporation of water from the tubes on the "Staudinger-Rad".

8.2.2.2 Ultracentrifugation and Gravimetric Determination of Particle Composition

Centrifugation, followed by decantation and redispersion in deionized water is currently the only effective but tedious procedure to purify microgel dispersions as it allows to remove low molecular weight polymers.[5]

Samples referred to in Chap. 3-6 were purified by ultracentrifugation using a Beck-Coulter Ultracentrifuge Model L8-55M with a titanium rotor Ti 70.1 at 25 °C in 10.4 ml centrifugation tubes. The rotation speed and time were chosen such that the microgel fraction clearly separated from the supernatant. Centrifugation time and rotation speed for each sample are listed in Tab. 8-3.

Tab. 8-3: Parameters for ultracentrifugation of microgel samples.

Sample	Time [min]	Speed [1000 rpm]
M71SU	45	50
PNIPMAM013SU	10	50
PNIPMAM014	20	50
PNIPMAM016SU	20	50
PNIPMAM017	60	50
CS010SU (CS-5/0.69)	30	50
CS018SU (CS-5/2.50)	10	50
CS017 (CS-5/1.42)	20	50
CS019 (CS-5/0.23)	45	50
CS009SU-T (CS-9/0.79)	30	50
CS011SU-T (CS-3/0.54)	30	50
CS013SU-T (CS-7/0.77)	45	50
INV002 (INV-1.4/0.79)	15	50

The supernatant was carefully removed with a Pasteur pipette. Three centrifugation tubes were labelled and the clear supernatants of three subsequent centrifugation cycles were merged and dried in the oven at 70 °C for three days. The transparent solution became turbid at higher temperatures, whereas the supernatant of a fourth centrifugation cycle did cloud indicating sufficient removal of low weight polymer. The microgel fraction was freeze dried. The final shell/core mass compositions were calculated from the synthesis composition (m_{core}, m_{shell}, BIS_{shell}) (ref.

Tab. 8-2) and the weight ratio of the freeze dried microgel fraction (CS) and the water soluble polymer (WSP). The conversion of the shell monomer is calculated according to the following equation:

$$shell\ conversion = \frac{\left(\frac{WSP}{CS + WSP}\right)}{\left(\frac{m_{shell} + BIS_{shell}}{m_{core} + m_{shell} + BIS_{shell}}\right)} \cdot 100\%$$

The core/shell composition obtained listed in Tab. 8-4 is obtained via:

$$\frac{m_{shell}}{m_{core}} = \frac{m_{shell} + BIS_{shell}}{m_{core}} \left(1 - \frac{\frac{WSP}{CS + WSP}}{\frac{m_{shell} + BIS_{shell}}{m_{core} + m_{shell} + BIS_{shell}}} \right).$$

Tab. 8-4: Particle composition and shell conversion determined by ultracentrifugation.

Sample	Synthesis composition			Ultracentrifugation analysis			m_{shell}/m_{core}	
	m_{core} [g]	m_{shell} [g]	BIS_{shell} [g]	WSP [g]	CS [g]	shell conv. %		average
CS010SU	8.14	8.14	0.5192	0.0241	0.1136	34.0	0.70	
(CS-5/0.69)				0.0256	0.1172	34.8	0.69	
				0.0253	0.1159	34.8	0.69	0.69
CS018SU	4.07	12.21	0.7789	0.0249	0.1215	22.3	2.48	
(CS-5/2.50)				0.0239	0.1185	22.0	2.49	
				0.0231	0.1209	21.1	2.52	2.50
CS017	0.185	0.37	0.0236	0.0243	0.0847	32.8	1.43	
(CS-5/1.42)				0.0241	0.0851	32.4	1.44	
				0.0246	0.0837	33.4	1.42	1.42
CS019	0.37	0.185	0.0118	0.0220	0.0891	57.0	0.23	
(CS-5/0.23)				0.0213	0.0871	56.6	0.23	
				0.0219	0.0877	57.5	0.23	0.23
CS009SU-T	0.37	0.37	0.0443	0.0237	0.1309	29.0	0.795	
(CS-9/0.79)				0.0239	0.1276	29.9	0.785	
				0.0242	0.1323	29.3	0.792	0.79
CS011SU-T	0.37	0.37	0.0138	0.0323	0.0998	48.0	0.539	
(CS-3/0.54)				0.0321	0.1032	46.6	0.554	
				0.0328	0.1029	47.5	0.545	0.54
CS013SU-T	0.37	0.37	0.0337	0.0217	0.1182	29.7	0.767	
(CS-7/0.77)				0.0211	0.1209	28.5	0.780	
				0.0209	0.1213	28.2	0.784	0.77
INV002	0.498	0.498	0.0962	0.0370	0.1689	33.0	0.799	
(INV-.4/0.79)				0.0380	0.1665	34.2	0.786	
				0.0380	0.1693	33.7	0.791	0.79

8.2.2.3 Freeze Drying

Water removal from the microgel dispersions and the determination of the solid content were done by freeze drying.

Larger amounts (> 100 ml) were freeze dried by Klaus Beneke (Lagaly group, University of Kiel) using a Christ Beta 1-8. Small amounts of dispersions could be freeze dried using an exsiccator with a vacuum pump (p < 3 mbar) equipped with a liquid nitrogen cold trap.

8.3 Characterization

8.3.1 Dynamic Light Scattering

Light scattering cuvettes were cleaned in an acetone fountain for at least 30 min to remove dust. The samples were prepared in the laminar flow box to prevent dust contamination. The sample concentration was adjusted to c≈0.01 wt% by diluting one droplet of the sample with heavy water. The samples were almost transparent in direct light. The samples were passed five times through a 1.2 µm filter (Minisart NML, Sartorius), filled into the cuvettes and sealed with teflon tape.

Dynamic light scattering experiments were carried out on an ALV goniometer setup (ALV-Laservertriebsgesellschaft mbH, Langen) which was modified by LSI (Light Scattering Instruments, Fribourg, Switzerland) with a Theta-Two-Theta extension. A HeNe-laser (Spectra Physics, Mod. 127, 35 mW) with a wave length of 632.8 nm was employed. The scattered light was detected at an angle of 90° over a period of 120 seconds. Hydrodynamic radii were calculated using second order cumulant fits[6] via Stokes-Einstein equation accounting for temperature dependent solvent viscosity.[7] The viscosity of heavy water as a function of temperature was given by:

$$\eta_{D_2O}(T) = 10^{(ViscA+ViscB\frac{1000}{T})}[cP]$$

with ViscA=-2.9559 und ViscB=0.89326 as constants for heavy water and the temperature given in K.[8]

Temperature dependent measurements of the particle size were carried out in the range of 20-55 °C with steps of 1 °C. The samples were allowed to equilibrate for 20 min at each temperature before the measurement. Heating and subsequent cooling cycles were performed. The change in particle size was fully reversible in the given time. Equilibration times shorter than 15 min during the cooling cycle revealed smaller particle sizes because the housing did not reach thermal equilibrium.

The light scattering apparatus was temperature calibrated with temperature insensitive polystyrene particles in water.[9] The actual sample temperature was calculated from the particle size and solvent viscosity by Stokes-Einstein equation. The sample temperature and the set temperature of the thermostat are related via:

$$T_{sample} = -0.88545 + 1.09822 \cdot T_{set} - 0.00266 \cdot T_{set}^2 \; [K].$$

All DLS measurements were evaluated with corrected values for sample temperatures and solvent viscosities.

8.3.2 Densitometry

Apparent specific densities were determined using a DMA 5000 densitometer (Anton Paar, Graz, Austria) by the laboratory technician Bente Olsen of J. S. Pedersen´s group at the University of Aarhus, Denmark.

The DMA 5000 density meter uses the oscillating-tube technique. The density determination is based on measuring the period of oscillation of a vibrating U-shaped hollow tube filled with the sample using the relationship between the period of oscillation and the density. This relationship is valid as long as the sample is not too viscous, otherwise the density has to be corrected accounting for the modified elastic modulus of the U-tube.[10,11]

The densitometer was daily calibrated at 20 °C using air and water as references. The sample volume needed was approximately 1.5 ml. Each measurement was at least repeated twice in the same day with fresh samples of concentrations 1-5 wt% in heavy water. The temperature was increased from 20 to 55 °C by steps of 1 °C with an accuracy of 0.002 °C. The measurements were run in the slow equilibrium mode (ca. 15 min equilibration time) to ensure the highest possible data quality.

PNIPMAM samples with molar cross-linker contents of 5 mol% (PNIPMAM013SU) and 7 mol% (PNIPMAM016SU) were investigated at concentrations of 1, 2, 5 wt% and 2, and 4 wt%, respectively. Temperature dependent apparent polymer densities of these samples are listed in Tab. 8-5 as well as the densities of a PNIPAM sample with 1.4 mol% cross-linker content corresponding to the core in the PNIPAM core-PNIPMAM shell samples that have been measured in a previous study on the same instrument.[12]

Tab. 8-5: Apparent specific polymer densities of PNIPAM and PNIPMAM samples.

Temperature [°C]	Apparent polymer density [g/cm^3]		
	PNIPMAM013SU (5 mol%)	PNIPMAM016SU (7 mol%)	PNIPAM M71 (1.4 mol%)
20	1.1947	1.1875	1.1563
25	1.1876	1.1835	1.1519
30	1.1801	1.1769	1.1459
35	1.1710	1.1689	1.1223
40	1.1632	1.1586	1.1133
45	1.1435	1.1436	-
50	1.1317	1.1351	-
55	1.1285	1.1290	-

The influence of molar cross-linker content on the density of the PNIPMAM samples is less than 0.5 %. Thus the apparent density of PNIPMAM was considered to be independent from the cross-linker content. Lacking a sufficient amount of material, PNIPMAM samples with 3 and 9 mol% cross-linker were not measured. Densities of these samples were adopted from the sample PNIPMAM013SU.

8.3.3 Small-Angle Neutron Scattering

Small-angle neutron scattering experiments were performed at the small-angle diffractometer D11 at the Institut Laue-Langevin (ILL), Grenoble, France.

The samples were prepared as follows. Microgel samples were measured at low weight concentration of ca. 0.2 wt%. The preparation of such low concentrated samples from dried polymer and solvent does not allow a sufficient accurate determination of the concentration which is obligatory for later data evaluation. For this purpose readily prepared stock solutions with a concentration of 1 wt% in heavy water were prepared. An aliquot of the stock solution was placed in a syringe on the balance and diluted with the fourfold amount of solvent. The final sample concentration was calculated from the initial concentration and the masses of stock solution and added solvent. The syringe was sealed and the samples were allowed to equilibrate over night on the Staudinger Rad. The dilute samples were directly transferred from the syringes to the sample containers (Hellma quartz cells 100-QS, 1 mm path) immediately before the SANS measurements. The quartz cells were sealed with a teflon plug and parafilm to prevent water evaporation from the cells during measurements at elevated temperatures.

The SANS measurements were run as follows. Scattering experiments were performed at a neutron wave length of λ=6 Å with a spread of $\Delta\lambda/\lambda$=9% (Dornier selector). The data were collected on a two-dimensional ^{3}He-detector with 64×64 pixels of 10×10 mm^2 size. A cadmium aperture for neutron beam collimation was chosen 7×10 mm^2. The maximum q-range was covered by three sample-detector distances of 2.5, 10.0, and 36.7 m. These settings allow a sufficient overlap between the distinct settings. Tab. 8-6 lists sample-detector distances, collimation length and q-range for a wave length of 6 Å.

Tab. 8-6: Detector settings and *q*-ranges at the D11 at 6 Å wavelength.

Detector distance [m]	Collimation length [m]	q-range [Å^{-1}]
36.7	40.5	1.43 10^{-3}-1.06 10^{-2}
10.0	10.5	5.16 10^{-3}-3.89 10^{-2}
2.5	2.5	2.18 10^{-2}-1.52 10^{-1}

The scattering experiment consists of the measurement of sample scattering as well as background and calibration measurements.

Sample scattering spectra were collected at detector distances of 2.5, 10.0, and 36.7 m and at temperatures 25, 39, and 50 °C. The acquisition time depended on the detector setting and temperature. A scattering spectrum with sufficient statistics required ca. 10^6 counts. An estimate of the total acquisition time was obtained from a short scattering experiment at the desired experimental condition (10-30 seconds). Tab. 8-7 gives typical acquisition times for a sample of 0.2 wt%.

Tab. 8-7: Typical SANS acquisition times for a microgel sample of 0.2 wt% at different temperatures.

Detector distance [m]	50 °C	39 °C	25 °C
36.7	900 s	1500 s	3600 s
10.0	900 s	900 s	3000 s
2.5	300 s	300 s	240 s

Transmission measurements and scattering from the empty cell and solvent were performed for background correction and absolute calibration. The calibration measurements are summarized in Tab. 8-8, where TRA and SCA denote either a transmission or scattering experiment. The numbers given represent the acquisition time in seconds (t) or monitor counts (m).

Tab. 8-8: SANS calibration measurements.

Calibration sample	Detector distance			
	36.7 m	10.0 m	2.5 m	5.0 m
empty beam	TRA 1000m	TRA 1000m	TRA 1000t	TRA 1000m
empty cell	SCA 3600t	SCA 3600t	SCA 3600t	TRA 1000m
D_2O (solvent)	SCA 1800t	SCA 1800t	SCA 1800t	TRA 1000m
H_2O (reference)	-	SCA 3600t	SCA 3600t	TRA 1000m
samples	-	-	-	TRA 1000m

ILL provided software $GRAS_{ANS}P$ by C. Dewhurst (Graphical Reduction and Analysis SANS Program, ver. 3.85) was used in order to subtract background and empty cell scattering and for azimuthal averaging. The incoherent scattering of H_2O at detector distances of 2.5 and 10.0 m was used for absolute calibration according to the standard procedures at the ILL.[13]
The $GRAS_{ANS}P$ home page provides a detailed manual including sample data.[14] The manual describes step by step the complete data reduction procedure.

8.3.4 Turbidimetry

Turbidity measurements reported in Chap. 2 were carried out with a Mettler Phototrode 550 (λ=550 nm) on samples of ca. 0.5 wt% in water. The output voltage range of the phototrode was between 0 and 1.0 V. The initial sample concentration was chosen to be ca. 0.7 V at 25 °C.
The sample and spectrode were placed in a test tube (diameter 12 mm). The sample temperature was controlled by placing the test tube in a heating vat (Lauda Ecoline E200).

The output voltage was received by a common multimeter (METEX 3640D) and transmitted to a computer. The temperature was increased from 25 to 50 °C with a rate of 0.25 °C/min. The data acquisition was fully controlled by a self-written BASIC program. The source code can be found in the appendix.

8.3.5 Differential Scanning Calorimetry

DSC experiments were performed on a Perkin Elmer Pyris 1 DSC at the group of Prof. Schick at the University of Rostock with kind support of Dr. Heiko Huth.

The samples were prepared as follows. The DSC experiments were carried out on samples of 6 wt% in heavy water. The freeze dried samples were weighted in a syringe on the balance and a calculated amount of heavy water was added. In order to disperse the samples the syringe were sealed with a plug and parafilm. Then the syringes were heated in a water bath to 45 °C for 10 min. The samples were removed from the water bath and intensively shaken until they cooled down to room temperature. This procedure was repeated at least three times until the samples looked completely homogeneous through the light.

Approximately 30 mg of the 6 wt% microgel dispersion were weighted in stainless steel pans with silicon rubber gaskets (Perkin Elmer supplies) as sample holders. DSC measurements were carried out in the temperature range from 25 to 55 °C with a heating rate of 2°C/min. For all samples at least two heating and cooling cycles were performed. The second heating run was exported from the Perkin Elmer software, baseline corrected and evaluated as explained in Chap. 6.

Heating and cooling rates of 0.5, 1, 2, 5, 10, and 20 °C/min were employed for sample CS010SU (CS-5/0.69). An influence on the thermal transitions was observed only at very high rates ≥ 10 °C/min.

8.3.6 Capillary Viscosimetry

Capillary viscosimetry experiments were carried out on a Lauda PVS 1 system equipped with a Lauda E200 heating vat using a micro-KPG-ubbelohde capillary (Typ 1, capillary constant=0.01027) with samples CS010SU (CS-5/0.69), CS018SU (CS-5/2.50), M71SU (PNIPAM core). The measurements on sample M71SU were done by the practical course student Judith Musch in Aachen.

Sample preparation. A 1 wt% stock solution was prepared from freeze dried sample and heavy water in a plugged syringe. Dispersions from 0.05 to 0.8 wt were obtained by defined dilution with heavy water.

The samples were passed into the ubbelohde capillary through a 5 µm filter (Sartorius) to remove dust. The cycle times of the pure solvent and the samples were measured in the temperature range from 20 to 50 °C. The measurements were repeated six times at each temperature. The average cycle time was calculated from at least three measurements with a standard deviation smaller than 3%.

The relative viscosities at a certain temperature were calculated from the cycle times via:

$$\eta_{rel}(T) = \frac{t_{sample}(T)}{t_{solvent}(T)}$$

and are depicted in the following figures for core-shell samples CS010SU (CS-5/0.69), CS018SU (CS-5/2.50), and the pure PNIPAM microgel M71SU:

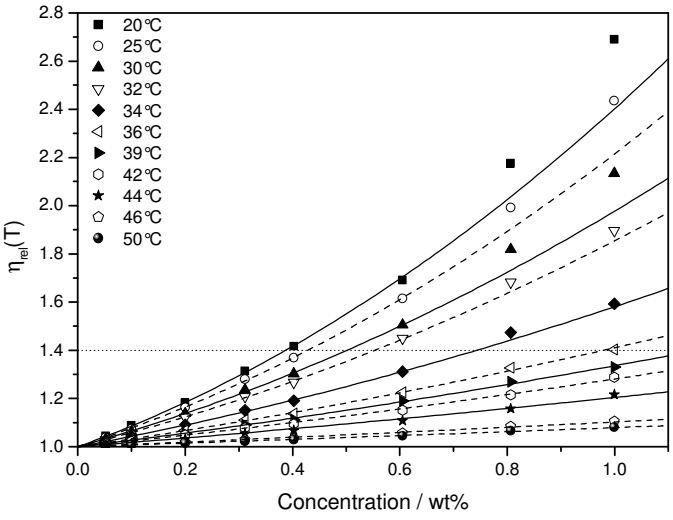

Fig. 8-1: Relative viscosity of core-shell microgel CS010SU (CS-5/0.69) in heavy water.

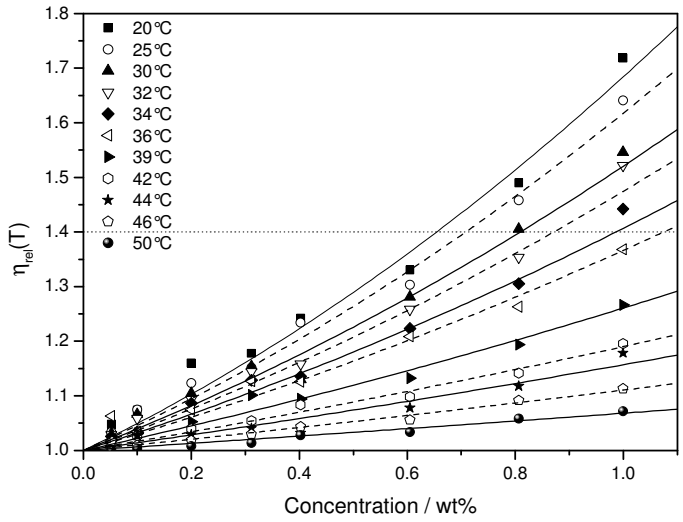

Fig. 8-2: Relative viscosity of core-shell microgel CS018SU (CS-5/2.50) in heavy water.

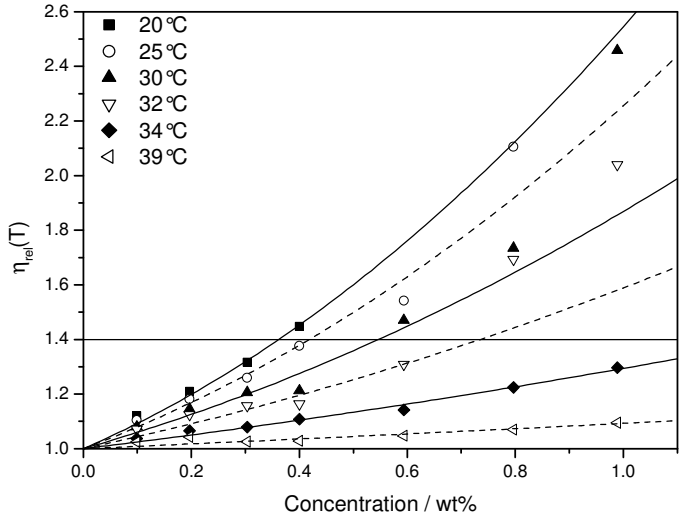

Fig. 8-3: Relative viscosity of PNIPAM microgel M71SU in heavy water.

In order to obtain the temperature dependent shift factors, the relative viscosities were plotted as a function of the concentration c. The experimental data were fitted to the Batchelor equation with $\eta_{rel} < 1.4$

$$\pi_{rel} = 1 + 2.5\Phi + 5.9\Phi^2 = 1 + 2.5(q \cdot c) + 5.9(q \cdot c)^2$$

where the volume fraction was substituted by the product of concentration (in wt%) and the temperature shift factor q. The shift factors of the three investigated samples in the temperature range from 20 to 50 °C are listed in Tab. 8-9.

Tab. 8-9: Shift factors obtained from the fitting of experimental viscosity data to the Batchelor equation.

Temperature	Sample		
[°C]	CS010SU (CS-5/0.69)	CS018SU (CS-5/2.5)	M71SU
20	0.31974	0.1892	0.34198
25	0.28906	0.17488	0.29587
30	0.24695	0.15297	0.22643
32	0.22372	0.14212	0.16844
34	0.16672	0.12551	0.09581
36	0.12647	0.11516	-
39	0.10726	0.08657	0.03424
42	0.09231	0.06585	-
44	0.07008	0.05548	-
46	0.0377	0.04037	-
50	0.02958	0.02569	-

9 Appendix

9.1 Curriculum Vitae

Personal Data

Name:	Ingo Berndt
Address:	Gravelottestraße 5 24116 Kiel Tel.: +49 431 6910463 Email: berndt@phc.uni-kiel.de
Date of birth:	20.09.1974 in Rendsburg, Schleswig-Holstein, Germany
Family status:	single
Nationality:	german

Early Education

1981-1985	Primary school Grund- und Hauptschule, Fockbek
1985-1994	High school Gymnasium Kronwerk, Rendsburg
25.06.1994	University entrance qualification

Military Service

07.1994-06.1995	Basic military service at Fernmeldebataillon 610 LJ, Flensburg

Higher Education

1995-1998	Pre-diploma study in Chemistry, University of Kiel, Germany
04.1998	Pre-diploma in chemistry: "sehr gut"
05.1998-05.2001	Diploma study in chemistry, University of Kiel
15.05.2001	Diploma in chemistry: "sehr gut" Diploma thesis at the Institute of Inorganic Chemistry: "Charakterisierung metalloxidmodifizierter Aerosile" with PD Dr. Ralf Zimehl in cooperation with Degussa-Hüls AG
07.2001-	Begin of PhD study in chemistry with Prof. Dr. Walter Richtering, Institute of Physical Chemistry, University of Kiel: "Structure of multi-temperature sensitive core-shell microgels"

Professional Experience

07/2001-04/2004	Scientific employee at University of Kiel
05/2004-	Scientific employee at RWTH Aachen University
2000-2003	Teaching assistant in GDCh courses "Moderne Methoden in der Kolloidchemie"
2001-2003	Co-supervision of two diploma students in chemistry and a practical course student in biochemistry, University of Kiel
2001-2004	Teaching assistant in laboratory courses in polymer and colloidal chemistry, University of Kiel

9.2 Patentschrift DE 102 40 956 B4

Based on the results presented in Chapter 2 parts of this work have been applied to patent at the Patent- und Markenamt of the Bundesrepublik German and finally accepted on 17.03.2005.

The original certificate titled "Heterogene Kern-Schale Mikrogele mit mehrstufigem Schaltverhalten" is reproduced on the following pages.

(19) **Bundesrepublik Deutschland**
Deutsches Patent- und Markenamt

(10) **DE 102 40 956 B4** 2005.03.17

(12) **Patentschrift**

(21) Aktenzeichen: **102 40 956.0**
(22) Anmeldetag: **05.09.2002**
(43) Offenlegungstag: **18.03.2004**
(45) Veröffentlichungstag der Patenterteilung: **17.03.2005**

(51) Int Cl.[7]: **B01J 13/02**
A61K 7/00, A61F 13/00, C09D 151/06, C08F 265/10

Innerhalb von 3 Monaten nach Veröffentlichung der Erteilung kann Einspruch erhoben werden.

(71) Patentinhaber:
Christian-Albrechts-Universität zu Kiel, 24118 Kiel, DE

(74) Vertreter:
BOEHMERT & BOEHMERT, 24105 Kiel

(72) Erfinder:
Richtering, Walter, Prof. Dr., 24119 Kronshagen, DE; Berndt, Ingo, 24105 Kiel, DE

(56) Für die Beurteilung der Patentfähigkeit in Betracht gezogene Druckschriften:
DE 198 56 432 A1
DE 100 63 197 A1
EP 03 56 953 A2

(54) Bezeichnung: **Heterogene Kern-Schale Mikrogele mit mehrstufigem Schaltverhalten**

(57) Hauptanspruch: Kern-Schale Mikrogel, bestehend aus einem Mikropartikel (Durchmesser < 1 µm) als Kern und wenigstens einer aus einem Polymer bestehenden Schale, die durch Emulsions-, Dispersions- oder Suspensionspolymerisation aus Monomeren unter Zugabe von Vernetzermonomeren gebildet wird bzw. werden, wobei die Schale(n) aus einem aus einem ersten Monomer gebildeten thermosensitiven Mikrogel mit einer ersten Schalttemperatur besteht bzw. bestehen, dadurch gekennzeichnet, dass wenigstens eine weitere Schale oder der Kern aus einem aus einem zweiten Monomer gebildeten thermosensitiven Mikrogel mit einer von der ersten Schalttemperatur unterschiedlichen zweiten Schalttemperatur besteht.

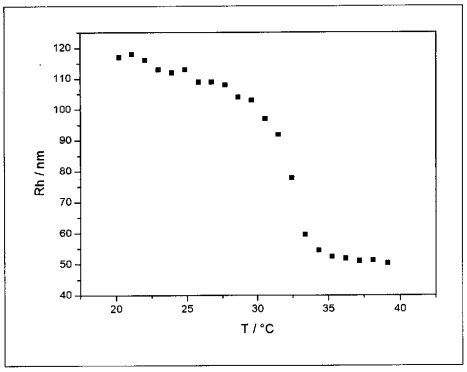

Beschreibung

[0001] Die Erfindung betrifft thermisch schaltbare Kern-Schale Mikrogele, aufgebaut aus wenigstens zwei verschiedenen thermosensitiven Polymeren mit unterschiedlicher Schalttemperatur, wobei der Kern selbst aus einem thermosensitiven Polymer besteht, sowie Kern-Schafe Mikrogele mit nicht thermosensitivem Kern, der von wenigstens zwei Schalen aus verschiedenen thermosensitiven Polymeren mit unterschiedlicher Schalttemperatur umgeben ist.

[0002] Dem Stand der Technik sind thermosensitive Mikrogele wohlbekannt (z.B.: Pelton und Chibante, Colloids and Surfaces, 20, 246–256 (1986), Pelton, Adv. Colloid Interface Sci., 85, 1–33 (2000)). Dabei handelt es sich um langkettige Makromoleküle, die z.B. durch Emulsions-, Dispersions-, oder Suspensionspolymerisation aus einem bestimmten Monomer gebildet und durch Zufügen von Vernetzermolekülen während der Synthese zu vernetzten, kugelförmigen Partikeln "geformt" werden. Zu den mit diesem Ziel am meisten verwendeten Monomeren zählt das N-Isopropylacrylamid (NIPAM), so dass vernetztes Poly-N-Isopropylacrylamid (PNIPAM) eines der geläufigsten thermosensitiven Mikrogele ist.

[0003] Die herausragende Eigenschaft dieser Mikrogele ist ihre Fähigkeit, ihre Größe bei Temperaturänderung zu verändern. Dabei werden Wassermoleküle reversibel in die Struktur der Mikrogele eingebaut oder ausgelagert und so die physikalischen Eigenschaften verändert. So kann sich z.B. der Radius eines PNIPAM-Mikrogels bei Temperaturerhöhung um das 2–2,5fache verringern, was eine Verringerung des Volumens um einen Faktor 10–16 bedeutet. Gequollene PNIPAM-Mikrogele sind als Funktion der Konzentration weitgehend transparent, dagegen trübt sich eine PNIPAM-Dispersion beim Schrumpfen der Partikel sichtbar. Speziell bei PNIPAM findet die Auslagerung des Wassers beim Erwärmen über eine relativ scharf definierten Temperaturgrenze von T_s = 32 °C hinweg statt, die in der Literatur als "lower critical solution temperature" (LCST) und hier kurz als Schalttemperatur bezeichnet wird.

[0004] Außer NIPAM sind eine Vielzahl weiterer Monomere bekannt, mit denen sich thermosensitive Mikrogele mit ähnlichem Verhalten darstellen lassen, beispielsweise N-Diethylacrylamid, N-Vinylisobutyramid, N-Acryloylpyrrolidin, N-Acroyloylpiperidin, N-Vinylpyrrolidon, N-Vinylpiperidon, N-Vinylcaprolactam (PVCap), N-Ethylmethacrylamid (NEMAM) oder etwa N-Isopropylmethacrylamid (NIPMAM), sowie eine Reihe weiterer substituierter Acrylamide.

[0005] Der Stand der Technik kennt weiterhin Verfahren, die Schalttemperatur thermosensitiver Mikrogele zu verschieben. Dies kann vor allem durch Zugabe anionischer/kationischer oder hydrophober Copolymere bei der Polymerisation des Mikrogels erreicht werden. Das Quellvermögen wiederum lässt sich in erster Linie durch den Vernetzungsgrad der Mikrogele steuern, d.h. durch Art und Menge der Vernetzerzugabe bei der Polymerisation. Als Vernetzer kommt dabei hauptsächlich N,N'-Methylenbisacrylamid zum Einsatz, aber auch Divinylbenzol (Senff und Richtering, Colloid Polym. Sci., 278, 830 pp. (2000)) oder Ethylenglykoldimethacrylamid (EGDMA) (Hazot et al., Macromol. Symp., 150, 291–296 (2000)). Bei radikalischen Polymerisationen werden Kaliumperoxodisulfat, AIBN, Wasserstoffperoxid/UV, 4,4'-Azobiscyanopentanoicacid oder speziellere, dem Monomer angepasste Verbindungen als Radikalstarter verwendet. Durch Copolymerisation mit ionogenen Monomeren wie Acrylsäure oder Acrylsäureamid (Pelton und Chibante, Colloids and Surfaces, 20, 247–256 (1986)), Methacrylsäure (Zhou, J. Phys. Chem. B, 102, 1364–1371 (1998)), Butylmethacrylamid, aminofunktionalisierten Acrylamiden (Duracher et al., Colloid Polym. Sci., 276, 219–231 (1998), Zha et al., Colloid Polym. Sci., 280, 1–6 (2002)) oder anderen Monomeren wie Styrol lassen sich neben Schalttemperatur und Quellvermögen auch Funktionalisierung der Mikrogele gezielt beeinflussen.

[0006] Die Anwendungsgebiete für thermosensitive Mikrogele umfassen beispielsweise Kosmetika (JP07285828A), Verbandsmaterial (JP05084288A), atmungsaktive Bekleidung (JP06220775A) oder auch thermisch veränderbare Membranfilter (JP01058303 A).

[0007] Eine weitere Anwendung thermosensitiver Polymere liegt in ihrer Verwendung als Träger katalytisch wirksamer Verbindungen. Trägergebundene Katalysatoren, insbesondere trägergebundene (immobile) Enzyme, werden benutzt z.B. in der medizinischen Analytik bei der Herstellung von Produkten aus Pharmazie und Pflanzenschutz, bei der Herstellung von Nahrungsmitteln sowie bei der Gewinnung optisch aktiver Substanzen. Die Rückgewinnung und erneute Verwendung des meist recht teuren Katalysators ist nicht zuletzt aus wirtschaftlichen Gründen interessant. Bereits in der EP 277473 B1 wird die Immobilisierung von Enzymen, Coenzymen, Antikörpern, Antigenen, Aminosäuren und Metallen oder Metallkomplexen durch Bindung insbesondere an NIPAM oder NIPMAM beschrieben. Das thermosensitive Verhalten der Polymere erlaubt das reversible Ausfällen der Polymerkonjugate und deren spätere Wiederverwendung mit nur unwesentlich verringerter Aktivität. Die fixierten Katalysatoren sind häufig gegenüber der freien Form stabilisiert. Die oben genannten Manipulationstechniken für das Quellverhalten der Mikrogele werden zur Anpassung der Trägerpolymere an die optimalen Reaktionsbedingungen ausgiebig verwendet.

[0008] Bei der Präparation von Platin-Partikeln auf

einem Polystyrol-Kern umgeben von einer PNIPAM-Schale wurde ferner gefunden, dass die katalytische Aktivität der Platin-Teilchen vom Quellverhalten der Schale beeinflusst wird (Chen et al., Chem. Commun., 831–832 (1998)). Die Reaktionsraten sinken messbar beim Überschreiten der Schalttemperatur der NIPAM-Schale.

[0009] Das zuletzt genannte Beispielsystem fällt unter den Oberbegriff der Kern-Schale-Mikrogele, bei denen ein etwa kugelförmiger Kern von ggf. mehreren Schalen umgeben ist, die aus verschiedenen Polymeren oder Copolymeren bestehen können. Derartige Kern-Schale-Teilchen mit einer thermosensitiven Außenschale werden u. a. benutzt in Lackfarben, als medizinische Carrier zum Wirkstofftransport oder in der biologischen Forschung sowie zur Rheologiemanipulation, etwa bei der Ausbeutung von Erdölreservoirs (GB 262 2 117A).

[0010] Bis heute werden nur Kern-Schale-Teilchen mit höchstens einem thermosensitiven Polymer verwendet, das gemeinhin die Schale bildet. Kern-Schale-Mikrogele, bei denen sowohl Kern als auch Schale thermosensitiv sind, wurden bis jetzt nur von Grundlagenforschern beschrieben (Jones und Lyon, Macromolecules 33, 8301 (2000); Gan und Lyon, J. Am. Chem. Soc., 123, 7511 (2001)). Dabei handelt es sich um Partikel bestehend aus einem vernetzten Poly-N-Isopropylacrylamid (PNIPAM) Kern und einer Schale aus vernetztem PNIPAM copolymerisiert mit Acrylsäure oder Butylmethacrylat. Die Besonderheit solcher doppelt thermosensitiven Moleküle liegt im Auftreten einer zweistufigen Quellverhaltens als Funktion der Temperatur infolge zweier diskreter Schalttemperaturen der benutzten Komponenten.

[0011] Die DE 100 63 197 A1 beschreibt Kern-Hülle Mikrogele aus unterschiedlichen Monomeren mit thermosensitiven Kern und nicht thermosensitiver Hülle. Aus der DE 198 56 432 A1 gehen ohne Vernetzermonomere dargestellte nanopartikuläre Kern-Schale-Systeme mit Wirkstoffen im Kern hervor, deren Hülle aus polymerem N-Vinylpyrrolidon und deren Kern aus Poly(N-isopropyacrylamid) besteht. Die EP 0 356 953 A2 offenbart ein Kern-Schale-Mikrogel aus unterschiedlichen Monomeren.

[0012] Der Nachteil der im Prinzip nur aus einem Monomer bestehenden Kern-Schale-Teilchen besteht darin, dass

a) beide Schalttemperaturen durch die Wahl des Monomers in engen Grenzen festgelegt sind und nicht beliebig weit voneinander entfernt gewählt werden können;

b) die aus dem Copolymer bestehende Schale zusätzliche ionische Gruppen enthält, welche ihr reversibles Quellvermögen gegenüber dem reinen Monomer abschwächen;

c) die Anwesenheit von Salzen (Ionen) in der Lösung das Quellverhalten des Kern-Schale-Mikrogels durch Wechselwirkung mit besagten ionischen Gruppen des Copolymers beeinflusst.

[0013] Es ist die Aufgabe der vorliegenden Erfindung, Kern-Schale Mikrogele mit mehrstufigem Schaltverhalten herzustellen, die die vorgenannten Nachteile nicht aufweisen. Diese Aufgabe wird gelöst durch die Merkmale des Anspruchs 1. Die Unteransprüche geben vorteilhafte Ausgestaltungen der Erfindung an.

[0014] Die Erfindung wird wie folgt erläutert:
Der Hauptnachteil der dem Stand der Technik bekannten Kern-Schale Mikrogele mit zweistufigem Schaltverhalten liegt in der Verwendung ionischer, Gruppen bei der Erzeugung der copolymerisierten Schale. Diese bewirkt u. a. eine zusätzliche Einlagerung von Wasser in das Mikrogel, was zunächst zu einer größeren Quellung führt als beim reinen Monomer. Allerdings wird dieses zusätzliche Wasser auch beim Erwärmen nicht oder nur in geringem Maße wieder abgegeben, so dass eine solche Schale beim Überschreiten ihrer Schalttemperatur nur relativ schwach schrumpft. Bildet man die Schale indes aus einem zweiten Monomer, dessen Polymer-Schalttemperatur sich von der des Kerns unterscheidet (→ „heterogenes Mikrogel"), so kann ein zweistufiges Schaltverhalten hervorgerufen werden, das anhand einiger Parameter feinjustierbar ist, die im Stand der Technik nicht bzw. nur in engen Grenzen zur Verfügung stehen. Insbesondere lassen sich dabei auch deutlich ausgeprägte Stufen mit etwa gleicher Stufenhöhe einrichten. Die Anwesenheit von Ionen in der Lösung stört obendrein dieses Schaltverhalten nicht.

[0015] Ein weiterer Vorteil heterogener Kern-Schale-Teilchen liegt in der Möglichkeit, die beiden Schalttemperaturen durch die konkrete Wahl der thermosensitiven Monomere vorzugeben. Grundsätzlich können so Kern-Schale Mikrogele geschaffen werden, deren Schalttemperaturen auch mehrere 10 °C voneinander entfernt liegen, z.B. indem der Kern aus PNIPAM und die Schale aus Polyvinylpiperidon besteht.

[0016] Die Vernetzung der Schale eines heterogenen Mikrogels beeinflusst besonders empfindlich den Bereich zwischen den Schalttemperaturen. Während sich die mittlere Partikelgröße in den weiter außen liegenden Temperaturbereichen bei „baugleichen" Mikrogelen mit unterschiedlich vernetzter Außenschale sehr ähnlich verhält, lassen sich im Zwischenbereich gezielt Rampen unterschiedlicher Steigung oder sogar ein Plateau einrichten. Die Feinjustierung des hydrodynamischen Radius als Funktion der Temperatur ist besonders interessant für (medizinische} Partikelfilter auf der Basis von Mikrogel-Arrays, wobei z.B. ein PNIPAM-Kern/PNIPMAM-Schale-System gerade den physiologisch relevanten Temperaturbe-

reich abdeckt (Umgebung der menschlichen Körpertemperatur). Ferner ist es für medizinische Zwecke i. a. eher vorteilhaft, wenn das Schaltverhalten durch Ionen z.B. im Blutkreislauf nicht beeinflusst wird.

[0017] Neben Monomerauswahl und Vernetzungsgrad spielt noch das Verhältnis von Schalendicke zu Kernradius für das effektive Schaltverhalten des heterogenen Mikrogels eine wichtige Rolle. Es wurde beispielsweise gefunden, dass bei vorgegebenem PNIPAM-Kern mit wachsender Mächtigkeit der PNIPMAM-Schale ein stetiger Übergang hin zum Schaltverhalten des reinen PNIPMAM vollzogen wird, d.h. die Thermosensitivität des Kerns ist bei zu mächtigen Schalen nicht mehr effektiv erkennbar. Die besten Ergebnisse werden erzielt, wenn man darauf achtet, dass das Massenverhältnis zwischen Kern und Schale ungefähr 1:1 beträgt, damit eine Feinabstimmung des Schaltverhaltens, insbesondere die Ausprägung eines Plateaus, zwischen den Schalttemperaturen durch Vernetzungsvariation der Schale erfolgen kann.

[0018] Zu den Anwendungen der heterogenen Kern-Schale Mikrogele zählen die disperse Trübung und die Aktivitätssteuerung von Katalysatoren.

[0019] Das Schaltverhalten thermosensitiver Mikrogele äußert sich unmittelbar in ihrer Lichttransmissivität. Wählt man den Arbeitspunkt der Mikrogel-Funktionalität in der Umgebung der ersten Schalttemperatur, so stellt die auch weiterhin gequollene Außenschale sicher, dass die getrübten Teilchen nicht ausflocken können. Zugleich kann die Ausflockung immer noch durch weitere Temperaturerhöhung erzwungen werden, was ggf. eine Rückgewinnung der Mikrogele erlaubt. Die Rückgewinnung ist gerade bei kostspieligen Mikrogelen von Bedeutung, wie beispielsweise bei solchen, die katalytische Verbindungen enthalten. Dabei ist das temperaturabhängige Quellvermögen der Trägerpolymere geeignet, die Aktivität der Katalysatoren zu steuern. Durch Temperaturänderung selbstgeregelte Katalysatoren sind interessant z.B. für exotherme Reaktionen, die in ihrer Ablaufgeschwindigkeit bzw. ihrem Stoffumsatz gedrosselt werden sollen. Um die Ausflockung während der Aktivitätssteuerung zu vermeiden, ist das Hinzufügen einer weiteren thermosensitiven Gelschale zweckmäßig, deren Schalttemperatur weit genug vom Arbeitspunkt der Katalysatorkontrolle entfernt liegt und die trotzdem die Rückgewinnung durch Ausfällen ermöglicht.

[0020] Weitere vorteilhafte Ausgestaltungen bestehen in der Synthese von Kern-Schale Mikrogelen mit mehr als einer thermosensitiven Schale, wobei der Kern nicht unbedingt selbst schaltbar sein muss. Vielmehr kann der Kern als temperaturstabiles Trägerpolymer (z.B. Polystyrol, allg. Latex) für weitgehend beliebige funktionelle Molekülgruppen fungieren, die im Wesentlichen an der Kernoberfläche aufgepropft sind. Eine erste umgebende, thermosensitive Polymerschale nimmt während einer Abkühlungsphase zusätzliches Lösungsmittel aus der Mikropartikel-Lösung auf und ermöglicht dessen Zugang zu den funktionellen Gruppen, etwa für eine chemische Reaktion. Eine zweite, i. a. die äußerste thermosensitive Schale hindert das Mikrogel am Ausflocken bis die Rückgewinnung gewünscht wird. Beim anschließenden Erwärmen wird Flüssigkeit mit Reaktionsprodukten wieder in die Lösung abgegeben. Von besonderem Vorteil bei der „Pumpwirkung" einer solchen thermosensitiven Schale ist die Möglichkeit, diese Schale selbst noch mit weiteren funktionellen Gruppen, etwa Katalysatoren, auszustatten. In der Theorie lassen sich so auch komplexe, mehrstufig schaltbare Mikrogele denken, die, beladen mit einer Reihe verschiedener Funktionsmoleküle, auch die Durchführung komplizierter Umsetzungen mit mehreren Phasen im Innern eines Mikroteilchens erlauben.

[0021] Die Erfindung wird näher beschrieben anhand eines Kern-Schale Mikrogels bestehend aus einem PNIPAM-Kern und einer PNIPMAM-Schale, bei dem Schalenstärke und -vernetzung variiert werden (siehe Beispielsynthesen). Die folgenden Abbildungen zeigen zugehörige Messergebnisse.

[0022] **Abb.** 1 zeigt als typisches Ergebnis die thermosensitive Antwort eines PNIPAM-Mikrogels auf Temperaturänderung. Die hydrodynamischen Radien wurden durch dynamische Lichtstreumessungen (DLS) bestimmt.

[0023] **Abb.** 2 zeigt das Ergebnis einer DLS-Messung für Poly-N-Isopropylmethacrylamid (PNIPMAM). Die Schalttemperatur ist nicht so scharf definiert wie bei PNIPAM und liegt zwischen 42 und 44 °C. Auch das Quellvermögen fällt im gezeigten Beispiel deutlich geringer aus als bei PNIPAM, d.h. das Radienverhältnis zwischen gequollenen und nicht gequollenen PNIPMAM-Mikropartikel liegt hier weit unterhalb von 2. Bei dem gezeigten PNIPMAM handelt es sich um ein hochvernetztes Mikrogel (9,0 mol%).

[0024] **Abb.** 3 verdeutlicht die Zunahme des Quellvermögens mit abnehmendem Vernetzungsgrad des Mikrogels am Beispiel des reinen PNIPMAM. Die Schalttemperatur wird ebenfalls schärfer.

[0025] **Abb.** 4 zeigt die thermosensitive DLS-Antwort eines Kern-Schale Mikrogels bestehend aus einem PNIPAM-Kern und einer PNIPMAM-Schale (mit Vernetzung 1,5 mol%, CS012). Die Schalttemperaturen der Einzelkomponenten übertragen sich auf das Kern-Schale Mikrogel.

[0026] **Abb.** 5 gibt das Ergebnis einer Trübungsmessung des Mikrogels aus **Abb.** 4 wieder.

[0027] **Abb.** 6 zeigt das Schaltverhalten verschiedener Kern-Schale Mikrogele mit PNIPAM-Kern und PNIPMAM-Schale, wobei die Schalenstärke variiert wird. Mit wachsender Mächtigkeit der Schale verschwindet der Einfluß des Kerns und das Schaltverhalten nähert sich dem des reinen Schalenmonomers an.

[0028] **Abb.** 7 stellt den hydrodynamischen Radius R_h dreier PNIPAM/PNIPMAM-Partikel (siehe Beispielsynthesen II) im Vergleich zum PNIPAM-Kern allein dar. Der Effekt unterschiedlicher Schalenvernetzung besteht bei ansonsten gleichartigen Teilchen, insbesondere CS011 und CS012, vor allem im Verlauf der Funktion $R_h(T)$ im Temperaturbereich zwischen den Schalttemperaturen von Kern und Schale.

Beispielsynthesen

[0029] Für alle Synthesen wurde als Kern das oben und in **Abb.** 1 beschriebene Mikrogel M71 verwendet. Dabei handelt es sich um ein mit 1,4 mol% BIS vernetztes PNIPAM-Mikrogel. Im Weiteren wird dieses Mikrogel als Kern bezeichnet.

I. Kern-Schale Mikrogele CS005/CS0061/CS008 mit variabler Schalenstärke

[0030] In einem 250 ml-Dreihalskolben mit mechanischem Rührer, Rückflusskühler und Gaseinleitungsrohr wurden 0,9/0,45/0,225 g in 50 ml Wasser dispergiertem Kern vorgelegt. Durch 30 min Einleiten von Stickstoff bei 70 °C wurde der Sauerstoff aus der Lösung vertrieben.

[0031] In einem anderen Kolben wurden bei 70 °C 50 ml deion. Wasser durch Stickstoffeinleiten sauerstofffrei gemacht, 1,19 g NIPMAM, 143,0 mg BIS und 10,3/10,0/10,0 mg SDS gelöst und weitere 15 min Stickstoff eingeleitet. Dieses Gemisch wurde zur Kern-Lösung gegeben, weitere 15 min Stickstoff eingeleitet und die Polymerisation durch Zugabe von 23,0 mg KPS, das in wenigen ml deion. Wasser gelöst wurde, gestartet.

[0032] Das Reaktionsgemisch wurde bei 70°C 6 h gerührt, abkühlen lassen und dann durch Glaswolle filtriert.

II. Kern-Schale Mikrogele CS009/CS011/CS012 mit variabler Vernetzung

[0033] In einem 250 ml-Dreihalskolben mit mechanischem Rührer, Rückflusskühler und Gaseinleitungsrohr wurden 0,54/0,45/0,45 g in 30/25/25 ml Wasser dispergiertem Kern vorgelegt. Durch 30 min Einleiten von Stickstoff bei 70 °C wurde der Sauerstoff aus der Lösung vertrieben.

[0034] In einem zweiten Kolben wurden bei 70 °C 30/25/25 ml deionisiertes Wasser durch Stickstoffeinleiten von Sauerstoff befreit, 0,57/0,47/0,47 g NIPMAM, 68,7/17,8/8,7 mg BIS und 4,8/4,1/4,1 mg SDS gelöst und weitere 15 min Stickstoff eingeleitet. Dieses Gemisch wurde zur Kern-Lösung gegeben, weitere 15 min Stickstoff eingeleitet und die Polymerisation durch Zugabe von 11,1/9,2/9,2 mg KPS, das in wenigen ml deionisiertem Wasser gelöst wurde, gestartet. Das Reaktionsgemisch wurde bei 70 °C 6 h gerührt, abkühlen lassen und dann durch Glaswolle filtriert.

Abkürzungen:

[0035] PNIPAM: Poly-N-Isopropylacrylamid, NIPMAM: N-Isopropylmethacrylamid, BIS: N,N'-Methylenbisacrylamid, SDS: Natrium-Dodecylsulfat, KPS: Kalium-Peroxodisulfat

Patentansprüche

1. Kern-Schale Mikrogel, bestehend aus einem Mikropartikel (Durchmesser < 1 µm) als Kern und wenigstens einer aus einem Polymer bestehenden Schale, die durch Emulsions-, Dispersions- oder Suspensionspolymerisation aus Monomeren unter Zugabe von Vernetzermonomeren gebildet wird bzw. werden, wobei die Schale(n) aus einem aus einem ersten Monomer gebildeten thermosensitiven Mikrogel mit einer ersten Schalttemperatur besteht bzw. bestehen, **dadurch gekennzeichnet**, dass wenigstens eine weitere Schale oder der Kern aus einem aus einem zweiten Monomer gebildeten thermosensitiven Mikrogel mit einer von der ersten Schalttemperatur unterschiedlichen zweiten Schalttemperatur besteht.

2. Kern-Schale Mikrogel nach Anspruch 1, dadurch gekennzeichnet, dass die Außenschale des Kern-Schale Mikrogels aus einem thermosensitiven Mikrogel besteht.

3. Kern-Schale Mikrogel nach Anspruch 2, dadurch gekennzeichnet, dass die Außenschale die höchste Schalttemperatur aufweist.

4. Kern-Schale Mikrogel nach Anspruch 2, dadurch gekennzeichnet, dass der Vernetzungsgrad der Außenschale bei der Polymerisation durch Zugabe von Vernetzermonomeren im Bereich 1,5–15 mol% gewählt wird.

5. Kern-Schale Mikrogel nach einem der vorangegangenen Ansprüche, dadurch gekennzeichnet, dass der Kern oder eine andere als die Außenschale aus einem Trägerpolymer mit daran gebundenen funktionellen Gruppen besteht.

6. Kern-Schale Mikrogel nach Anspruch 5, dadurch gekennzeichnet, dass die funktionellen Grup-

pen aus Enzymen, Coenzymen, Antikörpern, Antigenen, Aminosäuren, Metallen oder Metallkomplexen bestehen.

7. Kern-Schale Mikrogel nach einem der vorangegangenen Ansprüche, dadurch gekennzeichnet, dass als Monomere N-Isopropylacrylamid (NIPAM) und N-Isopropylmethacrylamid (NIPMAM) verwendet werden.

8. Kern-Schale Mikrogel nach einem der vorangegangenen Ansprüche, dadurch gekennzeichnet, dass das Kern-Schale-Teilchen aus einem thermosensitiven Kern und einer thermosensitiven Schale besteht, wobei Kern und Schale im Wesentlichen das Massenverhältnis 1:1 aufweisen.

Es folgen 4 Blatt Zeichnungen

Anhängende Zeichnungen

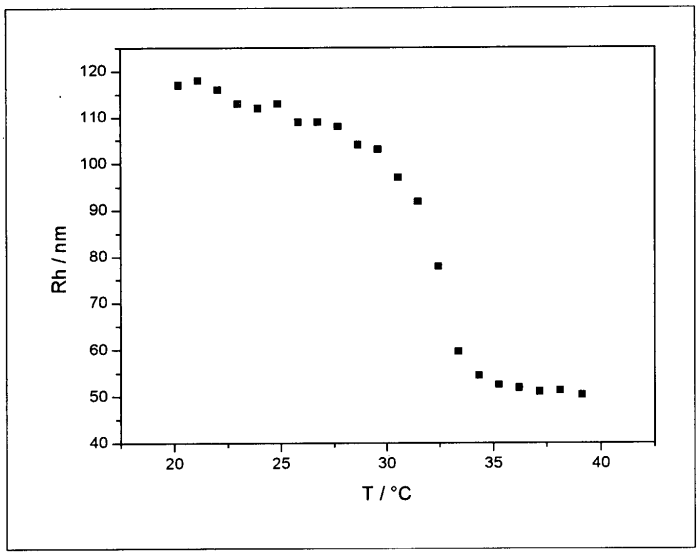

Abbildung-1 Hydrodynamischer Radius R_h der PNIPAM-Mikrogelpartikel M71 als Funktion der Temperatur. Die Schalttemperatur T_S = 32°C ist klar erkennbar.

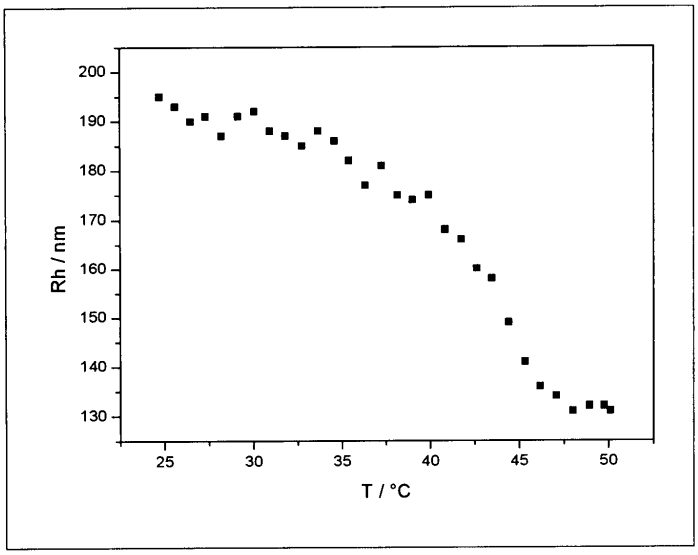

Abbildung-2 Hydrodynamischer Radius Rh der PNIPMAM-Mikropartikel als Funktion der Temperatur. Die Schalttemperatur T_S liegt zwischen 42°C und 44°C. Zudem fällt die Änderung von Rh über T_S hinweg deutlich geringer aus als bei PNIPAM.

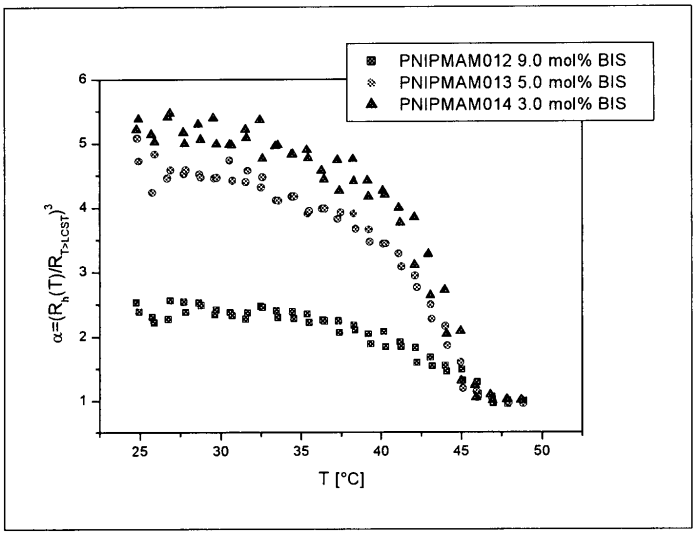

Abbildung-3 Zunahme des Quellvermögens mit abnehmender Vernetzung

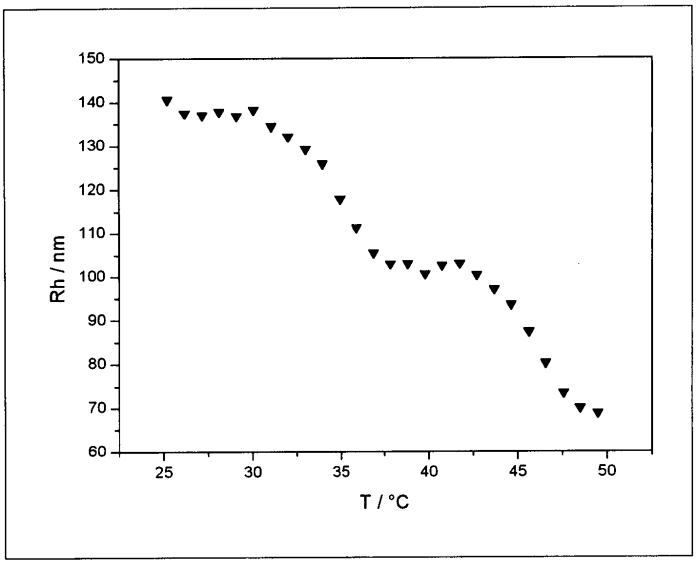

Abbildung-4 Hydrodynamischer Radius R_h eines PNIPAM/PNIPMAM Kern-Schale Mikrogels. Zwei diskrete Schalttemperaturen sind klar erkennbar.

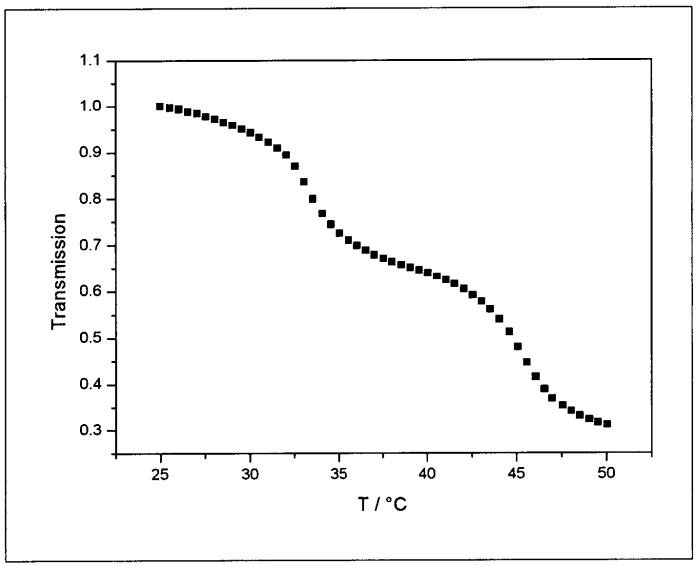

Abildung-5 Transmissionskurve des PNIPAM/PNIPMAM-Kern-Schale Mikrogels aus Abbildung-4. Die beiden Schalttemperaturen sind wie in der DLS zu erkennen.

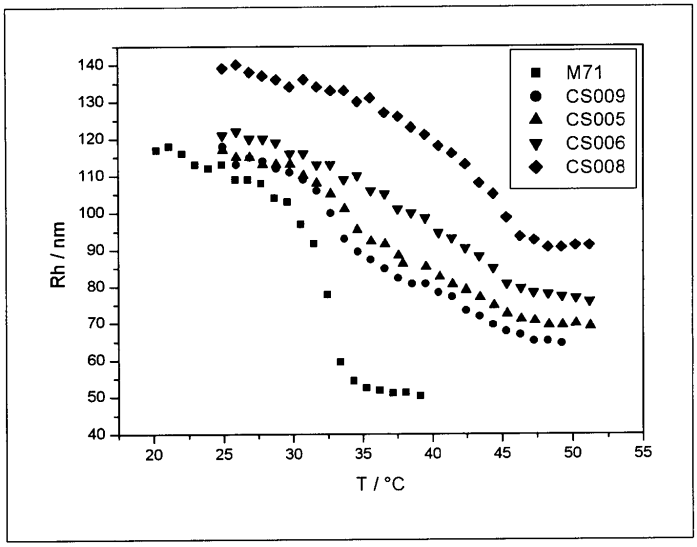

Abbildung-6 Hydrodynamische Radien verschiedener Kern-Schale-Mikrogele mit unterschiedlichen Schalenstärken. Zum Vergleich das PNIPAM-Mikrogel M71.

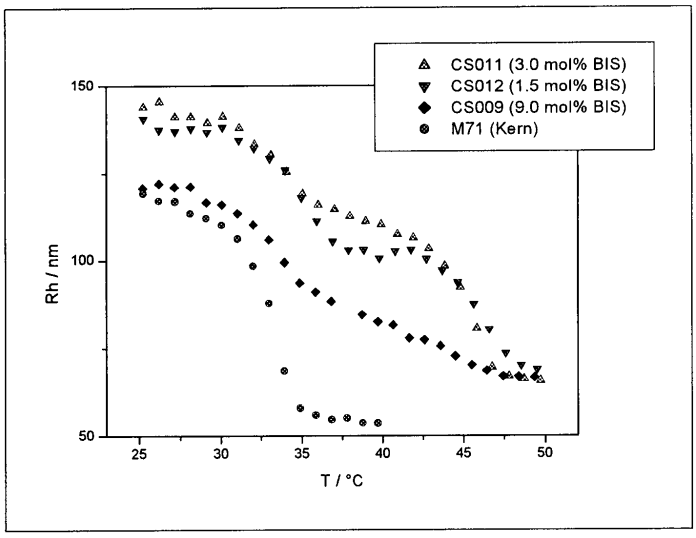

Abbildung-7 Hydrodynamischer Radius R_h der NIPAM/NIPMAM-Partikel CS009, CS011 und CS012 im Vergleich mit dem NIPAM-Kern (M71) allein. Die drei Kern-Schale Mikrogele unterscheiden sich im Vernetzungsgrad der Schale.

9.3 Source Code

This is the source code of control program used for optical transmission measurement with a Mettler DP550 phototrode and a Lauda E200.

The source code needs to be compiled with PowerBasic 3.20 (MS QBasic compatible).

```
DECLARE SUB Werteschreiben (i, TIst!, PhotoSig!, OutFile$, zeit)
DECLARE SUB Startbildschirm ()
DECLARE SUB Center (text$)
DECLARE SUB Parametereingabe (Probe$, TAnfang, TEnde, deltaT, intervall, dauer, OutFile$)
DECLARE SUB Thermostatbefehl (i)
DECLARE SUB Warten (intervall)
DECLARE SUB Werteholen (TIst, PhotoSig)
DECLARE SUB Parameterausgabe (OutFile$, Probe$, TAnfang, TEnde, deltaT, intervall)
'
ON ERROR GOTO Fehler
KEY(10) ON
ON KEY(10) GOSUB Abbruch

'Photrode METROHM Spectrode
'Ingo Berndt - 2003
'PowerBasic 3.20
'01.09.2003
'
'<----- HAUPTPROGRAMMM ----->
CALL Startbildschirm
CALL Parametereingabe(Probe$, TAnfang, TEnde, deltaT, intervall, dauer, OutFile$)
PRINT : PRINT
'
'<----- Warteschleife ----->
PRINT "Messung mit beliebiger Taste starten. Abbruch mit F10."
DO: LOOP UNTIL INKEY$ <> ""
'<----- Ende: Warteschleife ----->

CALL Startbildschirm
PRINT "Abbruch mit F10."

PRINT
'
' Parameter in das Ergebnisfile schreiben
CALL Parameterausgabe(OutFile$, Probe$, TAnfang, TEnde, deltaT, intervall)
'
'<----- Heizen ----->
nullzeit = TIMER
PRINT "T_soll", "T_ist", "DP550", "Zeit"
PRINT "================================================="
i = TAnfang
DO
        CALL Thermostatbefehl(i)
        CALL Warten(intervall)
        CALL Werteholen(TIst, PhotoSig)
        zeit = (TIMER - nullzeit) / 60
        CALL Werteschreiben(i, TIst, PhotoSig, OutFile$, zeit)
        PRINT USING "##.##"; i; : PRINT " øC", : PRINT USING "##.###"; TIst; : PRINT " øC", :
PRINT USING "#.####"; PhotoSig; : PRINT " V",
        PRINT USING "###.##"; zeit; : PRINT " min"
        i = i + deltaT
LOOP UNTIL i > TEnde
'<---- Ende: Heizen ---->
'
'<---- Kuehlen ----->
'i = TEnde
'DO
'     CALL Thermostatbefehl(i)
'     CALL Warten(intervall)
```

```
'     CALL Werteholen(TIst, PhotoSig)
'     zeit = (TIMER - nullzeit) / 60
'     CALL Werteschreiben(i, TIst, PhotoSig, OutFile$, zeit)
'      PRINT USING "##.##"; i; : PRINT " øC", : PRINT USING "##.##"; TIst; : PRINT " øC", :
PRINT USING "#.####"; PhotoSig; : PRINT " V",
'     PRINT USING "###.#"; zeit; : PRINT " min"
'     i = i - deltaT
'LOOP UNTIL i < TAnfang
'<----- Ende: Kuehlen ----->
'
PRINT : PRINT
CALL Thermostatbefehl(25)
PRINT "FERTIG!"
PRINT "Es wurden neue Daten fuer die Weltformel generiert."
'
END
'<---- Ende: Hauptprogrammm ----->

Abbruch:
       PRINT "Programm wurde abgebrochen."
       END

Fehler:
       PRINT "Es ist ein Fehler aufgetreten."
       PRINT "Programm wurde abgebrochen."
       END

SUB Parameterausgabe (OutFile$, Probe$, TAnfang, TEnde, deltaT, intervall)
'
DatNr = FREEFILE
OPEN OutFile$ FOR output AS #DatNr
       PRINT #DatNr, "*** Truebungsmessung mit METTLER Phototrode DP550 ***"
       PRINT #DatNr, " Ingo Berndt - AK Richtering - CAU Kiel - 2002"
       PRINT #DatNr,
       PRINT #DatNr, "Ausgabefile: "; OutFile$
       PRINT #DatNr, "Probenbezeichnung: "; Probe$
       PRINT #DatNr, "Starttemperatur: "; TAnfang
       PRINT #DatNr, "Endtemperatur: "; TEnde
       PRINT #DatNr, "Temperaturinkrement: "; deltaT
       PRINT #DatNr, "Zeitintervall: "; intervall
       PRINT #DatNr,
CLOSE #DatNr
'
END SUB

SUB Parametereingabe (Probe$, TAnfang, TEnde, deltaT, intervall, dauer, OutFile$)
PRINT
PRINT
PRINT "Bitte die Parameter f□r die Truebungsmessung eingeben!"
PRINT
INPUT "         Probenbezeichnung       : ", Probe$
PRINT
INPUT "         Anfangstempertur [øC]   : ", TAnfang
INPUT "         Endtemperatur [øC]      : ", TEnde
INPUT "         Temperaturinkrement [øC]: ", deltaT
PRINT
INPUT "         Zeitintervall [min]     : ", intervall
'dauer = 1 * ((TEnde - TAnfang) / deltaT + 1) * intervall
'PRINT "         Dauer der Messung: "; dauer; "min"
'IF 86400 - dauer * 60 < 86400 - TIMER THEN PRINT "           ACHTUNG: Messung laeuft ueber
Mitternacht"
PRINT
INPUT "         Ausgabedatei [Pfad, 8+3]: ", OutFile$
END SUB

SUB Startbildschirm
'
CLS
PRINT "*** Trübungsmessung mit METROHM Spectrode ***"
PRINT "Dipl.Chem. Ingo Berndt - (c) 2003"
'
END SUB

SUB Thermostatbefehl (i)
       befehl$ = "out_sp_00" + STR$(i)
```

```
        OPEN "COM1:9600,N,8,1" FOR RANDOM AS #1
               PRINT #1, befehl$
               INPUT #1, answer$
        CLOSE #1
END SUB

SUB Warten (intervall)
aktzeit = TIMER
DO
LOOP UNTIL TIMER - aktzeit > intervall * 60
END SUB

SUB Werteholen (TIst, PhotoSig)
'
'<----- Ist-Temperatur einlesen ----->
OPEN "COM1:9600,N,8,1" FOR RANDOM AS #1
PRINT #1, "in_pv_00"
INPUT #1, TIst
CLOSE #1
'<----- Ende: Ist-Temperatur einlesen ----->
'
'<----- Phototrodensignal einlesen ----->
'OPEN "COM2:1200,N,7,2,RS,CS,DS,CD" FOR RANDOM AS #2
'PRINT #2, "D"
'INPUT #2, antwort$
'PhotoSig = VAL(MID$(antwort$, 5, 5))
'CLOSE #2
PhotoSig = d10
'<----- Ende: Phototrodensignal einlesen ----->
'
END SUB

SUB Werteschreiben (i, TIst, PhotoSig, OutFile$, zeit)
'
OPEN OutFile$ FOR APPEND AS #3
PRINT #3, USING "###.##"; zeit;
PRINT #3, CHR$(9);
PRINT #3, USING "##.##"; i;
PRINT #3, CHR$(9);
PRINT #3, USING "##.###"; TIst;
PRINT #3, CHR$(9);
PRINT #3, USING "#.####"; PhotoSig
CLOSE #3
'
END SUB
```

9.4 SANS Data of Concentrated Core-Shell Microgel Dispersions

SANS measurements have been performed on concentrated samples (c=3-13 wt%) of CS-010SU (CS-5/0.69) and CS018SU (CS-5/2.50) at 25, 39 and 50 °C under the same experimental conditions as has been described in the experimental section.

For the sake of clarity some data were multiplied by constant factors as indicated. The intensity distribution of a highly diluted dispersion (0.2 wt%) is given for comparison.

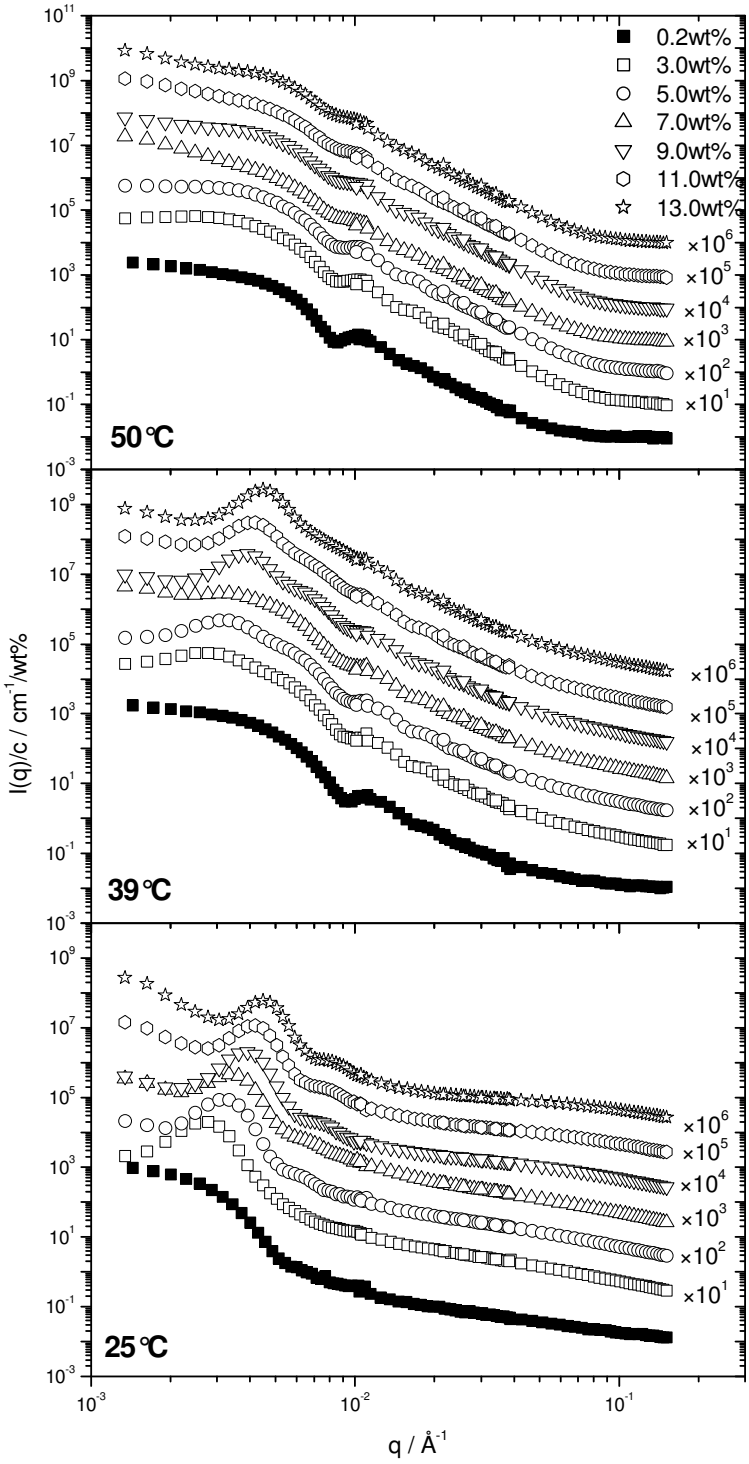

Fig. 9-1: Intensity distribution normalized on the concentration vs. momentum transfer q for various concentrations of the CS-5/0.69 core-shell microgel at 25, 39, and 50 °C.

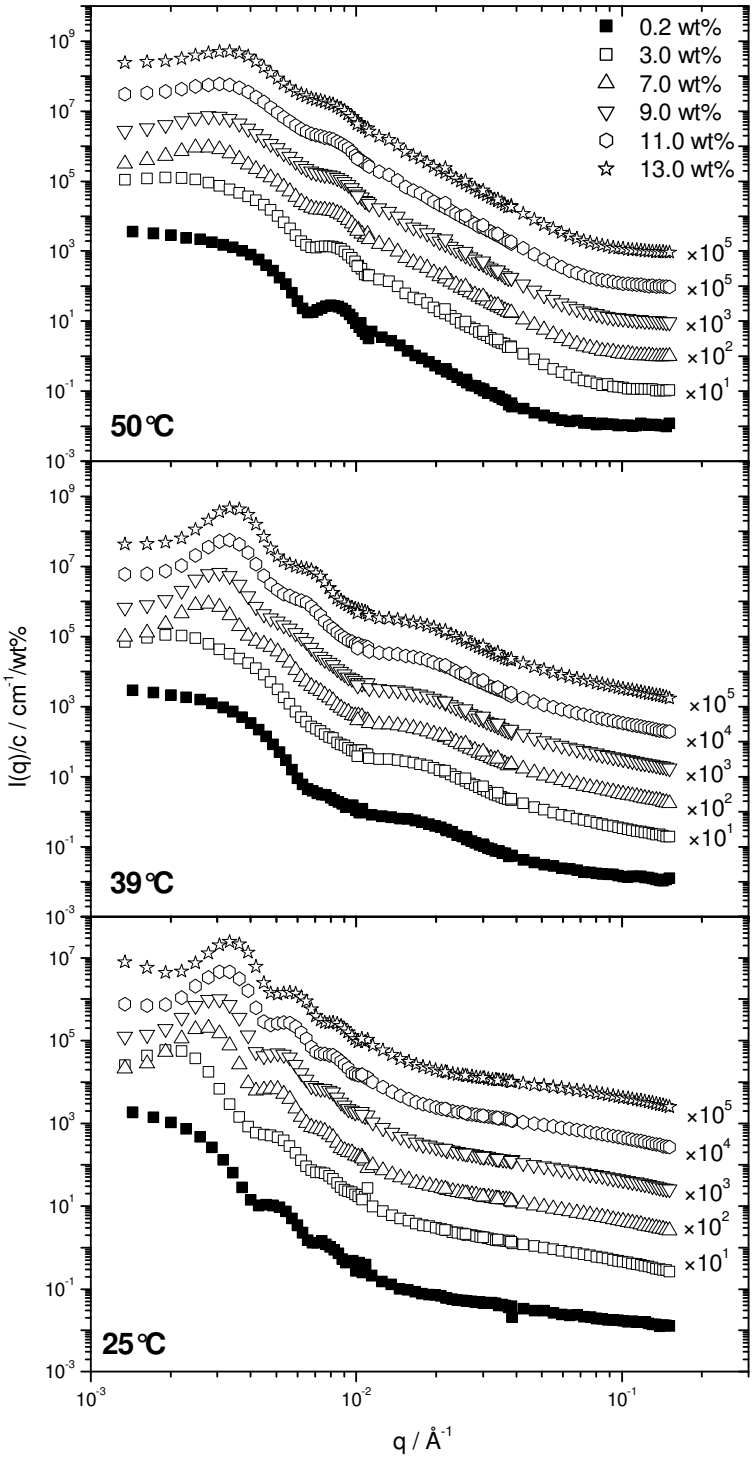

Fig. 9-2: Intensity distribution normalized on the concentration vs. momentum transfer q for various concentrations of the CS-5/2.50 core-shell microgel at 25, 39, and 50 °C.

9.5 PNIPMAM Microgels

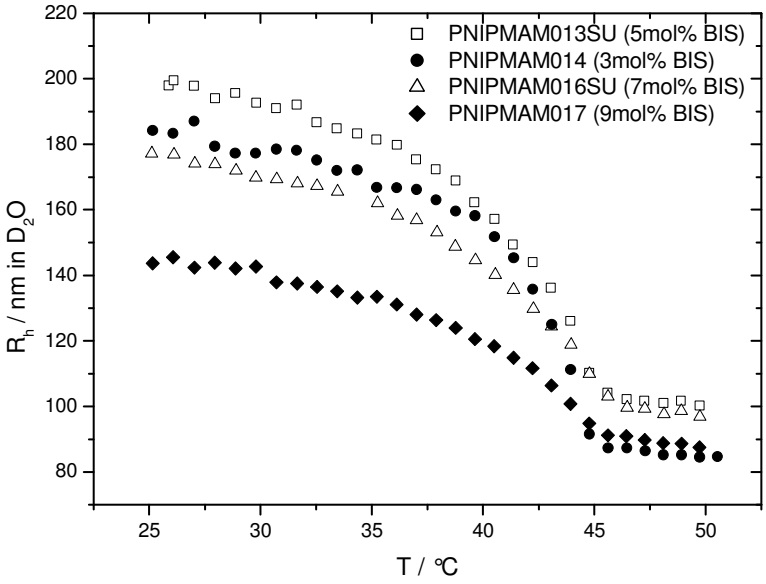

Fig. 9-3: Temperature dependence of the hydrodynamic radii of PNIPMAM microgels with molar cross-linker contents of 3, 5, 7, and 9 %.

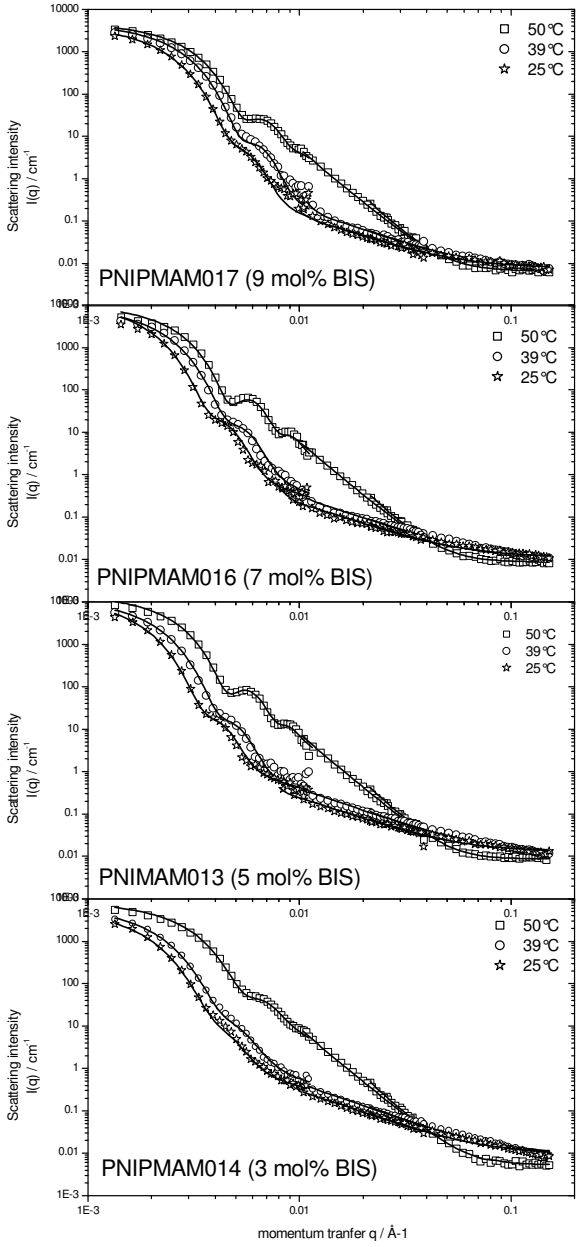

Fig. 9-4: Small-angle neutron scattering data and fit lines of PNIPMAM microgels with molar cross-linker contents of 3, 5,7, and 9 mol%.

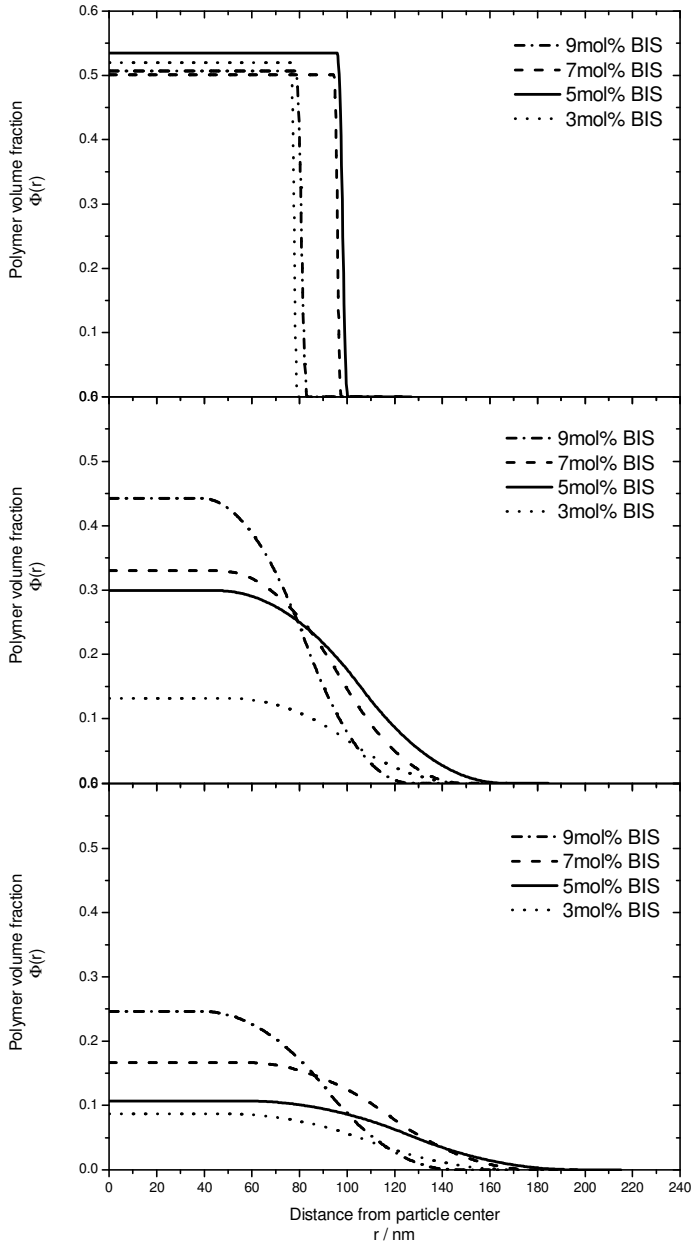

Fig. 9-5: Density profiles of PNIPMAM microgels with cross-linker contents 3, 5, 7, and 9 mol% calculated from the fits at 50, 39, and 25 °C

Tab. 9-1: Structural parameters of PNIPMAM microgels obtained from the modelling procedure employing a parabolic shaped density profile.

sample	T [°C]	R_{core} [nm]	σ_{core} [nm]	Φ_{core} [%]	σ_{rel} [%]	R_{SANS} [nm]	R_h [nm]
PNIPMAMM017	50	78.4	2.5	50.6	12.9	83	88
(9 mol% BIS)	39	38.1	44.2	44.3	11.4	126	123
	25	38.4	53.3	24.7	13.7	145	145
PNIPMAM016SU	50	94.5	1.5	50.1	9.8	97	98
(7 mol% BIS)	39	45.9	51.1	33.0	12.7	148	147
	25	55.9	61.8	16.7	13.1	180	177
PNIPMAM013SU	50	95.9	2.2	53.4	10.4	100	100
(5 mol% BIS)	39	45.5	60.2	29.9	12.4	166	168
	25	56.3	70.1	10.7	12.3	196	199
PNIPMAM014	50	76.4	1.4	52.0	16.9	79	85
(3 mol% BIS)	39	50.2	50.1	13.2	17.5	150	159
	25	48.0	61.9	8.7	18.2	172	180

10 References

Chapter 1

[1] S. H. Gehrke In: *Advances in Polymer Science*, Springer Verlag: Berlin, 1993.
[2] J. L. Drury, D. J. Mooney *Biomat.* **2003**, *24*, 4337.
[3]M. J. Serpe *PhD Thesis*, Georgia Institute of Technology, USA, **2004**; C. M. Nolan *PhD Thesis*, Georgia Insititue of Technology, USA, **2005**; S. P. Nayak *PhD Thesis*, Georgia Institute of Technology, USA**, 2005**.
[4] X.-C. Xiao, L.-Y. Chu, W.-M. Chen, J.-H. Zhu *Polymer* **2005**, *46*, 3199.
[5] W. Lin, Y. Zhou, Y. Zhao, Q. Zhu, C. Wu *Macromolecules* **2002**, *35*, 7407.
[6] H.-J. Kim, J.-H. Lee, M. Lee *Angew. Chem.* **2005**, *117*, 5960.
[7] Y. Li, T, Tanaka *J. Chem. Phys.* **1990**, *92*, 1365.
[8] J. Z. Zhang, N. A. Peppas *Macromolecules* **2000**, *33*, 102.
[9] S. Nayak, L. A. Lyon *Chem. Mat.* **2004**, *16*, 2623.
[10] S. Shimizu, T. Seyama, R. Sekine, K. Kurita *J. Appl. Christallogr.* **2003**, *36*, 694
[11] R. Freitag, F. Garret-Flaudy *Langmuir* **2002**, *18*, 3434.
[12] E. Daly, B. R. Saunders *Langmuir* **2000**, *16*, 5546.
[13] H. Hirose, M. Shibayama *Macromolecules* **1998**, *31*, 5336.
[14] R. H. Pelton *Adv. Colloid. Interf. Sci.* **2000**, *85*, 1.
[15] H. Feil, Y. H. Bae, J. Feijen, S. W. Kim *Macromolecules* **1993**, *26*, 2496.
[16] B. R. Saunders, B. Vincent *Adv. Colloid Interf. Sci.* **1999**, *80*, 1.
[17] C. D. Jones, L. A. Lyon *Macromolecules* **2000**, *33*, 8301.
[18] F. Seker, A. B. Ellis *J. Polym. Sci. Part A* **1998**, *96*, 2095.
[19] E. Djopke, W. Vogt *Macromol. Chem. Phys.* **2001**, *202*, 750.
[20] M. Stieger *PhD Thesis*, Universität Kiel, **2004**.

Chapter 2

[1] S. Chen, A. S. Hoffman *Macromol. Rapid. Commun.* **1995**, *16*, 175.
[2] D. E. Bergbreiter, B. L. Case, Y. S. Liu, C. W. Caraway *Macromolecules* **1998**, *31*, 6053.
[3] R. H. Pelton, P. Chibante *Colloids Surfaces* **1986**, *20*, 247.
[4] B. R. Saunders, B. Vincent *Adv. Colloid Interface. Sci.* **1999**, *80*, 1.
[5] R. Pelton Adv. Colloid Interface Sci. **2000**, *85*, 1.
[6] H. Senff, W. Richtering *J. Chem. Phys.* **1999**, *111*, 1705.
[7] H. Senff,W. Richtering *Colloid Polym. Sci.* **2000**, *278*, 830.
[8] S. Zhou, B. Chu *J. Phys. Chem.* **1998**, *102*, 1364.
[9] L. Zha, J. Hu, C. Wang, S. Fu, A. Elaissari, Y. Zhang *Colloid Polym. Sci.* **2002**, *280*, 1.
[10] M. Mielke, R. Zimehl *Ber. Bunsenges. Phys. Chem.* **1998**, *102*, 1698.

[11] E. Daly, B. R. Saunders *Langmuir* **2000**, *16*, 5546.
[12] C. D. Jones, L. A. Lyon *Macromolecules* **2000**, *33*, 8301.
[13] D. Gan, L. A. Lyon *J. Am. Chem. Soc.* **2001**, *123*, 7511.
[14] C. D. Jones, L. A. Lyon *Langmuir* **2003**, *19*, 4544.
[15] D. Duracher, A. Elaissari, C. Pichot *J. Polym. Sci. A* **1999**, *37*, 1823.
[16] D. Duracher, A. Elaissari, C. Pichot *Colloid Polym. Sci.* **1999**, *277*, 905.
[17] X. Wu, R. H. Pelton, A. E. Hamilelec, D. R. Woods, W. McPhee *Colloid Polym. Sci.* **1994**, *272*, 467.
[18] D. Duracher, A. Elaissari, C. Pichot *Macromol. Symp.* **2000**, *150*, 305.
[19] S. Seelenmeyer, I. Deike, S. Rosenfeldt, C. Norhausen, N. Dingenouts, M. Ballauf, T. Narayanan, P. Lindner *J. Chem. Phys.* **2001**, *114*, 10471.
[20] K. Kratz, T. Hellweg, W. Eimer *Ber. Bunsenges. Phys. Chem.* **1998**, *102*, 1603.
[21] K. Kratz, T. Hellweg, W. Eimer *Polymer* **2001**, *42*, 6631.
[22] H. M. Crowther, B. R. Saunders, S. J. Mears, T. Cosgrove, B. Vincent, S. M. King, G. E. Yu *Colloids Surf. A* **1999**, *152*, 237.
[23] I. Berndt, P. Lindner, J. S. Pedersen, W. Richtering *manuscript in preparation*.

Chapter 3

[1] R. H. Pelton, P. Chibante *Colloids Surf.* **1986**, *20*, 247.
[2] R. Pelton Adv. Colloid Interf. Sci. **2000**, *85*, 1.
[3] C. D. Jones, L. A. Lyon *Macromolecules* **2000**, *33*, 8301.
[4] D. Gan, L. A. Lyon *J. Am. Chem Soc.* **2001**, *123*, 7511.
[5] C. D. Jones, L. A. Lyon *Macromolecules* **2003**, *36*, 1988.
[6] C. D. Jones, L. A. Lyon *Langmuir* **2003**, *19*, 4544.
[7] I. Berndt, W. Richtering *Macromolecules* **2003**, *36*, 8780.
[8] D. Gan, L. A. Lyon *J. Am. Chem. Soc.* **2001**, *123*, 8203.
[9] C. D. Jones, J. G. McGrath, L. A. Lyon *J. Phys. Chem. B* **2004**, *108*, 12652.
[10] M. Stieger, W. Richtering, J. S. Pedersen, P. Lindner *J. Chem. Phys.* **2004**, *120*, 6197.
[11] A. Fernández-Barbero, A. Fernández-Nieves, I. Grillo, E. López-Cabarcos *Rhys. Rev. E* **2002**, *66*, 51803.
[12] B. R. Saunders *Langmuir* **2004**, *20*, 3925.
[13] I. Berndt, J. S. Pedersen, P. Lindner, W. Richtering *in preparation*.
[14] X. Wu, R. H. Pelton, A. E. Hamielec, D. R. Woods, W. McPhee *Colloid Polym Sci.* **1994**, *272*, 467.
[15] M. Kerker *The scattering of light*, Academic Press, San Diego, **1969**.
[16] J. S. Pedersen, D. Posselt, K. Mortensen *J. Appl. Cryst.* **1990**, *23*, 321.

Chapter 4

[1] D.E. Bergbreiter, B. L. Case, Y.-S. Liu, J. W. Caraway *Macromolecules* **1998**, *31*, 6053.
[2] V. Castro Lopez, S. L. Raghavan, M. J. Snowden *React. Funct. Polym.* **2004**, *58*, 175.
[3] G. Gerlach, M. Guenther, G. Suchaneck, J. Sorber, K.-F. Arndt, A. Richter *Macromol. Symp.* **2004**, *21*, 403.
[4] H. Kaşgöz, S. Ösgümüş, M. Orbay *Polymer* **2004**, *44*, 1785.

[5] V. J. Cornelius, M. J. Snowden, J. Silver, G. R. Fern *React. Funct. Polym.* **2004**, *58*, 165.
[6] H. Senff, W. Richtering *J. Chem. Phys.* **1999**, *111*, 1705.
[7] J. Kim, M. J. Serpe, L. A. Lyon *Angew. Chem.* **2005**, *117*, 1357.
[8] R. Pelton Adv. Colloid Interf. Sci. **2000**, *85*, 1.
[9] M. Heskins, J. E. Guilett *J. Macromol. Sci., Chem.* **1968**, *A2(8)*, 1441.
[10] M. Rasmusson, B. Vincent *React. Funct. Polym.* **2004**, *58*, 203.
[11] M. Mielke, R. Zimehl *Ber. Bunsenges. Phys. Chem.* **1998**, *102*, 1698.
[12] T. Hoare, R. Pelton *Macromolecules* **2004**, *37*, 2544.
[13] A. Mamada, T. Tanaka, D. Kungwatchakun, M. Irie *Macromolecules* **1990**, *23*, 1517.
[14] S. Nayak, L. A. Lyon *Angew. Chem.* **2004**, *116*, 6874.
[15] C. D. Jones, L. A. Lyon *Macromolecules* **2000**, *33*, 8301.
[16] I. Berndt, W. Richtering *Macromolecules* **2003**, *36*, 8780.
[17] S. J. Mears, Y. Deng, T. Cosgrove, R. Pelton *Langmuir* **1997**, *13*, 1901.
[18] H. M. Crowther, B. R. Saunders, S. J. Mears, T. Cosgrove, B. Vincent, S. M. King, G.-E. Yu *Colloids Surf. A* **1999**, *152*, 327.
[19] K. Kratz, T. Hellweg, W. Eimer *Polymer* **2001**, *42*, 6631.
[20] A. Fernández-Babero, A. Fernández-Nieves, I. Grillo, E. López-Cabarcos *Phys. Rev. E* **2002**, *66*, 051803.
[21] B. R. Saunders *Langmuir* **2004**, *20*, 3925.
[22] M. Stieger, W. Richtering, J. S. Pedersen, P. Lindner *J. Chem. Phys.* **2004**, *120*, 6197.
[23] X. Wu, R. H. Pelton, A. E. Hamielec, D. R. Woods, W. McPhee *Colloid Polym. Sci.* **1994**, *272*, 467.
[24] S. Meyer, W. Richtering *Macromolecules* **2005**, *38*, 1517.
[25] V. Boyko, S. Richter, I. Grillo, E. Geissler *Macromolecules* **2005**, 38, 5266.
[26] N. Dingenouts, C. Norhausen, M. Ballauff *Macromolecules* **1998**, *31*, 8912.
[27] S. Seelenmeyer, I. Deike, S. Rosenfeldt, C. Norhausen, N. Dingenouts, M. Ballauff, T. Narayan, P. Lindner *J. Chem. Phys.* **2001**, *114*, 10471.
[28] C. D. Jones, L. A. Lyon *Langmuir* **2003**, *19*, 4544.
[29] C. D.Jones, L. A. Lyon *Macromolecules* **2003**, *36*, 1988.
[30] D. Gan, L. A. Lyon *J. Am. Chem. Soc.* **2001**, *123*, 8203.
[31] C. D. Jones, J. G. Mc Grath, L. A. Lyon *J. Phys Chem. B*. **2004**, *108*, 12652.
[32] I. Berndt, J. S. Pedersen, W. Richtering *J. Am. Chem. Soc*. **2005**, *127*, 9372.
[33] J. S. Pedersen *Adv. Colloid Interf. Sci.* **1997**, *70*, 171.
[34] A neutron scattering length density calculator can be found at the NIST facility homepage: http://www.ncnr.nist.gov/resources/sldcalc.html
[35] J. S. Pedersen, D. Posselt, K. Mortensen *J. Appl. Crystallogr.* **1990**, *23*, 321.
[36] D. Duracher, A. Elaissari, C. Pichot *Macromol. Symp.* **2000**, *105*, 305.
[37] I. Berndt, J. S. Pedersen, W. Richtering *in preparation.*
[38] J. Pleštil *J. Appl. Cryst.* **2000**, *33*, 600.
[39] I. Berndt, C. Popescu, F.-J. Wortmann, W. Richtering *Angew. Chem. Int. Ed. accepted*.

Chapter 5

[1] S. Nayak, L. A. Lyon *Angew. Chem.* **2004**, *11*, 6874; *Angew. Chem. Int. Ed.* **2004**, *43*, 6706.
[2] J. Kim, S. Nayak, L. A. Lyon *J. Am. Chem. Soc.* **2005**, *127*, 9588.
[3] T. J. V. Prazeres, A. M. Santos, J. M. G. Martinho *Langmuir* **2004**, *20*, 6834.
[4] Y. Deng, W. Yang, C. Wang, S. Fu *Adv. Mater.* **2003**, *15*, 1729.

[5] Q. Sun, Y. Deng *Langmuir* **2005**, *21*, 5812.
[6] I. W. Hamley *The Physics of Block Copolymers*, Oxford University Press: Oxford, 1998.
[7] J. S. Pedersen, C. Svaneborg *Curr. Opin. Colloid Interface Sci*. **2002**, *7*, 158.
[8] K. B. Thurmond, T. Kowalewski, K. L. Wooley *J. Am. Chem. Soc.* **1997**, *119*, 6656.
[9] K. B. Thurmond, T. Kowalewski, K. L. Wooley *J. Am. Chem. Soc.* **1996**; *118*, 7239.
[10] T. K. Bronich, P. A. Keifer, L. S. Shlyakhtenko, A. V. Kabanov *J. Am. Chem. Soc.* **2005**, *127*, 8236.
[11] X.-S. Wang, A. Arsenault, G. A. Ozin, M. A. Winnik, I. Manners *J. Am. Chem. Soc.* **2003**, *125*, 12686.
[12] G. E. Oosterrom, J. N. H. Reek, P. C. J. Kamer, P. W. N. M. van Leeuwen *Angew. Chem. Int. Ed.* **2001**, *40*, 1828; *Angew. Chem.* **2001**, *113*, 1878.
[13] S. E. Stiriba, H. Kautz, H. Frey *J. Am. Chem. Soc.* **2002**, *124*, 9698.
[14] R. Haag Angew. Chem. **2004**, 116, 280; Angew. Chem. Int. Ed. **2004**, 43, 278.
[15] C. D. Jones, L. A. Lyon, *Macromolecules* **2000**, *33*, 8301.
[16] X. Li, J. Zuo, Y. Guo, X. Yuan *Macromolecules* **2004**, *37*, 10042.
[17] I. Berndt, W. Richtering *Macromolecules* **2003**, *36*, 8780.
[18] I. Berndt, C. Popescu, F.-J. Wortmann, W Richtering *Angew. Chem. Int. Ed.* **2005**, accepted.
[19] P. G. de Gennes, H. Hervet *J. Phys. Lett*. **1983**, *44*, L351.
[20] S. Rosenfeldt, N. Dingenouts, D. Pötschke, M. Ballauff, A. J. Berresheim, K. Müllen, P. Lindner *Angew. Chem. Int. Ed*. **2003**, *43*, 109; *Angew. Chem.* **2003**, *116*, 111.
[21] D. Boris, M. Rubinstein *Macromolecules* **1996**, *29*, 7251.
[22] M. Ballauff, C. Likos *Angew. Chem.* **2004**, *116*, 3060; *Angew. Chem. Int. Ed.* **2004**, *43*, 2998.
[23] D. Gan, L. A. Lyon *J. Am. Chem. Soc.* **2001**, *123*, 8203.
[24] C. D. Jones, J. G. McGrath, L. A. Lyon *J. Phys. Chem. B* **2004**, *108*, 12652.
[25] I. Berndt, J. S. Pedersen, W. Richtering *J. Am. Chem. Soc.* **2005**, *127*, 9372.
[26] I. Berndt, J. S. Pedersen, P. Lindner, W. Richtering *Langmuir*, accepted.
[27] D. Duracher, A. Elaissari, C. Pichot *Colloid Polym. Sci.* **1999**, *277*, 905.
[28] H. Senff, W. Richtering *J. Chem. Phys.* **1999**, *111*, 1705.
[29] X. Wu, R. H. Pelton, A. E. Hamielec, D. R. Woods, W. McPhee *Colloid Polym. Sci.* **1994**, *272*, 467.
[30] J. S. Pedersen, D. Posselt, K. Mortensen *J. Appl. Cryst.* **1990,** *23* 321.
[31] J. S. Pedersen Adv. Colloid Interface Sci. **1997**, 70, 171.
[32] M. Stieger, W. Richtering, J. S. Pedersen, P. Lindner *J. Chem. Phys.* **2004**, *120*, 6197.
[33] S. Meyer, W. Richtering *Macromolecules* **2005**, *38*, 1517.
[34] I. Berndt, J. S. Pedersen, W. Richtering, in preparation.

Chapter 6

[1] G. E. Oosterrom, J. N. H. Reek, P. C. J. Kamer, P. W. N. M. van Leeuwen *Angew. Chem. Int. Ed.* **2001**, *40*, 1828; *Angew. Chem.* **2001**, *113*, 1878.
[2] S. E. Stiriba, H. Kautz, H. Frey *J. Am. Chem. Soc.* **2002**, *124*, 9698.
[3] R. Haag *Angew. Chem.* **2004**, *116*, 280; *Angew. Chem. Int. Ed.* **2004**, *43*, 278.
[4] H. Huang, E. E. Remsen, T. Kowalewski, K. L. Wooley *J. Am. Chem. Soc.* **1999**, *121*, 3805.
[5] T. K. Bronich, P. A. Keifer, L. S. Shlyakhtenko, A. V. Kabanov *J. Am. Chem. Soc.* **2005**, *127*, 8236.

[6] R. Pelton *Adv. Colloid Interface Sci.* **2000**, 85, 1.
[7] C.D. Jones, L. A. Lyon *Macromolecules*, **2000**, *33*, 8301.
[8] S. Nayak, L. A. Lyon *Angew. Chem.* **2004**, *116*, 6874, *Angew. Chem. Int. Ed.* **2004**, *43*, 6706.
[9] C. D. Jones, L. A. Lyon *Macromolecules* **2003**, *36*, 1988.
[10] C. D. Jones, L. A. Lyon *Langmuir* **2003**, *19*, 4544.
[11] I. Berndt, W. Richtering *Macromolecules* **2003**, *36*, 8780.
[12] I. Berndt, J. S. Pedersen, W. Richtering *J. Am. Chem. Soc.* **2005**, *127*, 9372.
[13] P. Rennert, H. Schmiedel (Ed.) *Physik*, BI Wissenschaftsverlag: Mannheim, Leipzig 1995.
[14] H. Kawasaki, S. Sasaki, H. Maeda *Langmuir* **1998**, *14*, 773.
[15] H. Kawasaki, S. Sasaki, H. Maeda *Langmuir* **2000**, *16*, 3195.
[16] M. Schönhoff, A. Larsson, P.B. Welzel, D. Kuckling *J. Phys. Chem. B.* **2002**, *106*, 7800.
[17] S. Seelenmeyer, I. Deike, S. Rosenfeldt, Ch. Norhausen, N. Dingenouts, M. Ballauff, T. Narayanan, P. Lindner *J. Chem. Phys.* **2001**, *114*, 10471.
[18] D. Gan, L. A. Lyon, *J. Am. Chem. Soc.* **2001**, *123*, 8203.

Chapter 7

[1] T. Tokuhiro, T. Amiya, A. Mamada, T. Tanaka *Macromolecules* **1991**, *24*, 2936-2943.
[2]. H. Gao, W. Yang, K. Min, L. Zha, C. Wang, S. Fu *Polymer* **2005**, *46*, 1087.
[3] L. Zha, Y. Zhang, W. Yang, S. Fu *Adv. Mater.* **2002**, *14*, 1090.
[4] S. Nayak, D. Gan, M. J. Serpe, L. A. Lyon *Small* **2005**, *1*, 416.
[5] Y. Zhang, M. Jiang, J. Zhao, X. Ren, D. Chen, G. Zhang *Adv. Funct. Mat.* **2005**, *15*, 695.
[6] Y. Maeda, T. Higuchi, I. Ikeda *Langmuir* **2000**, *16*, 7503.
[7] Y. Maeda, T. Nakamura, I. Ikeda *Macromolecules* **2001**, *34*, 1391
[8] Y. Maeda, H. Yamamoto, I. Ikeda *Langmuir* **2001**, *17*, 6855.
[9] Y. Maeda, T. Nakamura, I. Ikeda *Macromolecules* **2001**, *34*, 8246.
[10] M. Schönhoff, A. Larsson, P. B. Welzel, D. Kuckling *J. Phys. Chem. B* **2002**, *106*, 7800.
[11] A. Larsson, D. Kuckling, M. Schönhoff *Colloids Surf. A* **2001**, *190*, 185.
[12] M. Schönhoff, B. Schwarz, A. Larsson, D. Kuckling *Progr. Colloid Polym. Sci.* **2002**, *121*, 80.
[13] L. Starovoytova, J. Spěváček, L. Hanyková, M. Ilavský *Polymer* **2004**, *45*, 5905.
[14] L. Starovoytova, J. Spěváček, M. Ilavský *Polymer* **2005**, *46*, 677.
[15] D. Gan, L. A. Lyon *J. Am. Chem. Soc.* **2001**, *123*, 8203.
[16] C. K. Chee, S. Rimmer, I. Soutar, L. Swanson *Polymer* **2001**, *42*, 5079.
[17] C. D. Jones, J. G. McGrath, L. A. Lyon *J. Phys. Chem* **2004**, *108*, 12652.
[18] H. Senff, W. Richtering *J. Chem. Phys.* **1999**, *111*, 1705.
[19] J. Wu, G. Huang, Z. Hu *Macromolecules* **2003**, *36*, 440.
[20] M. Stieger, J. S. Pedersen, P. Lindner, W. Richtering *Langmuir* **2004**, *20*, 7283.
[21] J. Zhang, N. A. Peppas *Macromolecules* **2000**, *33*, 102.
[22] X. Xia., Z. Hu *Langmuir* **2004**, *20*, 2094.
[23] X.-C. Xiao, L.-X.-C. Xiao, L.-Y. Chu, W.-M. Chen, J.-H. Zhu *Polymer* **2005**, *46*, 3199.
[24] E. Díez-Pena, I. Quijada-Garrido, P. Frutos, J. M. Barrales-Rienda *Macromolecules* **2002**, *35*, 2667.
[25] K. N. Plunkett, J. S. Moore *Langmuir* **2004**, *20*, 6535.

Chapter 8

[1] Deutero GmbH, Am Ring 29, D-56288 Kastellaun, Tel.: +49 6762 960231, Fax: +49 6762 960231. This supplier offers high quality deuterated solvents to much lower prices than the usual ones.
[2] H. Senff, W. Richtering *J. Chem. Phys.* **1999**, *111*, 1705.
[3] D. Duracher, A. Elaissari, C. Pichot *J. Poly. Sci. Part A* **1999**, *37*, 1823.
[4] C. D. Jones, L. A. Lyon *Macromolecules* **2000**, *33*, 8301.
[5] R. Pelton *Macromol. Symp.* **2004**, *207*, 575.
[6] D. E. Koppel *J. Chem. Phys.* **1972**, *57*, 4814.
[7] C. H. Cho, J. Urquidi, S. Singh, G. W. Robinson *J. Phys. Chem. B* **1999**, *103*, 1991.
[8] ALV-5000/E Reference Manual, p. 24, 1993.
[9] S. Pyett, personal communication, 2003.
[10] G. Fritz, G. Scherf, O. Glatter *J. Phys. Chem. B* **2000**, *104*, 3463.
[11] C. Sommer, J. S. Pedersen, P. C. Stein *J. Phys. Chem. B* **2004**, *108*, 6242.
[12] M. Stieger, W. Richtering, J. S. Pedersen, P. Lindner *J. Chem. Phys.* **2004**, *120*, 6197.
[13] P. Lindner, Scattering Experiments: Experimental Aspects, Initial Data Reduction and Absolute Calibration. In: *Neutrons, X-rays and Light: Scattering Methods Applied to Soft Condensed Matter*, 1st ed., P. Lindner, T. Zemb, Eds., North-Holland Delfa Series, Elsevier: Amsterdam, 2002.
[14] GRASP home page: www.ill.fr/lss/grasp/grasp_main.html